

Molecular and physiological dissection of GUN1 chloroplast-to-nucleus retrograde signaling



Dissertation der Fakultät für Biologie der Ludwig-Maximilians-
Universität München

vorgelegt von

Luca Tadini

01.08.2013



Molecular and physiological dissection of GUN1 chloroplast-to-nucleus retrograde signaling

Dissertation

zur Erlangung des Doktorgrades der Fakultät für Biologie
der Ludwig-Maximilians-Universität München

Erstgutachter: Prof. Dr. Dario Leister

Zweitgutachter: Prof. Dr. Jörg Nickelsen

Tag der Einreichung: 01.08.2013

Tag der mündlichen Prüfung: 26.09.2013

Summary

Retrograde signaling encompasses the molecular mechanisms that enable the cell organelles to communicate with the nucleus and to adapt Nuclear Gene Expression (NGE) to the organelle's needs. Regarding plastid-to-nucleus signaling, the Organellar Gene Expression (OGE), the Thylakoid Redox State (TRS), Reactive Oxygen Species (ROS) production and the tetrapyrrole biosynthesis are considered to be the main sources of signals. Here, we determined the molecular aspects of retrograde signaling by employing a genetics-based approach. To this end, the OGE-defective *prors1-1* mutant, knock-down of a dual-located Prolyl-tRNA Synthetase, was crossed with *chaos*, a mutant with altered light absorption properties. The phenotypic analysis of the double mutant allowed for the determination of a hierarchy among the signal sources: perturbations in OGE lead to an increase of the reduced fraction of the plastoquinone (PQ) pool, while the *chaos* mutation alleviates this effect. NGE analyses of the *prors1-1 chaos* double mutant indicate that the *chaos* mutation suppresses the down-regulation observed in the *prors1-1* mutant, implying that the TRS mediates the OGE-dependent retrograde signal. Furthermore, the introgression of the *gun1* mutation into an OGE defective genetic background like the *prors1-1* and some *prp* mutants, lacking plastid ribosomal proteins, enabled us to investigate the functional interaction of GUN1 with the OGE machinery. Moreover, the physical interaction with the Mg-chelatase suggests a role of GUN1 in coordinating OGE and chlorophyll biosynthesis with NGE. To determine whether other plastid Transcriptionally Active Chromosomes (pTACs) subunits exert a similar function, the effects of a mutation in the RNA helicase RH50 gene were analyzed in combination with the same set of OGE mutants. RH50, which is co-regulated and co-localizes with GUN1, was shown to modulate NGE in an OGE defective mutant background similar to GUN1, suggesting that a specific domain of the pTAC complexes, rather than GUN1 alone, is capable to mediate OGE-dependent signaling.

Zusammenfassung

Unter „retrograde Signaling“ werden jene molekularen Mechanismen zusammengefasst, die der Organellen-Kern Kommunikation dienen und es erlauben die nukleäre Genexpression (NGE) den Bedürfnissen der Organellen anzupassen. Als Hauptsignalquellen der Plastiden-Kern Kommunikation gelten die Genexpression der Organellen (OGE), der Redoxzustand der Thylakoide (TRS), reaktive Sauerstoffspezies und die Tetrapyrrole-Biosynthese. In dieser Arbeit wurden molekulare Aspekte der retrograden Signalübertragung mithilfe genetischer Ansätze untersucht. Dazu wurde die *prors1-1* Mutante, die einen Defekt in der OGE aufweist, mit *chaos*, einer Mutante mit veränderten Lichtabsorptionseigenschaften, gekreuzt. Deren Analyse erlaubte die Bestimmung einer Hierarchie unter den einzelnen Signalquellen: Störungen in der OGE erhöhen die reduzierte Fraktion des Plastoquinonpools (PQ) während die *chaos* Mutation diesen Effekt abschwächt. Die Analyse der NGE in der *prors1-1 chaos* Doppelmutante zeigt die kompensatorischen Eigenschaften der *chaos* Mutation hinsichtlich der verringerten Expression von kernkodierten Genen in der *prors1-1* Mutante. Somit scheint dem TRS eine Signalfunktion im OGE-abhängigen „retrograde Signaling“ zuzukommen. Die Einführung der *gun1* Mutation in *prors1-1* und einige *prp* Mutanten erlaubt es, die funktionale Interaktion von GUN1 mit den OGE Prozessen zu untersuchen. Zudem deutet die physikalische Interaktion von GUN1 mit der Mg-Chelatase auf eine Rolle von GUN1 in der Koordination von OGE und Chlorophyll-Biosynthese mit NGE hin. Zur Beantwortung der Frage, ob andere Untereinheiten der Plastidiären Transkriptionell-aktiven Chromosomen (pTACs) eine ähnliche Funktion wie GUN1 ausüben, wurden die Effekte einer Mutation im Gen der RNA Helikase RH50 in Kombination mit dem gleichen Set an OGE Mutanten analysiert. Die Mutation der stark mit GUN1 koregulierten und kolokalisierten RNA Helikase RH50 wies dabei ähnliche Anpassungseffekte der NGE in den OGE-Mutanten auf. Daraus lässt sich folgern, dass nicht GUN1 allein, sondern eine spezifische Domäne der pTAC-Komplexe in der Lage ist, die OGE-abhängige Signalübertragung zu vermitteln.

Index

Summary	i
Zusammenfassung.....	ii
Index	iii
Figures list.....	vii
Tables list	ix
Abbreviations.....	x
1. Introduction.....	1
1.1 Endosymbiotic origin of organelles, genetic rearrangement and intracellular communication.....	1
1.2 Retrograde plastid-to-nucleus signaling: the involvement of metabolites	3
1.3 Retrograde plastid-to-nucleus signaling in <i>Arabidopsis thaliana</i> : Organelle Gene Expression	6
1.4 Multiple Retrograde plastid-to-nucleus signaling pathways in <i>Arabidopsis thaliana</i> : thylakoid and chloroplast redox state and the formation of reactive oxygen species	7
1.5 GUN1, a possible integrator of different signaling pathways	9
1.6 GUN1 protein complex: a possible link between OGE and tetrapyrrole biosynthesis.....	11
1.7 Aims of the work	13
2. Material and Methods.....	15
2.1 Database analysis and software tools	15

2.2 Chemical material	15
2.3 Plant material and growth conditions.....	15
2.4 Chlorophyll fluorescence, pigment analysis and oxygen evolution measurements.....	17
2.5 Nucleic acids isolation.....	18
2.6 First strand cDNA synthesis.....	19
2.7 Northern blot analyses	19
2.8 Standard PCR and High fidelity PCR	23
2.9 Fluorescent protein localization.....	23
2.10 Yeast two-hybrid assay.....	24
2.11 Chloroplast isolation and sub-fractionation	26
2.12 Protein preparation and immuno-blot analysis	27
2.13 <i>In vivo</i> translation assay	27
2.14 Embryo analysis and TEM analysis	27
2.15 Bimolecular fluorescence complementation (BiFC)	28
3. Results and Discussions.....	30
3.1 Thylakoid redox signals are integrated into OGE-dependent retrograde signaling in the <i>prors1-1</i> mutant	30
3.1.1 The <i>chaos</i> mutation is capable of restoring a WT TRS in the <i>prors1-1</i> mutant	30
3.1.2. Protein composition of thylakoid membranes is influenced by the TRS	33
2.1.3. TRS influences nuclear and plastid gene expression	35

3.1.4. Discussion	39
3.2 GUN1 functionally interacts with the plastid gene expression machinery	42
3.2.1. <i>gun1-gun5</i> genetic interaction with <i>prpl11</i> and <i>prors1-1</i> mutants.....	42
3.2.2 GUN1 functionally interacts with different subunits of the plastid ribosomes.....	50
3.2.3 Discussion	51
3.3 GUN1 and the molecular mechanism behind.....	54
3.3.1 GUN1 is a component of the pTAC complex and interacts with the Mg-Chelatase.....	54
3.3.2 Discussion	59
3.4 The RH50 component of the pTAC complex shows similar features of GUN1 with respect to retrograde signalling	62
3.4.1 RH50 and GUN1 are subunits of the pTAC complex.....	62
3.4.2 RH50 is involved in plastid transcript processing.....	63
3.4.3 RH50 and GUN1 show similar genetic interactions	65
3.4.4 Discussion	68
3.5 GUN1 and RH50 are involved in the regulation of NGE.....	71
3.5.1 GUN1 and RH50 act as repressors of NGE in the <i>prors1-1</i> genetic background.....	71
3.5.2 Discussion	73
4. Conclusions.....	74

References	78
Acknowledgements.....	85
Curriculum vitae	86
Declaration / Eidesstattliche Erklärung	89

Figures list

Figure 1.1 Gene transfer during plastid evolution from cyanobacteria to the higher plants chloroplast and inter-organellar signaling.	3
Figure 1.2 Tetrapyrrole biosynthetic pathway and <i>gun</i> mutants identified within the pathway (red).	5
Figure 1.3 Schematic overview of the different pathways involved in retrograde signaling.	10
Figure 3.1 Schematic representation of <i>prors1-1</i> and <i>chaos</i> mutant alleles.	30
Figure 3.2 Phenotypes of <i>prors1-1</i> , <i>chaos</i> and <i>prors1-1 chaos</i> mutants..	31
Figure 3.3 Protein composition of thylakoid membranes.....	35
Figure 3.4 Synthesis rate of plastid-encoded proteins.	36
Figure 3.5 Expression analysis of nuclear- and plastid-encoded genes in <i>prors1-1</i> , <i>chaos</i> and <i>prors1-1 chaos</i> plants.....	38
Figure 3.6 Schematic representation of the employed mutants alleles. ..	43
Figure 3.7 Phenotypic analysis of <i>gun1 prpl11</i> mutant.	44
Figure 3.8 Phenotypic characterization of 26 days old <i>gun1 prpl11</i> and immutans plants.	46
Figure 3.9 Phenotypes of the <i>gun1-gun5</i> , <i>prpl11</i> and <i>prors1-1</i> single and <i>gun prpl11</i> and <i>gun prors1-1</i> double mutants... ..	47
Figure 3.10 Growth ratio measurements of <i>gun</i> mutants in <i>prpl11</i> and <i>prors1-1</i> genetic background.....	49
Figure 3.11 Phenotypic characterization of <i>gun1</i> and <i>prp</i> single and double mutants.....	51

Figure 3.12 GUN1-GFP localization.	55
Figure 3.13 BiFC assays to test the interaction of GUN1 with each of the following tetrapyrrole enzymes: HEMC, HEME, and CHLD.	58
Figure 3.14 Immuno-blot analyses on the accumulation of Mg-chelatase subunits in leaves of WT, <i>gun1</i> and 35S:GUN1-GFP transgenic lines.	59
Figure 3.15 <i>RH50</i> genomic locus and the employed T-DNA alleles.	62
Figure 3.16 Co-localization of 35S:RH50-YFP and 35S:GUN1-GFP in <i>A. thaliana</i> protoplasts.	63
Figure 3.17 Northern blot analyses on leaves from 14 days old <i>gun1</i> , <i>rh50</i> and <i>gun1 rh50</i> plants.	64
Figure 3.18 Phenotypic analyses of the <i>rh50</i> mutation in <i>prp</i> and <i>prors1-1</i> mutant genetic backgrounds.	66
Figure 3.19 Growth rate analyses of <i>rh50</i> mutant in combination with <i>gun1</i> and the OGE mutants.	67
Figure 3.20 Northern blot analyses on NGE in <i>gun1</i> , <i>rh50</i> and <i>prors1-1</i> single and double mutant backgrounds.	72
Figure 4.1 Working model of GUN1 and RH50 molecular function and heme and chlorophyll synthesis as signal molecules.	77

Tables list

Table 2.1 List of the mutant alleles employed in this work.....	16
Table 2.2 Sequences of the primers used for the genotyping analyses. .	17
Table 2.3 Sequences of the primers employed for northern blot radiolabeled probes.....	22
Table 2.4 Primer sequences employed in the Y2H assay.....	26
Table 2.5 Primer sequences used for BiFC assay, GUN1-GFP and RH50-YFP localization.....	29
Table 3.1 Photosynthetic performance and oxygen production of <i>prors1-1</i> , <i>chaos</i> and <i>prors1-1 chaos</i> mutants plants.	32
Table 3.2 Leaf pigment content of <i>prors1-1</i> , <i>chaos</i> and <i>prors1-1 chaos</i> mutants.....	33
Table 3.3 Segregation analyses on the progeny of four <i>gun1</i> alleles introduced into the <i>prpl11</i> mutant background.	45
Table 3.6 Photosynthetic efficiency measurements on <i>gun1 prps1</i> and <i>gun1 prps21</i> plants.	51
Table 3.7 Co-regulation data of GUN1 with the entire <i>Arabidopsis thaliana</i> transcriptome.....	56
Table 3.8 Data of the yeast-two-hybrid assay using GUN1 as bait.....	57
Table 3.9 Photosynthetic parameters (F_v/F_m , Φ_{II} and 1-qP) of rh50, <i>gun1</i> , <i>prors1-1</i> , <i>prpl11</i> , <i>prps1</i> and <i>prps21</i> single and double mutants.....	68

Abbreviations

°C	Degree Celsius
<i>A. thaliana</i>	<i>Arabidopsis thaliana</i>
ALA	5-aminolevulinic acid
CAO	Chlorophyll A Oxygenase
cDNA	Complementary DNA
Chl	Chlorophyll
Ci	Curie
cTP	Chloroplast transit peptide
Da	Dalton
DEPC	Diethylpyrocarbonate
DNA	Deoxyribonucleic acid
EDTA	Ethylene diamin tetraacetic acid
g	Gram
<i>g</i>	Gravity force
GFP	Green Fluorescent Protein
GUN	Genome Uncoupled
HEPES	4-(2-hydroxyethyl)-1-piperazineethanesulfonic acid
L	Liter
Lhc	Light harvesting complex
M	Mole(s) per liter
m	Milli
mol	Mole
mRNA	Messenger RNA
MRP	Mitochondrial Ribosomal Protein
MS	Mass spectrometry
PAGE	Polyacrylamide gel electrophoresis

PAM	Pulse amplitude modulation
PCR	Polymerase Chain Reaction
PRP	Plastid Ribosomal Protein
PSI/II	Photosystem I/II
PVDF	Polyvinylidene difluoride
qRT-PCR	Quantitative Real Time PCR
RNA	Ribonucleic acid
rRNA	Ribosomal RNA
RuBisCo	Ribulose-1,5-bisphosphate carboxylase oxygenase
SDS	Sodium Dodecyl Sulphate
TAE	Tris-acetate-EDTA
T-DNA	Transfer DNA
Tris	Tris(hydroxymethyl)-aminomethane
tRNA	Transfer RNA
v/v	Volume per volume
w/v	Weight per volume
WT	Wild Type
YFP	Yellow Fluorescent Protein
μ	Micro

1. Introduction

1.1 Endosymbiotic origin of organelles, genetic rearrangement and intracellular communication

Nowadays it is well accepted that organelles of eukaryotic cells originated from prokaryotic organisms. In particular, plant cells owe their photosynthetic capability to the uptake of a cyanobacterial ancestor that survived its endocytosis and established a symbiotic way of life inside the cytoplasm of the host cell (Martin and Kowallik, 1999). During the transition from a free living organism to an organelle, the endosymbiont partially retained its own genome as well as the ability to perform independent division cycles. However, the organellar genome size became strongly reduced with most of the genes being transferred from the endosymbiont to the nucleus of the host cell. Currently, the plastid genome encodes only 75 to 90 proteins, including subunits of the transcription and translation machinery, as well as of the photosynthetic complexes (Timmis et al., 2004), whereas about 95% of the plastid proteins, i.e. 2000 to 3000 polypeptides, are nuclear encoded (Martin et al., 2002; Barbrook et al., 2006). Therefore, plastid protein complexes and supercomplexes are chimeric structures of nucleus- and plastid-encoded proteins (Figure 1.1). In this scenario the necessity to effectively coordinate the gene expression of both genomes to allow for a correct plastid development and functionality becomes evident (Koussevitzky et al., 2007; Woodson and Chory, 2008). Moreover, also mitochondria and chloroplasts are strongly inter-dependent, with mitochondrial respiration being tightly linked to photosynthesis in the chloroplast (Hoefnagel et al., 1998). This mutual influence of the three genomes located within the plant cell clearly requires a concerted communication, both, for the coordination of functional assembly of chimeric protein complexes and for an efficient reorganization of protein complexes in response to environmental stimuli (Woodson and Chory, 2008). As extensively

described, the nucleus communicates with organelles via the anterograde signaling pathway (Figure 1.1), which comprises the synthesis of proteins that are targeted to organelles and involved in organelle gene expression. In this way the nucleus can directly influence organellar activity by acting on transcriptional, translational and post translational level. Plastid transcription is accomplished by two different polymerases, a plastid encoded polymerase (PEP) and a nucleus encoded polymerase (NEP). Interestingly, the transcription of the core of the PEP complex is performed by the NEP and PEP activity is modulated by nuclear encoded sigma factors (Hess and Borner, 1999; Shiina et al., 2005), thus showing the strict control that the nucleus exerts on the plastid genome. Conversely, any process that occurs in the organelles and influences nuclear gene expression can be defined as part of the retrograde signaling pathways. Such signals are required to communicate the organellar demands to the nucleus, both during development (biogenic control) and in fully developed plants (operational control). The developmental control of organelle biogenesis needs to be appropriately staged and the required subunits and cofactors need to be present in correct stoichiometry for accurate assembly. In fully developed plants the operational control is represented by rapid adjustments in response to environmental constraints with the objective to maintain optimal production and to limit the damages induced by oxidative stress (Leister, 2005; Pesaresi et al., 2007; Pogson et al., 2008; Woodson and Chory, 2008; Barajas-Lopez Jde et al., 2013). Various plastid-to-nucleus signaling pathways have been identified in *A. thaliana*, of which some will be described in more detail later on. The exchange of information between plastids and mitochondria is also an important issue. Indeed, it was shown that mitochondrial gene expression is able to influence the transcription of photosynthetic genes in the nucleus and that both plastids and mitochondria act synergistically to modulate nuclear gene expression (Pesaresi et al., 2006).

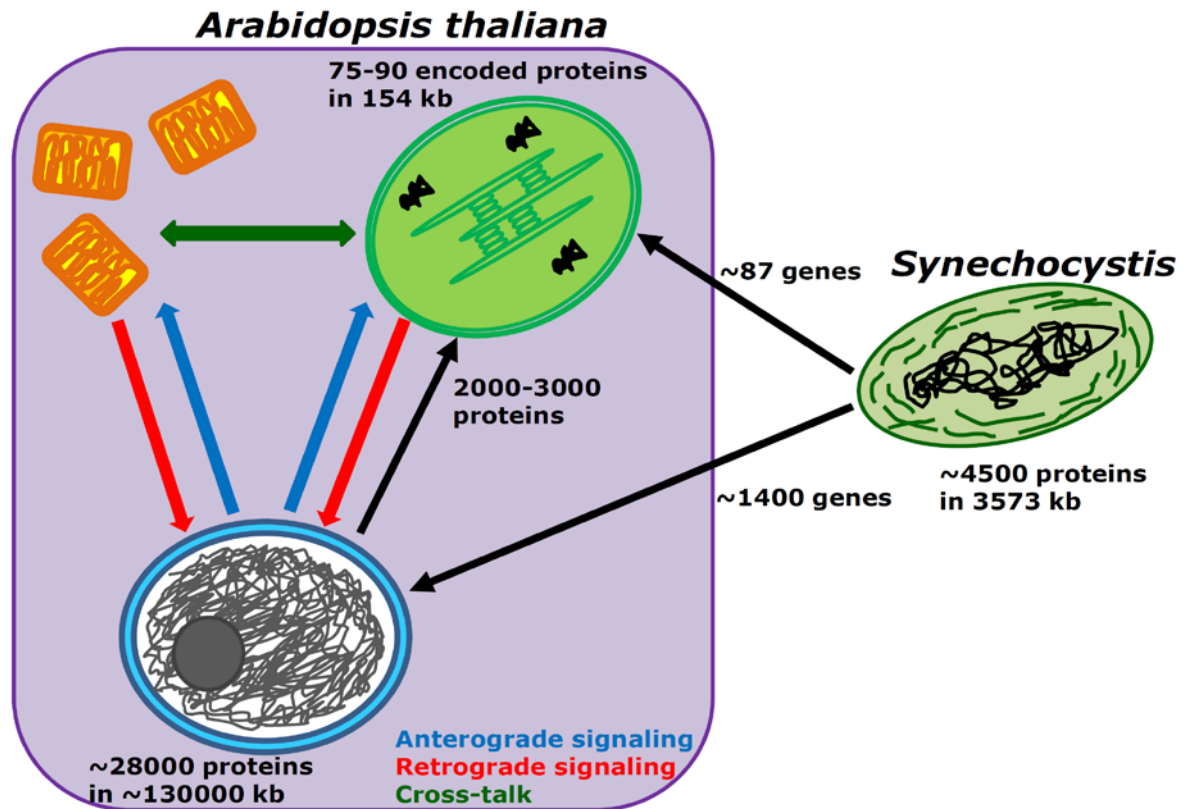


Figure 1.1 Gene transfer during plastid evolution from cyanobacteria to the higher plants chloroplast and inter-organellar signaling. Blue arrows indicate the anterograde pathways, red arrows the retrograde pathways and the green arrow represents the inter-organelle signaling pathway in plant cells.

1.2 Retrograde plastid-to-nucleus signaling: the involvement of metabolites

Arabidopsis thaliana mutants defective in retrograde signaling were first identified in 1993 by Joanne Chory's group (Susek et al., 1993). These mutants were described to be affected in plastid-to-nucleus communication and therefore named *genome uncoupled* (*gun*) mutants. A common feature of these mutants is that they still express nuclear encoded photosynthetic genes like *RbcS* and *Lhcb*, even though the chloroplast is disrupted by treatment with norfluorazon (Susek et al., 1993), a chemical that leads to photo-bleaching of chloroplasts by inhibiting β -carotene biosynthesis (Oelmüller et al., 1986). During this norfluorazon-based screen, five *gun* mutants were identified, named

gun1-to-5. Four of the affected genes, *GUN2*-to-5, play a role in the tetrapyrrole biosynthesis pathway, both at the chlorophyll-heme branching-point and downstream thereof (Figure 1.2). In particular, *gun2* is altered in heme-oxygenase activity responsible of phytochrome synthesis, whereas *gun3* carries a mutation in the phytychromobilin-synthase that operates downstream of the heme-oxygenase. On the other hand, *gun4* and *gun5* mutant plants are affected in their chlorophyll biosynthesis: *gun4* is hampered in the regulatory subunit of the Mg-chelatase and *gun5* carries a mutated CHLH subunit of the same enzymatic complex (Davis et al., 1999; Mochizuki et al., 2001; Larkin et al., 2003). Subsequently, it was shown that mutations in CHLD and both CHLI subunits of the Mg-chelatase confer a *gun* phenotype to the plant (Strand et al., 2003; Huang and Li, 2009). These observations suggested that the accumulation of Mg-protoporphyrinIX (Mg-ProtoIX), a precursor of chlorophyll, acts as a mobile signal responsible for the downregulation of nuclear photosynthesis gene expression (NGE) under specific stress conditions. However, the role of Mg-ProtoIX, as a plastid signal, has been widely questioned, since its accumulation following norfluorazon treatment could not be correlated with changes in NGE (Mochizuki et al., 2008; Moulin et al., 2008). Recently, a new *gun* mutant, named *gun6*, has been identified. The mutant is characterized by the over-expression of the FERROCHELATASE1 gene (Woodson et al., 2011) responsible for synthesizing Heme from Protoporphyrin IX (see also Figure 1.2). Because of these novel findings, Heme was proposed to be directly involved in organelle-to-nucleus communication acting as a positive stimulus for NGE (Woodson et al., 2011). According to this model, plants with altered heme-oxygenase (*gun2*) and phytychromobilin-synthase (*gun3*) show a *gun* phenotype as a consequence of the inhibition of heme conversion, whereas plants with altered Mg-chelatase activity (*gun4* and *gun5*) promote the transformation of Protoporphyrin IX into Heme at the expense of Mg-Protoporphyrin. More recently, several other metabolites

have been proposed to act as signaling molecules, including the phosphonucleotide 3'-phosphoadenosine 5'-phosphate (PAP), β -cyclocitral or methylerythritol cyclodiphosphate (MEcPP) (Estavillo et al., 2011; Ramel et al., 2012; Xiao et al., 2012).

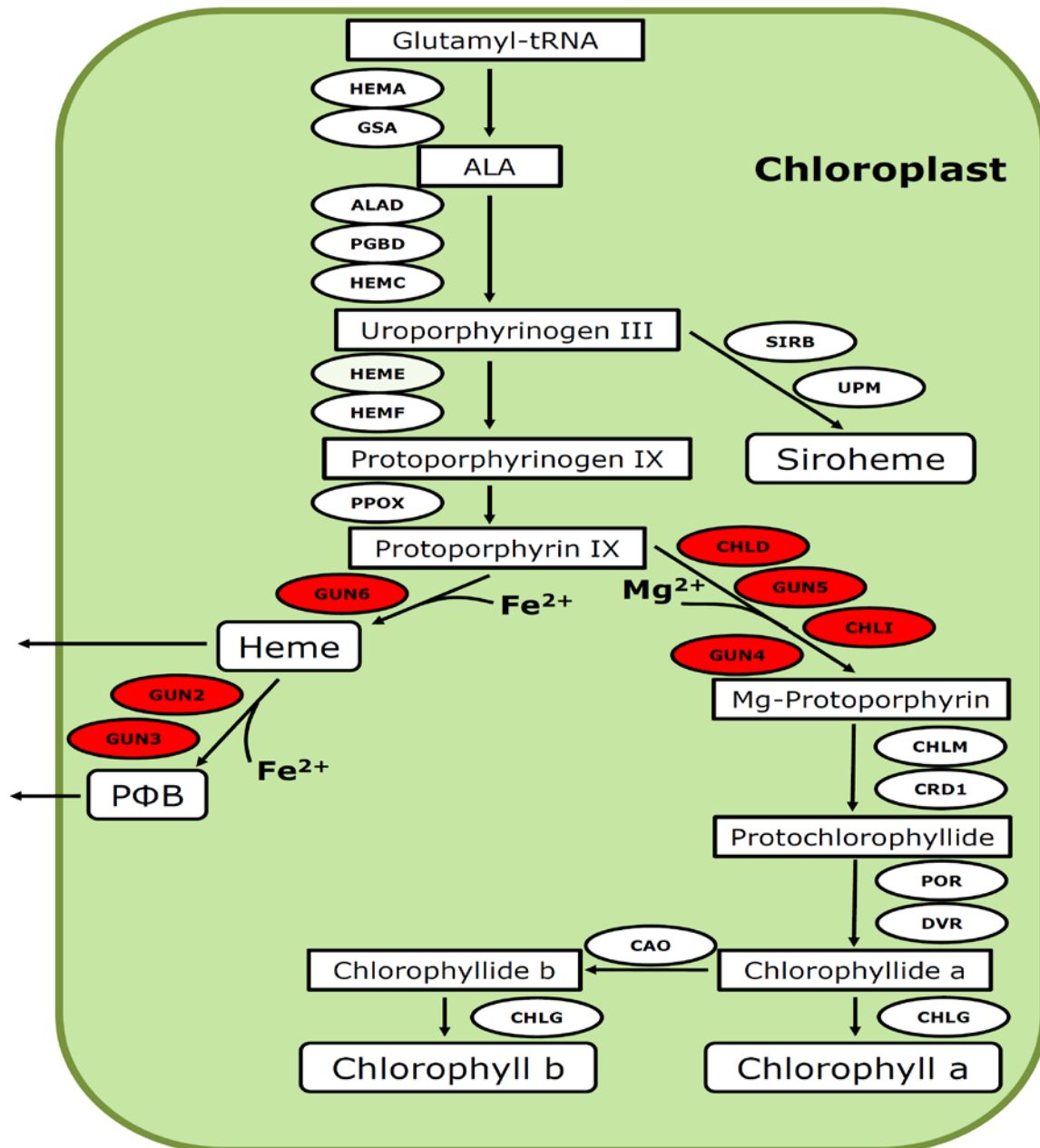


Figure 1.2 Tetrapyrrole biosynthetic pathway and gun mutants identified within the pathway (red). The *gun2* mutant is affected in the heme oxygenase enzyme (HO) which is responsible, together with the phytochromobilin-synthase (HY2, *gun3*) for the conversion of heme into the phytochrome chromophore, phytochromobilin. Recently, the *gun6* mutant has been reported to overexpress the Ferrochelatase 1 (FC1) that converts Protoporphyrin IX into Heme (Woodson et al., 2011). The other *gun* mutants such as

gun4 and *gun5* (altered CHLH subunit) are characterized by a defect in the Mg-chelatase enzyme that catalyzes the production of Mg-protoporphyrin. Note that alterations of other subunits of the Mg-chelatase, such as CHLD and CHLI, have been also reported to confer a *gun* phenotype, at least in *Arabidopsis* (Strand et al., 2003; Huang and Li, 2009).

1.3 Retrograde plastid-to-nucleus signaling in *Arabidopsis thaliana*: Organelle Gene Expression

Besides signaling pathways which are modulated by metabolites, precursors and byproducts, other plastid processes such as organellar protein synthesis have been shown to play an important role in retrograde-signaling. In particular, by employing prokaryote-specific inhibitors of plastid protein synthesis, Organellar Gene Expression (OGE) was observed to influence nuclear photosynthesis gene expression, strengthening the existence of communication pathways that coordinate the different genome activities. As a matter of fact, the expression of nuclear photosynthetic genes is dramatically affected in leaves treated with translation inhibitors like lincomycin or chloramphenicol (Oelmüller et al., 1986; Adamska, 1995; Gray et al., 1995; Yoshida et al., 1998; Sullivan and Gray, 1999). Moreover, similar results have been obtained by analyzing the *albostrians* mutant of barley, which is impaired in plastid ribosome function and, as a consequence, shows a strong down-regulation of photosynthetic nuclear genes (Bradbeer et al., 1979; Hess et al., 1994). A synergistic effect of the plastid and mitochondrial translation rate on nuclear gene expression has also been observed (Pesaresi et al., 2006). It was shown that *Arabidopsis mrpl11* and *prpl11* mutants, defective in mitochondrial and plastid ribosomal protein L11 respectively, exhibit a slight down-regulation of nuclear photosynthesis gene expression (Pesaresi et al., 2001; Pesaresi et al., 2006). In the *mrpl11 prpl11* double mutant, the down-regulation of photosynthetic nuclear genes is even more pronounced, similarly to the situation observed in *prors1-1* and *prors1-2*, where a dual targeted polyl-tRNA synthetase is knocked-down, supporting the notion that organellar translation rates act in a concerted

manner on the modulation of nuclear photosynthesis gene expression (Pesaresi et al., 2006). More recently, it has been shown that even mutants affected in plastid sigma factors like *sig2* and *sig6* and therewith possessing an altered plastid transcription, show a significant down-regulation of nuclear photosynthetic gene expression (Woodson et al., 2013). The observation is in agreement with the fact that the core of the PEP complex is encoded by the chloroplast genome; therefore, the inhibition of plastid translation causes the reduction of RNA synthesis (Gray et al., 2003).

1.4 Multiple Retrograde plastid-to-nucleus signaling pathways in *Arabidopsis thaliana*: thylakoid and chloroplast redox state and the formation of reactive oxygen species

Many environmental stimuli lead to changes in the Thylakoid Redox State (TRS) that influences nuclear and plastid gene expression to adapt the chloroplast in general, and more specifically its photosynthetic apparatus, to the altered environmental conditions. It has been shown that in the green alga *Dunaliella tertiolecta* *LchB* expression is influenced by the plastoquinone (PQ) pool redox-state (Escoubas et al., 1995). In higher plants nuclear expression of photosynthesis related genes was described to be possibly correlated with the redox-state of the thylakoid membrane via the phosphorylation of Lhcb proteins (Pursiheimo et al., 2001). This potential involvement of Lhcb phosphorylation leads to the hypothesis that STN7, the Lhcb kinase, could be involved in the TRS signaling pathway as a regulatory component. The phenotypic characterization of *Arabidopsis stn7* mutant plants further supported the notion that STN7 might represent the link between short- and long-term regulatory mechanisms (Bonardi et al 2005; Pesaresi et al., 2009). Furthermore, Reactive Oxygen Species (ROS) production is strongly correlated with TRS. Changes in TRS are very dangerous to chloroplasts as alterations in the photosynthetic electron transport chain perturb the balance between Reactive Oxygen

Species (ROS) production and scavenging, leading to a transient ROS accumulation (Eltner, 1991). ROS represent byproducts of photosynthesis, with singlet oxygen ($^1\text{O}_2$) being produced at PSII and superoxide anions ($\text{O}_2^{\bullet-}$) being formed at PSI as a consequence of the over-reduction of electron carriers. $\text{O}_2^{\bullet-}$ is further processed to H_2O_2 which is less reactive and therefore less dangerous to the chloroplast (Mullineaux and Karpinski, 2002; Apel and Hirt, 2004). ROS production leads to changes in NGE in order to improve the scavenging if needed. However, even though all ROS species cause similar damages, different ROS activate different signaling pathways (Foyer and Noctor, 2005). H_2O_2 is able to act as a signaling molecule itself with specific aquaporins allowing H_2O_2 to reach the cytosol under physiological conditions and to activate a broad array of stress responses (Bienert et al., 2007; Mubarakshina et al., 2010). Moreover, TRS also acts in a complex signaling network by regulating proteins via post-translational modifications. Besides protein phosphorylation, the TRS affects the disruption and/or formation of disulphide bridges between cysteine residues (Buchanan, 1980). Several protein elements involved in protein synthesis have been found to be regulated by TRS via thioredoxin proteins, a family of small proteins sensitive to the redox state of the stroma and able to transfer the redox state by becoming a reducing component. Indeed, the diverse group of thioredoxin targets comprises several plastid ribosomal proteins (i.e. PRPS1, PRPS5, PRPS30, PRPL4 and PRPL21), elongation factors, RNA-binding proteins and transcription factors (Balmer et al., 2003; Balmer et al., 2004; Stroher and Dietz, 2008; Tillich et al., 2009; Stern et al., 2010). On the other hand, mutant plants affected in chloroplast protein synthesis, like plastid ribosomal mutants or leaky *prors1* mutants, also show an altered TRS. In these mutants the electron pressure on thylakoids is higher than the impaired photosystems can handle, causing an over-reduction of the plastoquinone pool and therewith affecting the general thylakoid redox state, clearly indicating that any perturbation in

chloroplasts implies an altered over-reduction of the thylakoid electron transport chain itself and ROS generation (Pesaresi et al., 2006). These alterations lead then to retrograde signaling.

1.5 GUN1, a possible integrator of different signaling pathways

All retrograde signals described above, have been hypothesized to converge into a single retrograde signaling pathway to the nucleus, in which GUN1 has a major regulatory function (Koussevitzky et al., 2007). GUN1 has been proposed to be the integrator of several signals originating from inside the chloroplast (see the model in Figure 1.3), since the *gun1* mutation, identified in the same screen as the other *gun* mutants (Susek et al., 1993), is able to maintain NGE under a wide range of conditions and genetic backgrounds. This includes norfluorazon and lincomycin treatment and mutations where either protein import (*ppi2* mutant) or plastid transcription (*sig2* mutant) are affected (Koussevitzky et al., 2007; Kakizaki et al., 2009; Woodson et al., 2013). GUN1 is a plastid-located pentatricopeptide-repeat (PPR) protein that belongs to a subfamily of proteins with nucleic acids binding activity. Proteomic studies and localization assays, using GUN1-GFP protein fusions indicate that GUN1 is a component of the plastid Transcriptionally Active Chromosomes (pTACs), i.e. mega-dalton protein complexes required for gene expression and protein synthesis (Koussevitzky et al., 2007; Olinares et al., 2010). The role of GUN1 as a retrograde-signal integrator inside the chloroplast might be linked to a recently described protein, reported to be physically able to transfer signals from the chloroplast to the nucleus. This protein named PTM (for PHD type transcription factor with transmembrane domains) is a nuclear encoded protein attached to the outer plastid envelope and able to act as an abscisic acid (ABA) receptor (Figure 1.3). PTM can migrate to the nucleus and bind the promoter region of the *ABA INSENSITIVE 4 (ABI4)* transcription factor to activate its expression, thereby acting as an epigenetic regulator (Sun et al., 2011). ABI4 is

sensitive to most of the potential plastid-to-nucleus signals and was therefore proposed to be the main cytosolic signaling component of the GUN1-dependent signaling pathway. To be more precise, ABI4 acts as a negative regulator of *Lhcb* expression by binding its G-box promoter region (Koussevitzky et al., 2007). On the nuclear side, can be observed the activity of a second transcription factor, GOLDEN LIKE 1 (GLK1). GLK1 appears to play a role in the retrograde signal deriving from an altered plastid import (Kakizaki et al., 2009). Unlike ABI4, GLK1 acts as a positive regulator of *Lhcb* expression, that can be regulated by plastid signals, both at the post-translational and transcriptional level (Waters et al., 2008; Waters et al., 2009).

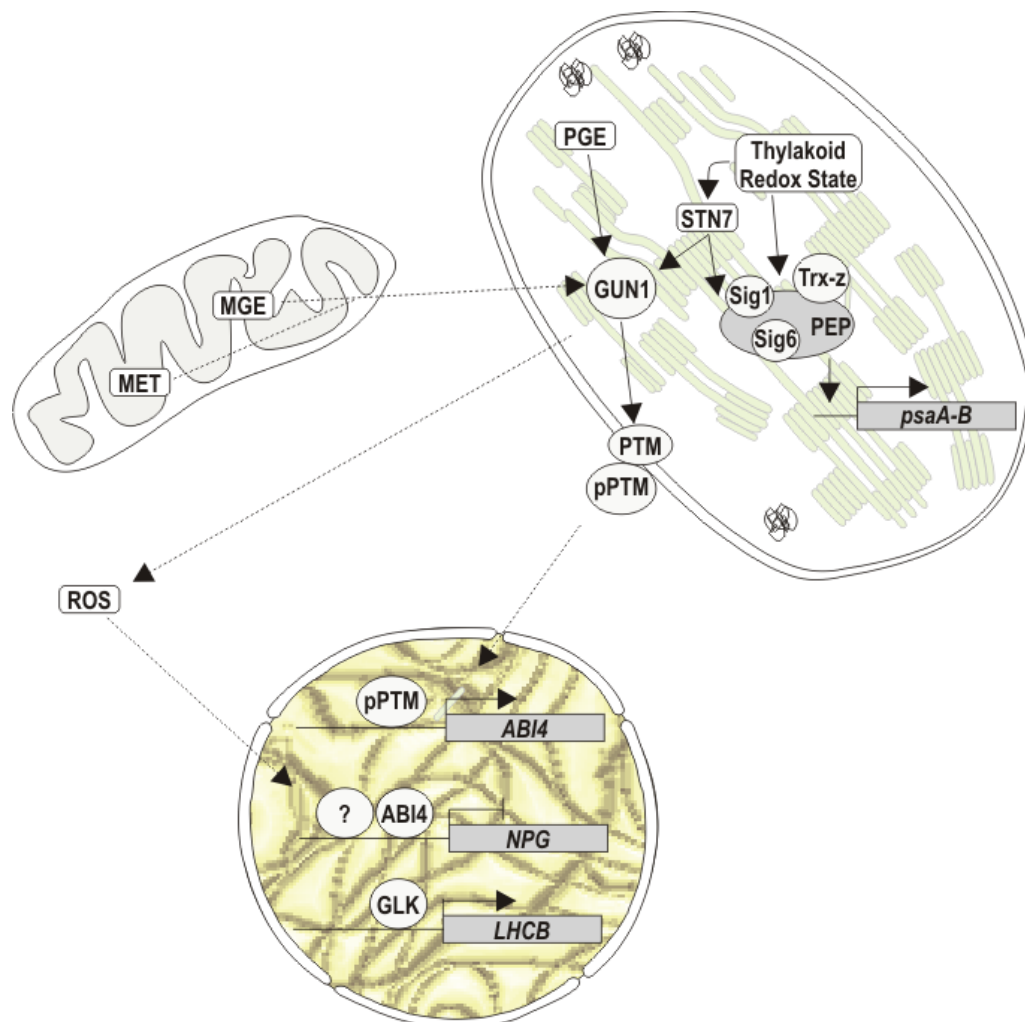


Figure 1.3 Schematic overview of the different pathways involved in retrograde signaling. The model proposes that GUN1 may act as the major integrator of retrograde

signals originating from both chloroplasts and mitochondria. Subsequently, the signal is transduced to the nucleus via the processed form of the PTM transcription factor (pPTM), where it activates the transcription of the *ABI4* gene and possibly modulates the activity of the GLK transcription factor. On the other hand, Reactive Oxygen Species (ROS) are supposed to be able to reach the nucleus directly, and are responsible to repress the expression of photosynthesis-related genes in combination with *ABI4*.

1.6 GUN1 protein complex: a possible link between OGE and tetrapyrrole biosynthesis

Plastid Transcriptionally Active Chromosomes (pTACs) are soluble megadalton complexes containing DNA, RNA and proteins. The composition of the pTAC complexes was investigated by MS-analyses, resulting in the identification of many factors involved in OGE like ribosomal proteins (PRPs), the PEP-core enzyme and proteins involved in transcription, translation and RNA metabolism (Olinares et al., 2010). Helical repeat proteins, like octatricopeptide, pentatricopeptide or tricopeptide-repeat (OPRs, PPRs, TPRs) proteins, are particularly abundant in pTAC complexes, which is in agreement with their primary role in modulating gene transcription and RNA editing, maturation or stability. The PPR proteins, which GUN1 belongs to, are defined by a characteristic 35 amino-acid sequence, repeated up to 30 times (Small and Peeters, 2000). Although GUN1 has been shown to be a constituent of the pTACs, nothing is known about its interaction partners and the molecular details of its function as an integrator of plastid retrograde signals. RH50 is another subunit of pTACs identified as well via MS analyses, *RH50* encodes a plastid-located RNA-helicase belonging to the DEAD-helicase family (Olinares et al., 2010). DEAD box helicases owe their name to the characteristic amino-acid sequence Asp-Glu-Ala-Asp (DEAD) as a part of the Walker B motif (Cordin et al., 2006). RNA helicases are proteins involved in the synthesis, maturation, cleavage and degradation of RNAs, translation initiation and ribosome assembly by remodeling RNA and displacing RNA-protein complexes. Mutants of RNA helicases often show dramatic phenotypes associated with an altered RNA metabolism

(Banroques et al., 2011; Linder and Jankowsky, 2011). Taken together, these data suggest that GUN1 might act in a complex composed of nucleic acids, other RNA/DNA binding proteins involved in gene expression, and components of the transcriptional/translational machinery.

1.7 Aims of the work

Beside the uncertainty on the identity of messenger molecules, little is known about the extent to which different signals can be integrated into common pathways of organellar-to-nucleus signaling. Attempts to distinguish between different retrograde signaling pathways have been hampered by difficulties in discriminating between primary and secondary effects caused by chemical inhibitors, and a lack of genetic mutants that influence organelle function in a specific, well-defined manner (Leister, 2012; Barajas-Lopez Jde et al., 2013). Indeed, most of the *gun* mutants have a defect in chlorophyll accumulation, as shown by the pale-green-yellow colored leaves of *gun2*, *gun3*, *gun4* and *gun5*, leading to a decrease in light absorption and, as a consequence, a more oxidized thylakoid electron transport chain in comparison to WT plants. That may explain, at least in parts, the capability of these mutants to partially prevent the repression of nuclear photosynthesis-related genes under stress conditions. On the other hand, the excessively reduced state of the thylakoid electron transport chain observed in the *prors1-1* mutant, supports the notion that many alterations in plant cell metabolism directly or indirectly impinge on the redox state of photosynthetic electron transport components, making the photosynthetic apparatus a major sensor of physiological imbalances (Pfannschmidt and Yang, 2012). Therefore, changes in thylakoid excitation pressure may be associated with major modifications in gene expression at the organellar and nuclear level. Certainly, the WT-like phenotype of *gun1* and *gun6* mutants indicate that other factors, beside the amount of light absorbed and the redox state of thylakoid membranes and chloroplast stroma, play a role in retrograde signaling.

Here, we have specifically addressed the role of light and GUN1 in retrograde signaling by:

- introducing the *chaos* mutation into *prors1-1* plants. The mutation in the *CAO* gene reduces the size of the PSII antenna, thus mimicking a major adaptive mechanism that plants have evolved to protect themselves against the damaging effects of excess light energy (Oelze et al., 2008). Down-regulation of the *CAO* gene, which codes for the cpSRP43 subunit involved in the insertion of Lhcb proteins into the thylakoids (Klimyuk et al., 1999), has actually been implicated in the system that remodels the photosynthetic machinery to safeguard against photo-oxidative stress (Klenell et al., 2005).
- introducing the *gun1* mutation into various of *Arabidopsis* mutants affected at different levels and in different steps of plastid gene expression, such as reduced levels of mitochondrial and plastidial aminoacyl-tRNA synthetase (*prors1-1*), lack of plastid ribosomal proteins (*prp* mutants) and of enzymes involved in transcript processing (RNA helicase *rh50*)

The objective was to increase our knowledge on the factors that trigger the retrograde signal(s) and on the plastid-located molecular mechanisms that initiate its/their transduction to the nucleus.

2. Material and Methods

2.1 Database analysis and software tools

Gene models, mRNAs and EST sequences have been obtained from the NCBI and TAIR databases (www.ncbi.nlm.nih.gov, www.arabidopsis.org), nucleic acid sequence analysis was performed using the Gene Runner (www.generunner.net) and BioEdit Sequence Alignment Editor (www.mbio.ncsu.edu/bioedit/bioedit.html) software. Sub-cellular localizations and chloroplast transit peptides were predicted by consulting the TargetP database (www.cbs.dtu.dk/services/TargetP). ImageJ software (rsbweb.nih.gov) was used for growth measurements.

2.2 Chemical material

Standard chemicals were purchased from Roth (Karlsruhe, Germany), Duchefa (Haarlem, Netherlands), Applichem (Darmstadt, Germany), Serva (Heidelberg, Germany), Invitrogen (Darmstadt, Germany) and Sigma-Aldrich (Steinheim, Germany).

2.3 Plant material and growth conditions

Arabidopsis thaliana T-DNA and transposon insertion mutant lines were isolated from different collections shown in Table 2.1. All T-DNA and transposon lines were identified via the SIGNAL database (signal.salk.edu/cgi-bin/tdnaexpress), insertion flanking regions were then confirmed by PCR and sequenced (primer sequences listed in table 2.2). *Arabidopsis thaliana* WT and mutant seeds (ecotype Col-0 and Ler) were incubated in the dark on wet Whatman paper for two days at 4 °C, then transferred to soil under controlled climate chamber conditions (PFD: 80 $\mu\text{mol m}^{-2}\text{s}^{-1}$ 16h/8h dark/light). High-light treatment was performed with a light intensity of 400 $\mu\text{mol m}^{-2}\text{s}^{-1}$. Plants under low-light conditions were grown with 25 $\mu\text{mol m}^{-2}\text{s}^{-1}$ light at a 16h/8h dark/light cycle. For phenotypic analyses and NF treatment, plants were grown for 14 days on

Murashige and Skoog (MS) medium (Duchefa) with or without 1% (w/v) sucrose at $80 \mu\text{mol m}^{-1}\text{s}^{-1}$ at 16h/8h dark/light cycle.

Table 2.1 List of the mutant alleles employed in this work. Additionally, the primer combinations used for genotyping are shown.

Allele	Type of mutant	Reference	Gene primers	T-DNA primers
<i>gun1-1</i>	Point mutation	Koussevitzky et al., 2007	Lap45 + Lap56	X
<i>gun1-9</i>	Point mutation	Koussevitzky et al., 2007	Lap17 + Lap18	X
<i>gun1-101</i>	T-DNA insertion	Ruckle et al., 2007	Lap17 + Lap18	Lap17 + LB3
<i>gun1-102</i>	T-DNA insertion	Unpublished allele	Lap17 + Lap18	Lap17 + LB3
<i>gun2</i>	Point mutation	Susek et al., 1993	Lap11 + Lap60	X
<i>gun3</i>	Point mutation line	Susek et al., 1993	Gun3 S + Gun3 AS	X
<i>gun4</i>	Point mutation line	Larkin et al., 2004	Lap14 + Lap59	X
<i>gun5</i>	Point mutation line	Mochizuki et al., 2001	Gun5 S + Gun5 AS	X
<i>rh50-1</i>	T-DNA line	Unpublished allele	Lap70 + Lap76	Lap76 + LBGK1
<i>rh50-2</i>	T-DNA line	this work	Lap70 + Lap76	Lap70 + dSpm32
<i>prps1</i>	T-DNA line	Romani et al., 2012	Lap166 + Lap188	Lap188 + LB3
<i>prps17</i>	T-DNA line	Romani et al., 2012	Lap141 + Lap142	Lap142 + Ds5.4
<i>prps21</i>	T-DNA line	this work	Lap36 + Lap37	Lap37 + LB3
<i>prpl11</i>	T-DNA line	Pesaresi et al., 2001	Lap21 + Lap22	Lap21 + LBGK1
<i>prpl24</i>	T-DNA line	Romani et al., 2012	Lap5 + Lap6	Lap5 + LBB1.3
<i>prors1-1</i>	T-DNA line	Pesaresi et al., 2006	Lap25 + Lap26	Lap25 + LBGK1
<i>chaos</i>	Transposon	Unpublished allele	Cao S + Cao AS	Cao AS + EnR

Table 2.2 Sequences of the primers used for the genotyping analyses.

Primer name	Sequence (5' to 3')	Primer name	Sequence (5' to 3')
Lap 45	GCTCATCTTTCACAGACTACTC	Lap 22	GGGTCTTGAGAATAAACGTG
Lap 56	GCTCAATCCTTCTATTCGTC	Lap 5	GGACAGTAGTATAGCTGAAG
Lap 17	GAGAGTAACAACCGAACGAC	Lap 6	GCCACTTTACTCAATGTGAG
Lap 18	AAAGTGCCAAAGCATGTCAG	Lap 25	AACCAAGCATGAGTTTCTCG
Lap 11	AACCATGGCGTATTTAGCTC	Lap 26	ATCCGGAAGAGGTCTGTTC
Lap 60	GAACCTTGAACCTTAGTAACAGC	Gun3 S	CGTATAAGGAATTCGCAGAG
Lap 14	CTGGCTTTGTTTCATACATCC	Gun3 AS	CATGCCTGATAGTACTCTAG
Lap 59	ACAAACGCCTCCGCCACAAC	Gun5 S	AAGGACAGGTGGTGGATGTG
Lap 70	TGTTTCGTAACGGCGGAGGAG	Gun5 AS	GTATCAGCAATTGGTCTCAC
Lap 76	CAAAACGCCTATCTTCTCTAC	Cao S	ATGCAAAAGGTCTTCTTGGC
Lap 166	ACCCAACGATAAAACGCAGG	Cao AS	CCTCTCTCGTCTTCCACTTC
Lap 188	TCTAACGTCACGCTGTTTAG	LB3	CTGAATTCATAACCAATCTCGATACAC
Lap 141	CATCGATTGATTCCAAATC	LBB1.3	TTTTGCCGATTTCGGAAC
Lap 142	CCATAAATTACACTGGTTCC	LBGK1	CCCATTGACGTGAATGTAGACAC
Lap 36	TCAATGATAGCTTGTGATGG	dSpm32	CGAATAAGAGCGTCCATTTTAG
Lap 37	TTTCCAACCTCACAATGTACC	Ds5.4	TACGATAACGGTCGGTACGG
Lap 21	CTTCTCTACATCCCAACTCC	EnR	GAGCGTCGGTCCCCACACTTCTATAC

2.4 Chlorophyll fluorescence, pigment analysis and oxygen evolution measurements

Chl *a* fluorescence was measured *in-vivo* with the non-invasive Dual-PAM 100 (Walz, www.walz.com/) as described by Pesaresi et al. (2009). After 20 minutes of dark adaption the minimal fluorescence (F_0) was measured. With a pulse (0.8 sec) of saturating white light ($5,000 \mu\text{mol photon m}^{-2} \text{s}^{-1}$) the maximum fluorescence (F_m) was determined. The ratio $(F_m - F_0) / F_m$ was calculated as F_v / F_m , the maximum quantum yield of PSII. After 10 minutes of actinic red light ($80 \mu\text{mol photon m}^{-2} \text{s}^{-1}$), the steady state fluorescence (F_s) was measured and with a second saturation pulse the F_m' was determined. The PSII effective quantum yield (Φ_{II}) was calculated

as the ratio $(F_v - F_s)/F_m'$. Leaf pigment content was analyzed by reverse-phase HPLC according to (Farber et al., 1997).

Oxygen evolution rates were measured on leaf discs (diameter approx. 6 mm) isolated from 28 days old plants. The discs were dark-adapted for 30 min in a buffer containing 1 mM NaHCO₃ (pH 9) to provide a CO₂-saturated atmosphere (Chow et al., 1989). A Clark-type O₂ electrode (Oxygraph, Hansatech, www.hansatech-instruments.com) provided with an electrode conditioning unit was used for measurements. At the end of the dark adaption period, no O₂ was detectable in the chamber. Then, the chamber was illuminated with white light, at a flux rate of approximately 80 $\mu\text{mol photon m}^{-2} \text{ sec}^{-1}$, and oxygen production was measured for 30 minutes.

2.5 Nucleic acids isolation

Genomic DNA was isolated from *A. thaliana* leaves or cotyledons. Nucleic acids were extracted with a DNA extraction buffer (200 mM Tris-HCl pH 7.5, 250 mM NaCl, 25 mM EDTA and 0.5% (w/v) SDS) and precipitated with 0,8 volumes of isopropanol at 16,000 g for 20 minutes. The pellet was then washed in 70% ethanol and resuspended in 200 μl of ddH₂O. No RNase treatment step was needed for PCR analysis. For expression analyses the leaf material of 28 days old plants was harvested after 8 hours of light-adaption and ground in liquid nitrogen. The total RNA was extracted from ground tissue using one volume of extraction buffer (300 mM NaCl, 50 mM TRIS-HCl pH 7.5, 20 mM EDTA, 0.5% SDS) and one volume of Phenol-Chloroform-Isoamylalcohol (PCI) followed by solubilization at 65°C for 5 minutes. After a centrifugation step (10 minutes at 7,000 g), the supernatant was mixed with one volume of 8 M LiCl, incubated for two hours at -20°C and centrifuged for 30 minutes at 4°C at 7,000 g. The pellet was then washed with 75% ethanol and resuspended in 80 μl of DEPC-treated water.

2.6 First strand cDNA synthesis

For cDNA synthesis the iScript reverse transcriptase kit (Bio-Rad, www.biorad.com) was employed. In a total volume of 5 μ l, 1 μ g of RNA, 0.5 μ l of 10x PCR buffer (Quiagen, www.qiagen.com) + $MgCl_2$ and 0.5 units DNase were combined. This mix was incubated at room temperature for 30 minutes. Then 2.5 mM EDTA were added and the mix was incubated for 15 minutes at 65°C. To each sample 2 μ l of 5x iScript reaction mix buffer and 0.5 μ l of iScript reverse transcriptase were added. The samples were topped up to 10 μ l with DEPC H_2O . The first-strand cDNA synthesis was performed according to the following protocol by using a thermocycler (BioRad): 5 minutes at 25 °C, 40 minutes at 42°C and 5 minutes at 85 °C.

2.7 Northern blot analyses

Northern blot analyses were performed according to Sambrook and Russel (2001) loading 15 μ g of total RNA. To 15 μ l of RNA 15 μ l of formamide, 4 μ l of formaldehyde and 3 μ l of 10x MEN (0.2 M MOPS, 50 mM Na acetate, 10 mM EDTA; pH 7.0) buffer were added. The samples were incubated at 65°C for 15 minutes and afterwards put on ice for 5 minutes. Then 8 μ l of 6x loading dye were added, the samples were loaded on an agarose gel (2% agarose, 6% formaldehyde, 1x MEN buffer) and then ran at 40 V for 3 hours. The blotting sandwich was built up as follows. A glass basin was filled with 20x SSC (2 M NaCl, 0.2 M Na-citrate; pH 7.0) buffer and on top of this basin a glass plate was positioned that did not cover the whole basin. On top of this plate a paper bridge was assembled, consisting of 2 pieces of 3 MM whatman paper of the same size that were wetted in 10x SSC buffer and reached into the 10x SSC buffer in the basin. On top of the bridge 2 pieces of 3 MM whatman paper were added that had the same size as the gel and were also wetted with 10x SSC buffer. Next, the gel was put upside down on the paper, followed by the positively charged

nylon membrane upfront pre-incubated in 2x SSC buffer. On top of the membrane 2 further sheets of whatman paper were added, also pre-wetted in 2x SSC buffer and about 10 cm of paper towels and a weight to drive the flux of the blotting buffer via capillary force. The blotting assembly was allowed to run over night for approximately 16 hours and the membrane was afterwards UV-crosslinked. For the pre-hybridization-step the hybridization buffer was preheated to 60°C. 20 ml of hybridization buffer and 160 µl of previously denaturated (100 °C, 5 minutes) herring sperm DNA (10 ng/µl) were added. The tube was incubated in a rotating oven at 65 °C overnight. For probe preparation approximately 100 ng of PCR-product were filled up to 12 µl with ddH₂O, denaturated at 100°C for 5 minutes and cooled down on ice for 5 minutes. Afterwards, 4 µl of 1x NEBuffer 2, 1 µl of Klenow DNA polymerase, 33 µM dNTPs (without CTP) and 3 µl of radioactive ³²P-dCTP were added to the probe followed by incubation over night at room temperature. For probe purification illustra MicroSpin™ G-25 Columns were used according to the producer's instructions. For the washing step the washing buffer (0.1% SDS, 0.2 M NaCl, 20 mM NaH₂PO₄, 5 mM EDTA; pH7.4) was pre-warmed in a water bath to 60 °C. The probe was discarded and 10 ml of washing buffer were added and further incubated at 65 °C. The washing buffer was kept at 65 °C. After 30 minutes the washing buffer was exchanged and the tubes were put back to 65°C for 15 minutes. The washing buffer was discarded and the membrane was washed again at room temperature in 6 mM NaH₂PO₄, 1 mM EDTA, 0.2% SDS; pH 7.0 for one hour on a shaker. The membrane was then exposed to a radioactive sensitive screen overnight. Primers used to amplify the probes are listed in Table 2.3. The probe used for the 23S-4.5S intergenic region was synthesized using a 73 bp primer complementary to the region (5´-GAGCACAGCCGAGACAGCAACGGGTTCTCCGCCCTGCGGGGATGGAGTGACAGAAGTTTTGAGAATTCAAGA -3´) labeled at the 5´ end with ³²P-γATP with the T4 PNK (NEB, www.neb.com/). The 5´ labeling reaction of the probe

was carried out for 30 minutes at 37°C in a total volume of 50 µl using 50 pmol of primer, 5 µl of 10x PNK buffer, 2 µl of PNK enzyme and 3 µl of 3^{32}P -γATP. Signals were acquired and quantified with a phosphoimager and IMAGEQUANT (Typhoon, GE Healthcare, www3.gehealthcare.com). For quantitative real-time PCR (qRT-PCR) 4 µg of total RNA were treated with DNase I (Roche Applied Science, www.roche-applied-science.com) before usage for the iScript first-strand cDNA synthesis according to the supplier's manual (Bio-Rad, www.bio-rad.com).

Table 2.3 Sequences of the primers employed for northern blot radiolabeled probes.

Genes	Sense primer (5' to 3')	Antisense primer (5' to 3')
<i>16S rRNA</i>	AGTCATCATGCCCCCTTATGC	CAGTCACTAGCCCTGCCTTC
<i>23S rRNA</i>	GTTCGAGTACCAGGCGCTAC	CGGAGACCTGTGTTTTTGGT
<i>2CPA</i>	ATGGCGTCTGTTGCTTCTTC	TGCAAGGTGAGAGAACACAC
<i>4,5S rRNA</i>	GAAGGTCACGGCGAGACGAGCC	GTTCAAGTCTACCGGTCTGTTAGG
<i>5S rRNA</i>	TATTCTGGTGTCTAGGCGTAG	ATCCTGGCGTCGAGCTATTTTTCC
<i>AOX1</i>	GGTTCTGAATGGAAGTGAAC	GGAGCTGGAGCTTCCTTTAGT
<i>CAT1</i>	CTTCTTTGACTGTGCGAACTC	CCAGTATCCTCCAGTTCTCC
<i>Ferritin1</i>	ATGGCCTCAAACGCACTCTC	ATGCCCTCTCTCTTCCTCAC
<i>Lhca1</i>	GTCAAGCCACTTACTTGGGA	GGGATAACAATATCGCCAATG
<i>Lhca2</i>	GAGTTCCTAACGAAGATCGG	AAGATTGTGGCGTGACCAGG
<i>Lhca3</i>	AGGCTGGTCTGATTCCAGCA	ACTTGAGGCTGGTCAAGACG
<i>Lhca4</i>	TGAGTGGTACGATGCTGGGA	GTGTTGTGCCATGGGTCAGA
<i>Lhcb1.2</i>	GACTTTCAGCTGATCCCGAG	CGGTCCCTTACCAGTGACAA
<i>Lhcb2</i>	GAGACATTCGCTAAGAACCG	CCAGTAACAATGGCTTGGAC
<i>Lhcb4</i>	AGCTAGTGGATGGATCATCT	CAGGAGGAAGAGAAGGTATC
<i>Lhcb5</i>	CTGGTGCTTTGCTTCTTGATG	TCCAGCGATGACGGTAAGCA
<i>Lhcb6</i>	GCATGGTTTGAAGCTGGAGC	ACAAACCAAGAGCACCGAGA
<i>PRPL2</i>	GAGGAATAATTACCGCAAGG	CTCTACCCAAACTTTTCTGG
<i>PRPS3</i>	AGACTTGGTACAACCCAAAG	TGTAAAGGAACTCTGCCTTC
<i>PRPS8</i>	ATGGGGAAAGACACCATTGC	TCCGCCGATTCTTTTTAGTC
<i>psaB</i>	GTATTGCTACCGCACATGAC	CCACGAAACTCTTGGTTTCC
<i>PsaD1</i>	AAGCCGCCGGGATCTTCAAC	CTAAGCCTTGTCCCCAAAGC
<i>PsaE1</i>	ATGGCGATGACGACAGCATC	TGTTGGTCGATATGTTGGCG
<i>PsaF</i>	GTTCGACAACTACGGGAAGT	CTTAGCAATGAGATCACCAT
<i>PsaK</i>	ATGGTCTTCG AGCCACCAAA	CGTTCAGGTGCATGAGAATA
<i>PsaO</i>	ATGGCAGCAACATTTGCAAC	GTAATCTTCAGTCCTGCCCT
<i>psbA</i>	CGGCCAAAATAACCGTGAGC	TATACAACGGCGGTCTTATG
<i>PsbO2</i>	AGACGGAAGCGTGAAGTTCA	CAATCTGACCGTACCAAACC
<i>PsbQ</i>	ACAGATAACTCAGACCAAGC	GCTTGGCAAGAACATTGTTC
<i>PsbT2</i>	ATGGCGTCAATGACCATGAC	CAGTTACGGCATATCTTGGC
<i>PsbX</i>	ATGGCTTCTACCTCCGCGAT	TAGGTTCTCTTGACAGGGTC
<i>PsbY</i>	ATGGCAGCAGCTATGGCAAC	CTCCGGAGGTGGAGTCAAAA
<i>RbcL</i>	CGTTGGAGAGACCGTTTCTT	CAAAGCCCAAAGTTGACTCC
<i>RbcS</i>	ATGGCTTCCTCTATGTTCTC	CGGTGCATCCGAACAATGGA

2.8 Standard PCR and High fidelity PCR

For genotyping of plant material 1 µl of DNA was used as a template for PCR analysis. For this purpose the PCR was performed in a total volume of 20 µl containing 2 µl of 10x PCR-buffer (QIAGEN), 100 µM dNTPs, 200 µM primers (Table 2.2), 0.5 units of Taq polymerase. The PCR product was then loaded on a 1%-agarose gel. The genes of interest were amplified from Col-0 cDNA with the Phusion High-Fidelity DNA Polymerase (Finnzymes). Reactions were performed in a total volume of 20 µl each. The reaction contained 200 µM of each primer, 250 µM dNTPs, 4µl of 5x Phusion HF reaction buffer and 0.4 units Phusion HF DNA Polymerase. The PCR-products were loaded on a 1% agarose TAE (150 mM Tris-HCl, 1.74 M Acetic acid, 1 mM EDTA) gel and then cut from the gel and purified via the QIAGEN gel extraction kit following the producer's instructions. Plasmids for yeast cell transformation and plant transformation were obtained with different methods and strategies. PCR fragments amplified with Phusion High-Fidelity DNA Polymerase (Finnzymes, according to the manual) were purified from a 1% agarose TAE gel and purified with QIAGEN gel extraction kit following producer's instructions.

2.9 Fluorescent protein localization

The cloning procedure in binary vectors for protein expression of GUN1-GFP and RH50-YFP in plants was carried out using the GATEWAY™ reaction strategy. The coding sequences of GUN1 and RH50 were amplified using cDNA as template, primers are listed in Table 2.5. First an entry clone (pDonor207, Invitrogen) was produced using BP ClonaseII enzyme mix reaction (see the Invitrogen GATEWAY™ instruction manual). After purification of the donor vector from *E. coli* (QIAprep Spin Miniprep Kit, following producer's instructions) the LR reaction (LR Clonase II enzyme mix, Invitrogen) was used to clone the gene of interest in the GFP (pB7FWG2) and YFP (pB7YWG2) destination vectors.

Stable plant transgenic mutant lines, expressing chimeric protein with GUN1-GFP and RH50-YFP fused to the C-terminal end of coding sequence of interest, were used for protoplast isolation.

Four weeks old leaf material was cut with a razorblade and digested with 2.5 mg/ml macerozyme and 2.5 mg/ml cellulase in an isoosmotic buffer (2-(N-morpholino)ethanesulfonic acid 10 mM, 20 mM CaCl_2 , 500 mM mannitol, 550 mOsm; pH 5.8) for four hours at room temperature. Afterwards the released protoplasts were centrifuged at 50 g for 10 minutes and the pellet was resuspended in 100 μl of the isolation buffer described before. Pictures were acquired with the AxioCam MRc5 (Zeiss) equipped with filters for chlorophyll, GFP and YFP supported by the Axiovision program V 4.1.

2.10 Yeast two-hybrid assay

For yeast two hybrid analyses, the classic restriction enzymes cloning strategy was chosen. The PCR products (primers listed in Table 2.4) were digested with one or two enzymes for 60 min at 37°C, for the cutting procedure EcoRI and BamHI were used in a single or double digest in NEB buffer 4. GUN1, PRPL11, HEMA, GSA2, HEMC and HEME1 were cloned using EcoRI and BamHI, PRPL24 and CHL11 using EcoRI and RH50, GSA1, HEME2, HEMF1, PPOX, CHL12 and CHLD performing a BamHI single digest. The set of vectors used for the assays was pGadt7 as AD-Vector and pGbkt7 as BD-Vector (Clontech), to cut them a restriction reaction was incubated for 2 hours at 37°C and for 15 minutes at 65°C to inactivate the enzyme. To avoid self-ligation of the plasmids, Calf Intestine Phosphatase (NEB) was added to the reaction and incubated at 37°C for 30 min. The sample was then purified with the QIAquick PCR Purification Kit. The ligation step was performed at 4°C for 24 hours using a T4 DNA ligase (NEB).

The yeast strain PJ69-4a was inoculated in YPD liquid medium (10 g/l yeast extract, 20 g/l peptone, 20 g/l glucose) over night at 30°C. After the OD₆₀₀ reached approximately 0.6, the cells were spun down in the centrifuge for 10 minutes at 2,300 g. After centrifugation, the supernatant was removed and the cells were washed with 1.000 µl sterile ddH₂O. The cells were centrifuged again for 10 minutes at 2,300 g, the supernatant removed and the pellet washed in 500 µl LiTe buffer. The centrifugation-step was repeated and the pellet was resuspended in 500 µl LiTe buffer (10 mM Tris-HCl pH 7.5, 1 mM EDTA pH 8, 100 mM LiAc). For each transformation 50 µl of the washed yeast cells, 1 µg of each construct, 7 µl Carrier-DNA (DNA from fish sperm 2 mg/ml), 7 µl dimethylsulfoxid (DMSO) and 300 µl LiTePEG (10 mM Tris-HCl pH 7.5, 1 mM EDTA pH 8, 100 mM LiAc, 40% PEG) were combined. These preparations were incubated for 30 minutes at 28°C and for 14 minutes at 42 °C. Afterwards the cells were centrifuged down for 10 minutes at 2.300 g, resuspended in 100 µl of sterile ddH₂O and plated on SC-Drop-out (-W-L) plates. The plates were incubated at 30 °C. Of each positive plate a few colonies were streaked out on SC-Drop-out (-W-L-H) plates. For representative reasons, colonies of the SC-Drop-out (-W-L) plates were inoculated in 10 ml liquid SC-Drop-out (-W-L) medium overnight. The OD₆₀₀ was measured and brought to the same value. The cells were then centrifuged down at 2,300 g for 10 minutes and resuspended in 40 µl sterile H₂O. 20 µl of the cell suspension was then brought as a drop onto SC-Drop-out (-W-L-H) and SC-Drop-out (-W-L-H + 3mM 3AT)-plates. The SC-Drop-out was prepared with 6.67 g/l yeast nitrogen base (w/o amino acids), 20 g/l glucose, 0.83 g/l Synthetic Complete Drop Out Mix (-W-L/ -W-L-H/-W-L-H+3mM 3-Amino-1,2,4-triazole; pH 5.6).

Table 2.4 Primer sequences employed in the Y2H assay. The restriction sites used for the cloning procedure are not displayed.

Genes	Sense primer (5' to 3')	Antisense primer (5' to 3')
<i>GUN1</i>	GCTCATCTTTACAGACTACTC	CACAGAGCCAAACATTGTTAGG
<i>RH50</i>	TGTTTCGTAACGGCGGAGGAG	GGTCAAGATGAAGAGTTACTTAGGTTGTG
<i>PRPL11</i>	GCCATGGCTCCACCTAAACCC	ATAGAAACTACCAACCAGGC
<i>PRPL24</i>	CTTGCAAAGCTCAAGCGTTG	CTAAGATGCGGAGGTAAGTCTG
<i>HEMA</i>	TCTGCTTCTTCTGATTCTGCG	TTACTTCTGTTGTTGTTCCGCC
<i>GSA1</i>	CCGTCGACGAGAAGAAGAAAAG	CTAGATCCTACTCAGTACCCTC
<i>GSA2</i>	GCTTCTTCGTCGTCCAACC	TCCAGAGACATTTTAGAGCCGAC
<i>HEMC</i>	GCTCAAGCATACGAGACGC	CTTCTTCGAATGGCTCAGTTG
<i>HEME1</i>	GCTGCAAAAGGGCAAGCC	TCAGACAACCAATTCAGGTTTCAG
<i>HEME2</i>	GTTCCGTCGAGGGAAGTAC	TTAATATCTAATTTCTTGAGCAACCTC
<i>HEMF1</i>	TCTCAATTGAGAAAGAAGTTCC	CAATGGGAAACACAGGCTAGATC
<i>PPOX</i>	CCACCATCACGACGGATTG	ATTTACTTGTAAGCGTACCGTGACATG
<i>CHLI1</i>	TCGGTTATGAATGTAGCCACTG	TCAGCTGAAAATCTCGGCG
<i>CHLI2</i>	CTGTTATGAATGTCGCTACAGAG	CTAAGTGAAAACCTCATAGAACTTC
<i>CHLD</i>	GTGCCTCCGCGAATGCTAC	GTATTGCAGACAAAATGAGGTCAAG

2.11 Chloroplast isolation and sub-fractionation

Four weeks old light-adapted plants were homogenized in 0.45 M Sorbitol, 20 mM Tricine-KOH pH 8.4, 10 mM EDTA, 10 mM NaHCO₃ and 0.1% BSA. The material was then filtered through a single-layer of Miracloth (Calbiochem), and the filtrate was centrifuged at 4°C and 700 g for 7 minutes. The pellet was resuspended carefully in resuspension buffer (0.3 M Sorbitol, 20 mM Tricine-KOH pH 8.4, 2.5 mM EDTA and 5 mM MgCl₂). The suspension was centrifuged using a two-step Percoll gradient (40%-80% (v/v) in resuspension buffer) at 4°C and 6,500 g for 20 minutes. Intact chloroplasts were collected at the interface of the percoll gradient and washed once with resuspension buffer.

The isolated chloroplasts were then fractionated. To this end, intact chloroplasts were lysed in 30 mM HEPES-KOH pH 8.0, 60 mM KOAc and 10 mM MgOAc by passing the suspension through a 24-gauge syringe 20

times. Then the solution was centrifuged at 4°C and 16,000 g for 20 minutes. The supernatant was collected as stroma fraction. The pellet was washed again with 1 ml of the same buffer, centrifuged again at 4°C and 16,000 g for 20 minutes and collected as thylakoid fraction.

2.12 Protein preparation and immuno-blot analysis

Frozen plant material was homogenized in 2X Laemmli buffer (200 mM Tris-HCl pH 6.8, 4% SDS, 20% glycerol, 5% β -mercaptoethanol), and solubilized for 15 minutes at 65°C. After a centrifugation step (16,000 g, 10 min) the supernatant was boiled 5 minutes to denature the sample. Stroma and thylakoid samples were treated in the same way. The total protein extraction was then loaded on a Tris-glycine 12% SDS-PAGE (Schägger and von Jagow, 1987), afterwards, proteins were transferred to PVDF membranes (Ihnatowicz et al., 2004) and immuno-decorated with antibodies.

2.13 *In vivo* translation assay

The *in vivo* labeling assay was performed basically as described by Pesaresi, 2011. To this end, 6 mm leaf discs were incubated in 1 mM K_2HPO_4 – KH_2PO_4 pH 6.3, and 0.1% (w/v) Tween-20 and 20 μ g/ml cycloheximide to block cytosolic translation. [35 S] methionine was added to the buffer in a final concentration of 0.1 mCi/ml and vacuum-infiltrated into the leaf tissue. The material was then exposed to light (20 μ mol photon $m^{-2} s^{-1}$) and four leaf discs were collected at each time point (5, 15 and 30 min). Total proteins were extracted as described above and fractionated by Tris-glycine SDS-PAGE (12% PA).

2.14 Embryo analysis and TEM analysis

To analyze lethal mutants at the embryo and seedling stage, heterozygous mutant siliques were fixed in an ethanol and acetic acid solution (9:1, v/v) overnight, followed by two washes in 90% and 70% ethanol and clearing

in a chloral hydrate:glycerol:water solution (8:1:2, w/v/v) according to Yadegari, 1994. Siliques were manually dissected and observed with a Zeiss Axiophot D1, equipped with a differential interface contrast optics, focusing on the embryo development. Pictures were acquired with the AxioCam MRc5 (Zeiss) supported by the Axiovision program V 4.1.

Leaf tissue from light-adapted plants was fixed with 2.5% glutaraldehyde in fixation buffer (75 mM sodium cacodylate, pH 7. 0.2 mM MgCl₂) for 1 hour at room temperature. Afterwards leaves were rinsed several times in the same buffer, and post- fixed for 2 hours with 1% osmium tetroxide in fixation buffer at room temperature, as described previously (Aseeva et al., 2007). All micrographs were taken using a Zeiss EM 912 electron microscope.

2.15 Bimolecular fluorescence complementation (BiFC)

Full-length cDNA fragments of the target genes were cloned into the pDONR207 (Invitrogen) using gene specific primers (Table 2.5) and then recombined into the gateway compatible pVYNE and pVYCE plasmids (Gehl et al., 2009) carrying either the N-terminal part or C-terminal part of the Venus protein (YFP derivate), respectively. For BiFC assays (Walter et al., 2004) the constructs were transformed into *Agrobacterium tumefaciens* GV2260. Transient co-expression of tagged putative interaction partners was achieved by transformation of *Nicotiana tabacum* leaves with the infiltration technique. After 2-3 days of dark incubation, leaf discs were analyzed by confocal laser scanning microscopy using a Leica TCS SP2 (Leica, www.leica-microsystems.com), at λ_{ex} 514 nm, λ_{em} 530-555 nm for YFP and 600-700 nm for Chl emission.

Table 2.5 Primer sequences used for BiFC assay, GUN1-GFP and RH50-YFP localization. Tail sequences employed for cloning are not reported.

Genes	Sense primer (5´ to 3´)	Antisense primer (5´ to 3´)
<i>GUN1</i>	TCCTTTCAATGGCGTCAACG	ACAAAAGAAGAGGCTGTAAAGCAAACG
<i>RH50</i>	AGATGTTGGCGAGAGCTCCAC	TTGTGAACTCGTAAGCGTTTGG
<i>HEME2</i>	ATGTCAATCCTTCAAGTCTCTAC	AATATCTAATTTCTTGAGCAACC
<i>HEMC</i>	TCGCTCCTCCACCTGAATCCATG	CGTTGCCGAAGAAGCCAGGAC
<i>CHLD</i>	TTGAAAATGGCGATGACTCC	AAGAATTCTTCAGATCAGATAGTGC

3. Results and Discussions

3.1 Thylakoid redox signals are integrated into OGE-dependent retrograde signaling in the *prors1-1* mutant

3.1.1 The *chaos* mutation is capable of restoring a WT TRS in the *prors1-1* mutant

In order to verify the extent to which signals related to light and photosynthetic electron transport contribute to the OGE-dependent retrograde signaling pathway, the *chaos* mutation was introduced into the *prors1-1* genetic background.

The *prors1-1 chaos* mutant was generated by crossing the two single mutants and the double homozygous plants were isolated within the F2 generation. The scheme of the genes and the insertions present in the mutated alleles is displayed in Figure 3.1.

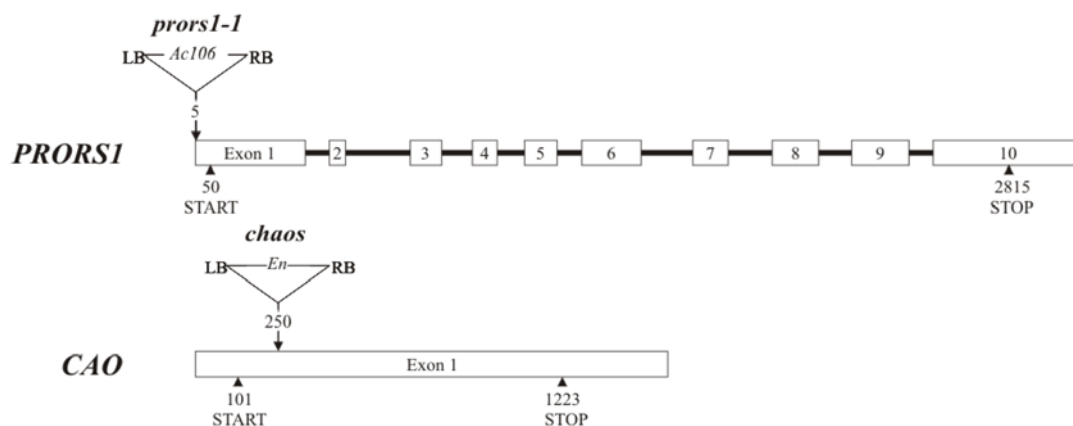


Figure 3.1 Schematic representation of *prors1-1* and *chaos* mutant alleles. Numbered boxes indicate the exons, while black lines represent the introns. Arrowheads indicate the start and stop codons of translation. T-DNA (*Ac106*) and transposon (*En*) insertions, not drawn to scale, are also indicated together with the position of the insertion. LB, left border; RB, right border.

Like the previously described single mutants (Klimyuk et al., 1999; Pesaresi et al., 2006), the *prors1-1 chaos* double mutant showed pale-green cotyledons and true leaves and a diminished growth. In particular, 28 days after germination (d.a.g.), the size of *prors1-1* and *chaos* plants

was about 80% of WT, whereas *prors1-1 chaos* double mutants showed a reduction in size by about 50%. However, the number of leaves during the plant life cycle was comparable between mutant and WT plants (Figure 3.2), indicating that the developmental stage among the genotypes was identical. Chlorophyll a fluorescence measurements were used to analyze the photosynthetic performance of 28 days-old WT and mutant plants.

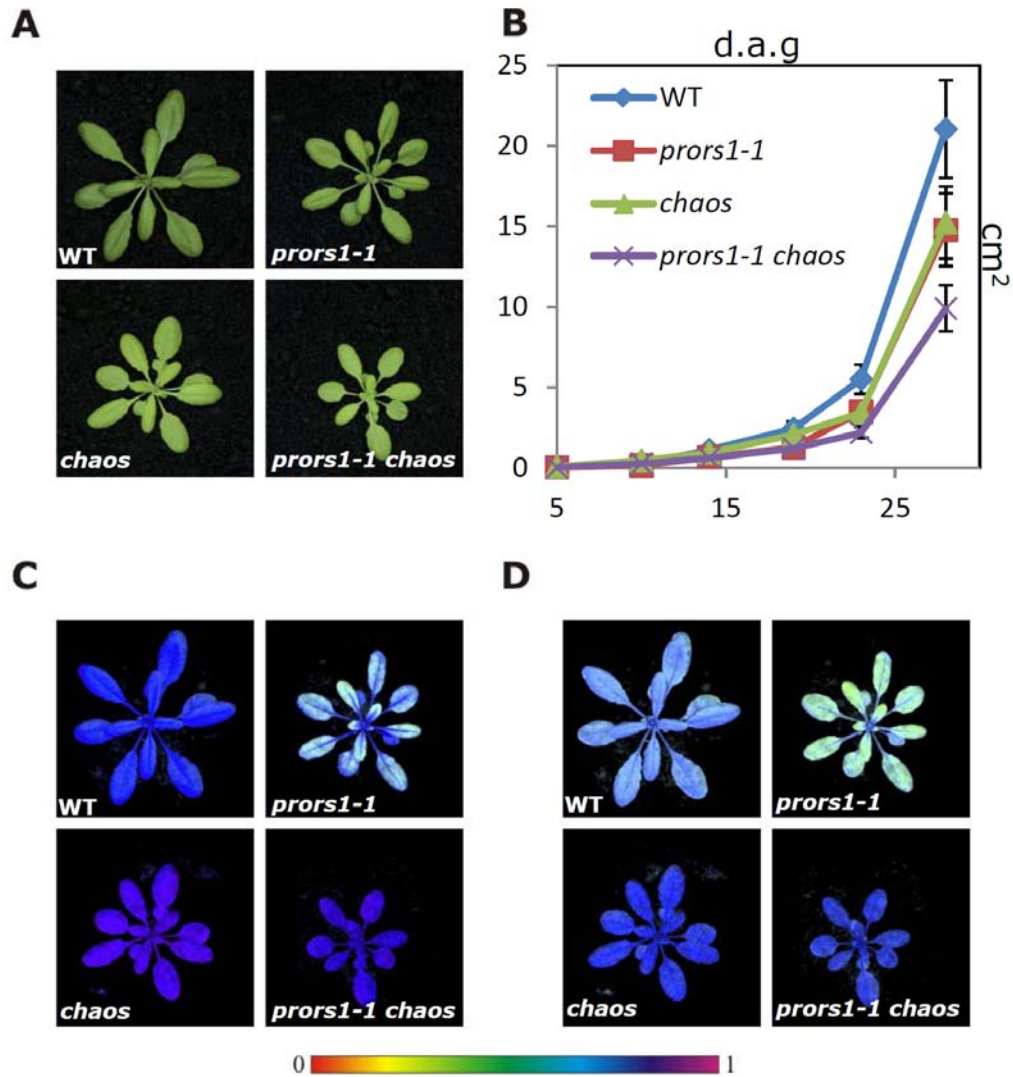


Figure 3.2 Phenotypes of *prors1-1*, *chaos* and *prors1-1 chaos* mutants. Pictures taken at 28 d.a.g. (A). Growth rate of the mutants was measured in cm² (y-axis) at 4, 10, 14, 19, 23 and 28 d.a.g. (x-axis) (B). F_v/F_m (C) and Φ_{II} (D) values of PSII are displayed in heat map colors based on the color scale below where violet color corresponds to 1 and red to 0 (Tadini et al., 2012).

Photosynthetic parameters highlight that *prors1-1* displayed a diminished maximum quantum yield of PSII (F_v/F_m) (Figure 3.2C), whereas *chaos* conversely showed a higher value than the WT. In the double mutant, the *chaos* mutation seemed to restore the F_v/F_m values to a WT level (Figure 3.2C). The effective quantum yield of PSII (Φ_{II}) measured after 10 minutes of actinic light exposure was reduced in *prors1-1* and increased in *chaos* and *prors1-1 chaos* if compared to the WT (Figure 3.2D). Moreover, the 1-qL parameter, used for an indirect estimation of the redox-state of the PQ pool, appeared to be decreased in *chaos* and *prors1-1 chaos* leaves. To further investigate the thylakoid electron transport rate, a Clark-type oxygen electrode was employed to measure the oxygen production of leaves under growth light conditions. The oxygen production in comparison with Col-0 was slightly reduced in *prors1-1* and significantly reduced in *chaos* and *prors1-1 chaos* leaves (Table 3.1).

Table 3.1 Photosynthetic performance and oxygen production of *prors1-1*, *chaos* and *prors1-1 chaos* mutants plants. The measures of photosynthetic parameters (F_v/F_m , Φ_{II} and 1-qP) and O_2 production were conducted at 28 d.a.g., the O_2 production is expressed in $\mu\text{mol } O_2 \text{ m}^{-2} \text{ h}^{-1}$.

	F_v/F_m	Φ_{II}	1-qP	NPQ	O_2 production
Col-0	0.83 ± 0.01	0.76 ± 0.01	0.08 ± 0.01	0.152 ± 0.01	0.03 ± 0.00
<i>prors1-1</i>	0.74 ± 0.02	0.63 ± 0.02	0.10 ± 0.02	0.116 ± 0.01	0.02 ± 0.00
<i>chaos</i>	0.86 ± 0.01	0.81 ± 0.01	0.04 ± 0.02	0.086 ± 0.01	0.01 ± 0.00
<i>prors1-1 chaos</i>	0.84 ± 0.01	0.78 ± 0.01	0.05 ± 0.02	0.077 ± 0.01	0.01 ± 0.00

Pigment analyses performed by HPLC showed that all the mutants have a reduced amount of total chlorophyll (Chl a+b). In detail, *prors1-1* contains 80% of WT chlorophyll, *chaos* 40% and the *prors1-1 chaos* double mutant about 35%. The chlorophyll a to b ratio (Chl a/b) was also altered, lower in *prors1-1* (2.55 ± 0.15 in comparison to 2.71 ± 0.09 in Col-0) and higher in *chaos* and *prors1-1 chaos*, 3.69 ± 0.08 and 3.01 ± 0.09 , respectively. In addition, the carotenoid pool, usually associated with the

PSII antenna [neoxanthin (Nx), lutein (Lut), and the VAZ pool (violaxanthin + antheraxanthin + zeaxanthin)], was markedly reduced in *chaos* and *prors1-1 chaos* mutants (Table 3.2). Taken together, these data indicate that the reduction of the PSII antenna size in the *prors1-1 chaos* mutant, as consequence of the *chaos* mutation, restores the altered TRS of *prors1-1* by decreasing the total amount of the light absorbed. Consequently, PSII is able to better process the electronic pressure generated by the antenna. However, the rescue-effect, observed at the TRS level, does not imply a rescue of the physiological functions of *prors1-1 chaos*. The double mutant was indeed smaller and produces less oxygen in comparison to the two single mutants.

Table 3.2 Leaf pigment content of *prors1-1*, *chaos* and *prors1-1 chaos* mutants. Measures expressed in pmol/mg (fresh weight) of leaf material analyzed by HPLC. Nx, neoxanthin; Lut, lutein; B-car, B-carotene; Chl a, Chlorophyll a; Chl b, chlorophyll b; Vaz, violaxanthin + antheraxanthin + zeaxanthin; Chl a + b, total chlorophyll.

Genotypes	Nx	Lut	Chl b	Chl a	B-Car	Vaz	Chl a+b	Chl a/b
Col-0	60±5	197±15	580±34	1574±54	211±7	66±5	2154±53	2,71±0,09
<i>prors1-1</i>	45±3	154±10	480±28	1225±71	121±8	66±1	1705±68	2,55±0,15
<i>chaos</i>	29±1	103±9	197±6	728±34	176±7	34±3	925±40	3,69±0,08
<i>prors1-1 chaos</i>	24±3	92±9	165±12	497±39	174±10	43±4	742±61	3,01±0,09

3.1.2. Protein composition of thylakoid membranes is influenced by the TRS

To define the protein composition of the photosynthetic machinery, immuno-blot analyses were performed on isolated thylakoids and total protein preparations fractionated on 1D SDS-PAGE (Figure 3.3). As previously described by Klimyuk et al. (1999), PSII-associated antenna complexes (Lhcb1, Lhcb2 and Lhcb3) were markedly reduced in the *chaos* mutant (30% of WT levels), and similar reductions could also be observed in *prors1-1 chaos* leaves. Conversely, Lhca1 seemed to be more reduced

in *prors1-1 chaos* than in the respective single mutants. Due to the *prors1-1* mutation, plastid encoded photosystem subunits were in general slightly reduced in *prors1-1* and *prors1-1 chaos*, as well as the α - and β -subunits of the ATPase that are reduced to 50% of WT levels. Other subunits belonging to the PSI antenna (Lhca2), PSII antenna (Lhcb5), PSI core (PsaD and PsaF), PSII core (D1, CP43 and D2) and oxygen evolving complex (PsbQ) were increased in their amounts in thylakoids of the double mutant compared to *prors1-1* (Figure 3.3). Immuno-blot analyses were also performed on dark- and light-adapted leaf material, by employing phosphothreonine-specific antibodies (p-Thr), to investigate the phosphorylation status of PSII core and LHCII proteins. In general only faint signals were visible in dark-adapted leaves, however in *prors1-1* LhcII phosphorylation is slightly increased. In light-adapted samples thylakoid proteins were strongly phosphorylated with *prors1-1* showing a significantly higher phosphorylation of CP43 and a slightly increased phosphorylation of D1/D2 and LHCII proteins. Contrarily, in *chaos* and *prors1-1 chaos* a marked decrease in D1, D2, and CP43 phosphorylation could be observed. The diminished phosphorylation of CP43, D1 and D2 in *prors1-1 chaos* is most likely a consequence of the reduced injections of electrons into the thylakoid electron transport chain and possibly leads to a slower protein turn-over in the thylakoids (Figure 3.3). This in turn may explain the higher accumulation of some nuclear-encoded photosynthetic proteins observed in *prors1-1 chaos* leaves with respect to *prors1-1*.

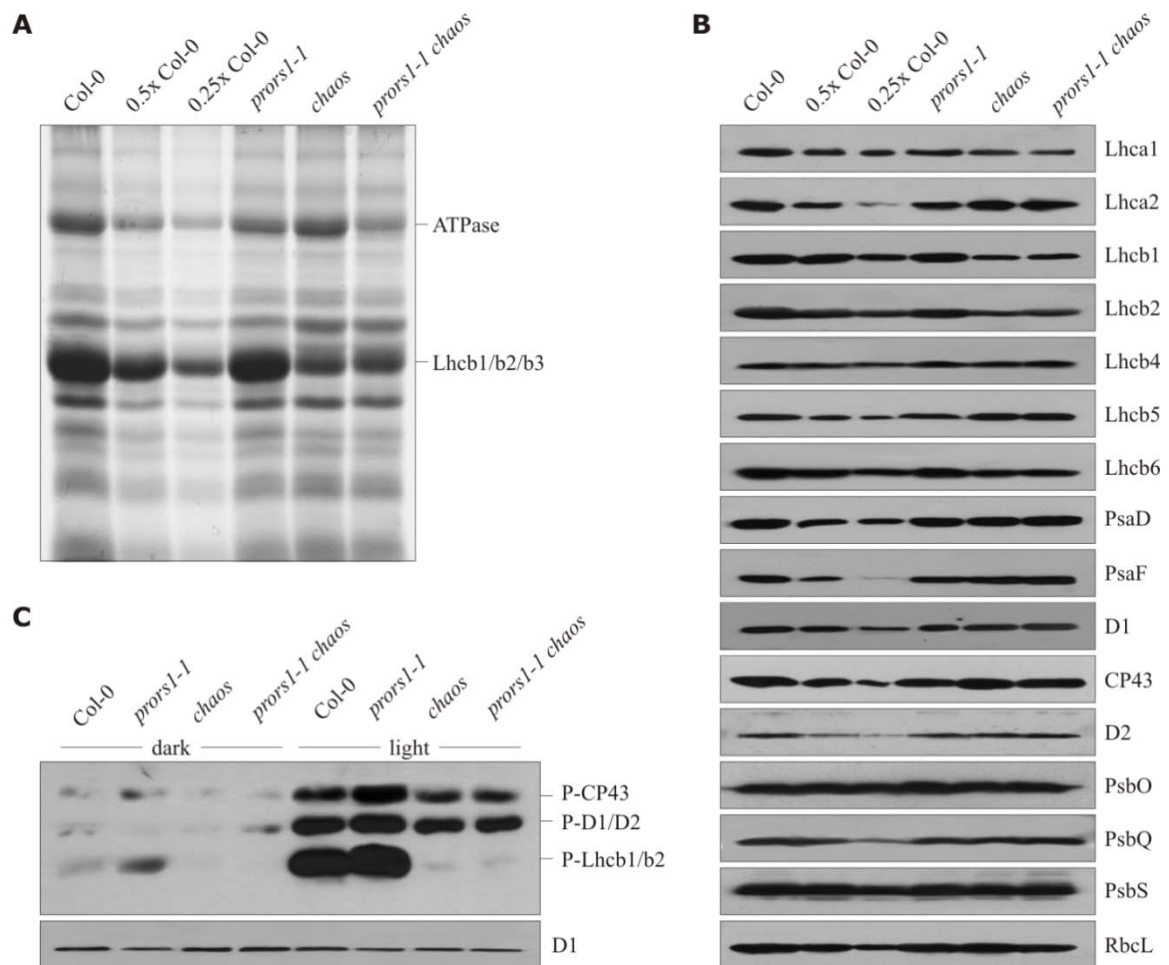


Figure 3.3 Protein composition of thylakoid membranes. Thylakoids and total proteins were extracted from an equal amount of leaf fresh weight. Thylakoids were isolated, fractionated by SDS-PAGE and stained with Coomassie Brilliant Blue (A). Immuno-blot analysis on total protein extracts were performed using antibodies against LHC and PS subunits. 0.50x Col-0 and 0.25x Col-0 indicate dilutions of WT control (B). Dark- and light-adapted total leaf extracts were probed with a Phospho-Threonine (P-Thr) specific antibody, D1 immuno-blotting was used as loading control (C) (Tadini et al., 2012).

2.1.3. TRS influences nuclear and plastid gene expression

To analyze the functional and physiological interaction between the TRS and OGE at the plastid level and their contribution to NGE, *in-vivo* labeling and northern blot analyses were performed. Leaf discs were collected after 5, 15 and 30 minutes of incubation with [35 S] methionine in the presence of light and inhibitors of cytoplasmic protein synthesis. To assess the protein synthesis rate, RbcL and D1 synthesis was monitored. As previously described in Pesaresi et al. (2006), *prors1-1* showed a slightly

slower protein synthesis rate (Figure 3.4), whereas no alterations could be detected in the *chaos* mutant, indicating that the reduced LhcII accumulation does not influence the translational machinery. The amounts of RbcL labeled in *prors1-1* and *prors1-1 chaos* plants were comparable and equivalent to about 55% of the WT levels (Figure 3.4).

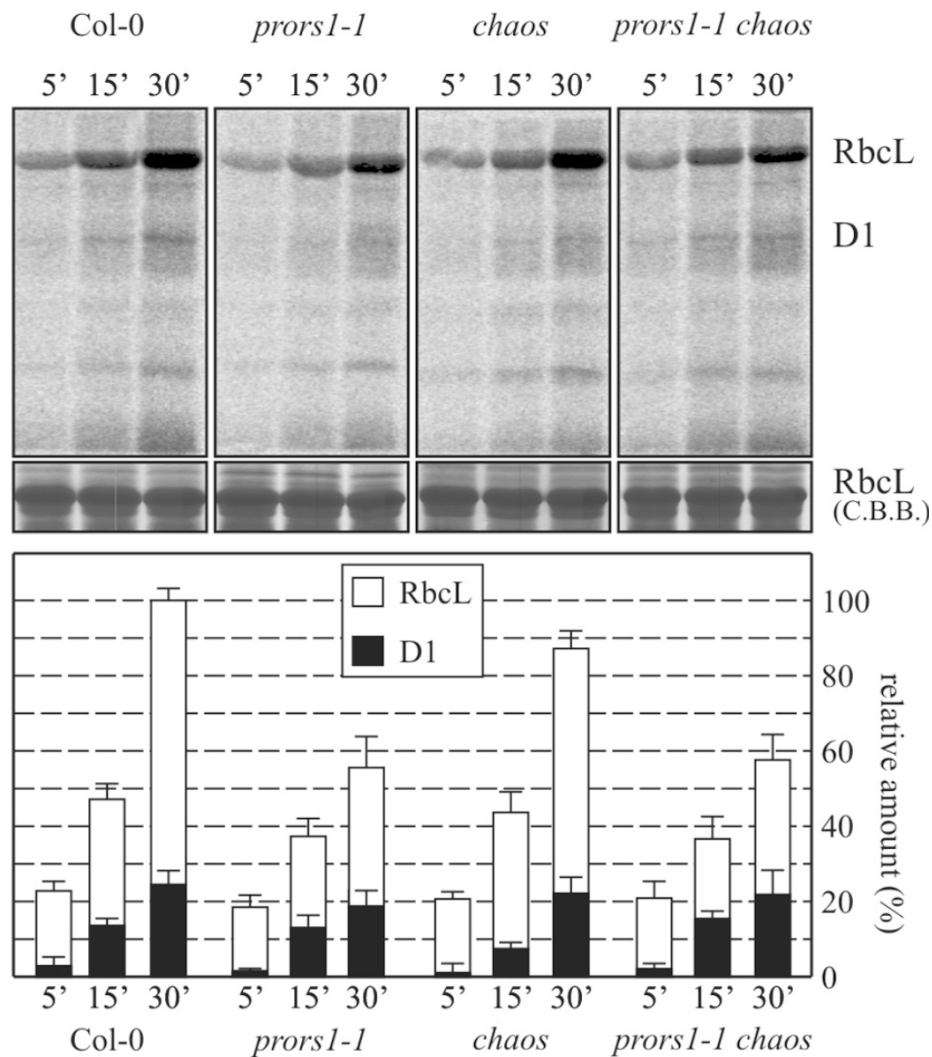


Figure 3.4 Synthesis rate of plastid-encoded proteins. *In-vivo* labeled total proteins were fractionated on SDS-PAGE. The presence of cycloheximide ensures protein synthesis to take place only in the organelles. RbcL and D1 protein accumulation was monitored and quantified (Tadini et al., 2012).

As described before (Pesaresi et al., 2006) the *prors1-1* mutant showed, as consequence of plastid-to-nucleus retrograde signaling, a diminished expression of nuclear-encoded photosynthetic genes. Expression analyses

were performed on 28 days old leaves to define the relative contribution of photosynthetic electron transport and the associated changes in TRS to the OGE-dependent signaling pathway (Figure 3.5). In the *prors1-1 chaos* double mutant, 15 of the 17 nuclear encoded photosynthetic genes analyzed were up-regulated in comparison to *prors1-1*. In particular, the expression of *Lhca1*, *Lhca2*, *PsaE1*, *PsaF*, *PsaK*, *PsaO*, *Lhcb1*, *Lhcb2*, and *PsbX* in *prors1-1 chaos* leaves was similar to those of the WT. In addition, *PsaD1*, *Lhcb3*, *Lhcb4*, *PsbO2* and *RbcS* transcripts accumulated in *prors1-1 chaos* leaves at higher levels than in *prors1-1*. Exceptions were represented by *Lhca3* and *Lhca4* genes which were down-regulated in both, *prors1-1* and *prors1-1 chaos* mutants. The limited capacity for light absorption caused by the *chaos* mutation also influenced plastid gene expression, as shown by the marked drop in *psaA-B* expression in *chaos* and *prors1-1 chaos* mutants, whereas *psbA* and *RbcL* levels were almost unchanged in mutant plants. Expression of genes involved in scavenging or preventing the formation of ROS was also investigated. The transcript levels of *Ferritin1*, mitochondrial alternative oxidase (*AOX1*), catalase (*CAT1*) and 2-Cys-peroxiredoxin-A (*2CPA*), whose expression was reported to be stimulated by increases in ROS production, were only slightly altered in the mutant genotypes (Figure 3.5), suggesting no significant alteration in the accumulation of ROS in those leaves.

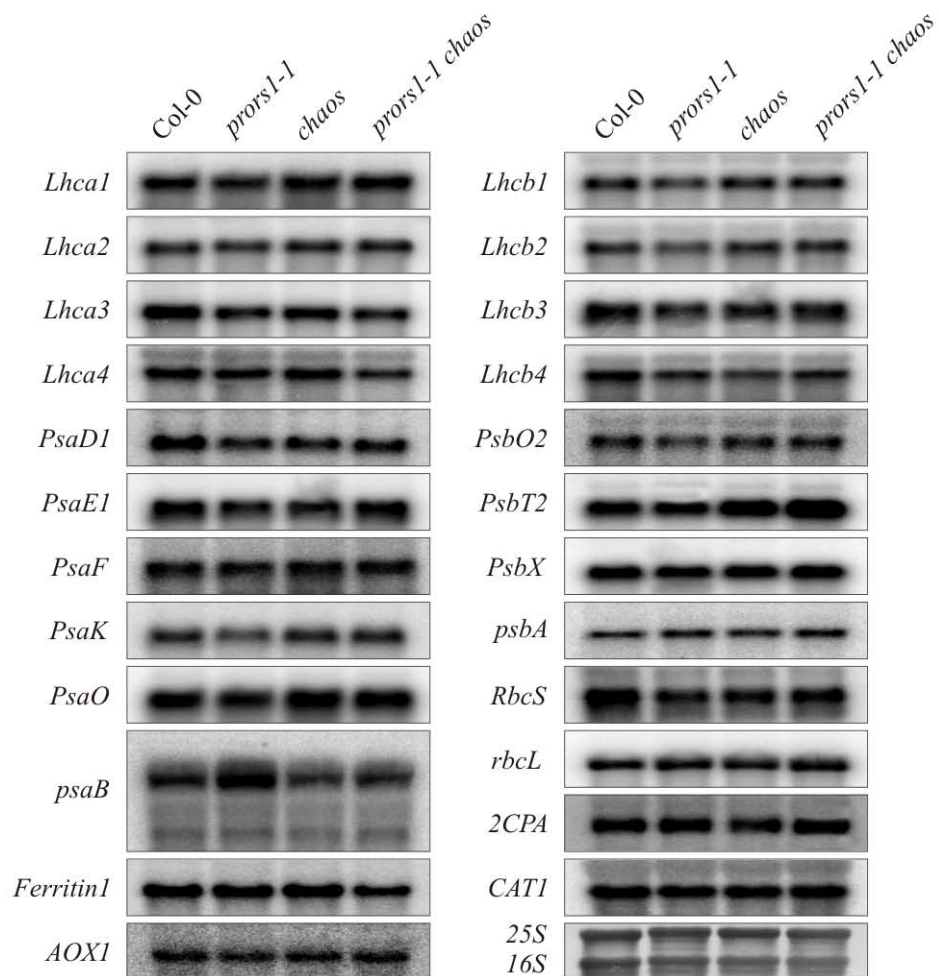
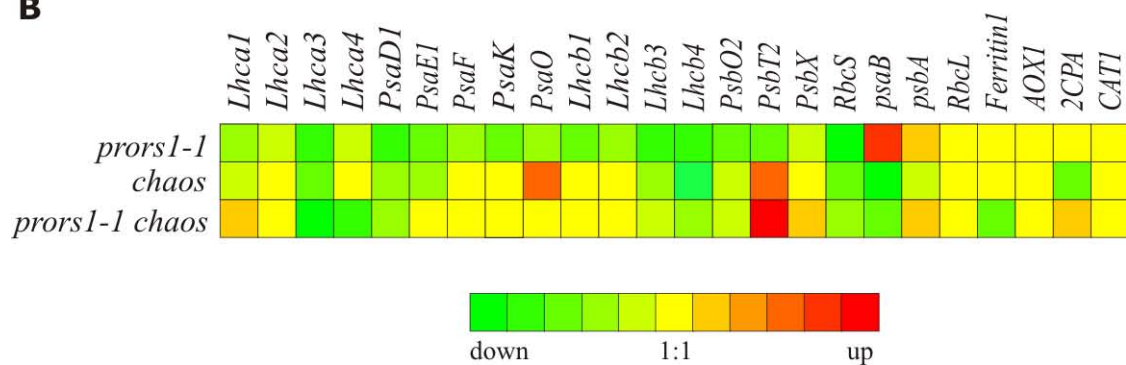
A**B**

Figure 3.5 Expression analysis of nuclear- and plastid-encoded genes in *prors1-1*, *chaos* and *prors1-1 chaos* plants. Northern blot analysis on photosynthesis and antioxidant genes (A), the equal loading was verified by methylene blue staining, where the 25S and 18S rRNA are shown. Gene expression was then quantified and depicted in a heat map representation (B) (Tadini et al., 2012).

3.1.4. Discussion

As mentioned before in this work, chemicals used to characterize the different retrograde signaling pathways have a wide range of secondary effects, which do not allow for a distinction between primary and secondary effects of the respective treatment. To avoid possible secondary effects and to identify the primary source of the signaling event, a genetic platform was employed, based on the *prors1-1* being a mutant slightly impaired in organellar protein synthesis but otherwise comparable to Col-0 (e.g. developmental stage). It has been described before by Pesaresi et al. (2006) and in this work that the translational defects observed in the *prors1-1* mutant have a clear effect on the TRS, which is supported by photosynthetic measurements and the enhanced thylakoid phosphorylation. This observation strengthens the notion that the photosynthetic machinery, and in particular the PQ pool, act also as the major sensor for physiological imbalances in the chloroplast (Pfannschmidt and Yang, 2012). Nevertheless, changes of the TRS, caused by alterations of the pressure across the electron transport chain, lead to modifications of the gene expression at the nuclear side. The introduction of the *chaos* mutation into the *prors1-1* genetic background intended to compensate the altered TRS of *prors1-1*, thus mimicking the physiological ability of the chloroplast to adapt to an excessive light exposure. The lack of cpSRP43 in the *chaos* mutant, responsible for the insertion of Lhcb proteins into the thylakoid membrane, results in a decrease of the PSII antenna and consequently a decrease in the light absorption capability of the electron transport chain (Klimyuk et al., 1999). As shown by Φ_{II} and NPQ measurements and by the phosphorylation-state of the thylakoid proteins, the TRS of *prors1-1* is restored to a WT-like level by the *chaos* mutation. Due to the *chaos* mutation, the accumulation of PSII antenna proteins (Lhcb1, Lhcb2, Lhcb3 and Lhcb6) is indeed markedly decreased in *prors1-1 chaos*. It must be noted that chloroplast-encoded *psaA-B* operon mRNA is decreased in *chaos* and *prors1-1 chaos* and more abundant in *prors1-1*,

since transcription of the chloroplast-encoded *psaA-B* operon is under control of the PQ pool redox-state (Pfannschmidt et al., 1999; Allen and Pfannschmidt, 2000). This observation supports the idea of a hyper-oxidized-PQ pool in *chaos* and *prors1-1 chaos* genetic background, on the other hand, plastid translation rate, analyzed by *in-vivo* labeling, revealed that the mitigation of *prors1-1* TRS by *chaos* mutation does not imply an OGE improvement. Protein synthesis of *prors1-1 chaos* is indeed comparable to *prors1-1* single mutant. We can therefore conclude that the OGE has a direct impact on the over-reduction of the TRS but, however, an over-oxidized TRS is not positively influencing the OGE when compromised. Nevertheless, the increased accumulation of some plastid-encoded subunits in *prors1-1 chaos* (relative to *prors1-1*) has to be attributed to post translational events which might affect protein stability as a consequence of a lower level of oxidative damage. The TRS mitigation effect, due to the introduction of the *chaos* mutation, does not improve the physiological functions as demonstrated by growth rate and O₂ production measurements of the *prors1-1 chaos* plants. Interestingly, the *prors1-1 chaos* plants show a general de-repression of those genes which are down-regulated in *prors1-1* single mutants, even though not all the genes show the same behavior. According to their de-repression pattern, four groups of genes can be defined: genes which are expressed at higher level than in the WT (e.g. *PsbT2*), genes expressed at levels similar to the WT (e.g. *Lhca1*, *Lhca2*, *PsaE1*, *PsaF*, *PsaK*, *PsaO*, *Lhcb1*, *Lhcb2*, and *PsbX*), genes expressed at levels higher than in *prors1-1* but lower than in the WT (e.g. *PsbO2* and *RbcS*) and those which are not influence in their expression by the *chaos* mutation (e.g. *Lhca3*, *Lhca4*). Since the TRS only partially suppresses the retrograde signaling pathway triggered by OGE, we could conclude that TRS and OGE act in distinct overlapping pathways which exert a synergistic effect on NGE. Moreover, these two components of the organelles-to-nucleus signaling act together in a gene-specific manner. Pesaresi et al. (2006) have already shown that

OGE-triggered retrograde signaling is widely independent of light-correlated processes like photosynthesis and TRS. Indeed, the down-regulation of nuclear genes in the *prors1-1* genetic background persists even after dark-adaptation, which implies that plants retain a certain memory of the stress conditions induced by light exposure. Moreover, it can be concluded that the specific retrograde-signaling observed in *prors1-1* is not triggered by ROS (this work and Pesaresi et al., 2006), since no expression changes of genes involved in ROS detoxification (*2CPA*, *CAT1*, *Ferritin1* and *AOX1*) was noted in the corresponding studies performed on WT and mutant plants.

3.2 GUN1 functionally interacts with the plastid gene expression machinery

The *gun* mutants have been reported to alter retrograde signaling, with *GUN1* being specifically involved in the OGE-dependent signaling pathway. In this part of the study we investigated a possible role of GUN proteins and other members of the pTAC complex in transducing the OGE-signal to the nucleus.

3.2.1. *gun1-gun5* genetic interaction with *prpl11* and *prors1-1* mutants

As mentioned before, *gun* mutants have been described to be impaired in the plastid-to-nucleus signaling, however the *gun*-phenotype has always been observed employing chemicals which heavily affect physiological functions (Susek et al., 1993; Koussevitzky et al., 2007). Since chemicals like norfluorazon (NF) or lincomycin (Lin) have a wide range of secondary effects on chloroplast functions, these experimental setups give only limited information about the signaling under physiological conditions. To analyze the role of *gun*-mediated signaling under more physiological conditions, a large set of double mutants was generated, by introducing the *gun1-gun5* mutations into the *prpl11* and *prors1-1* genetic backgrounds (Figure 3.6).

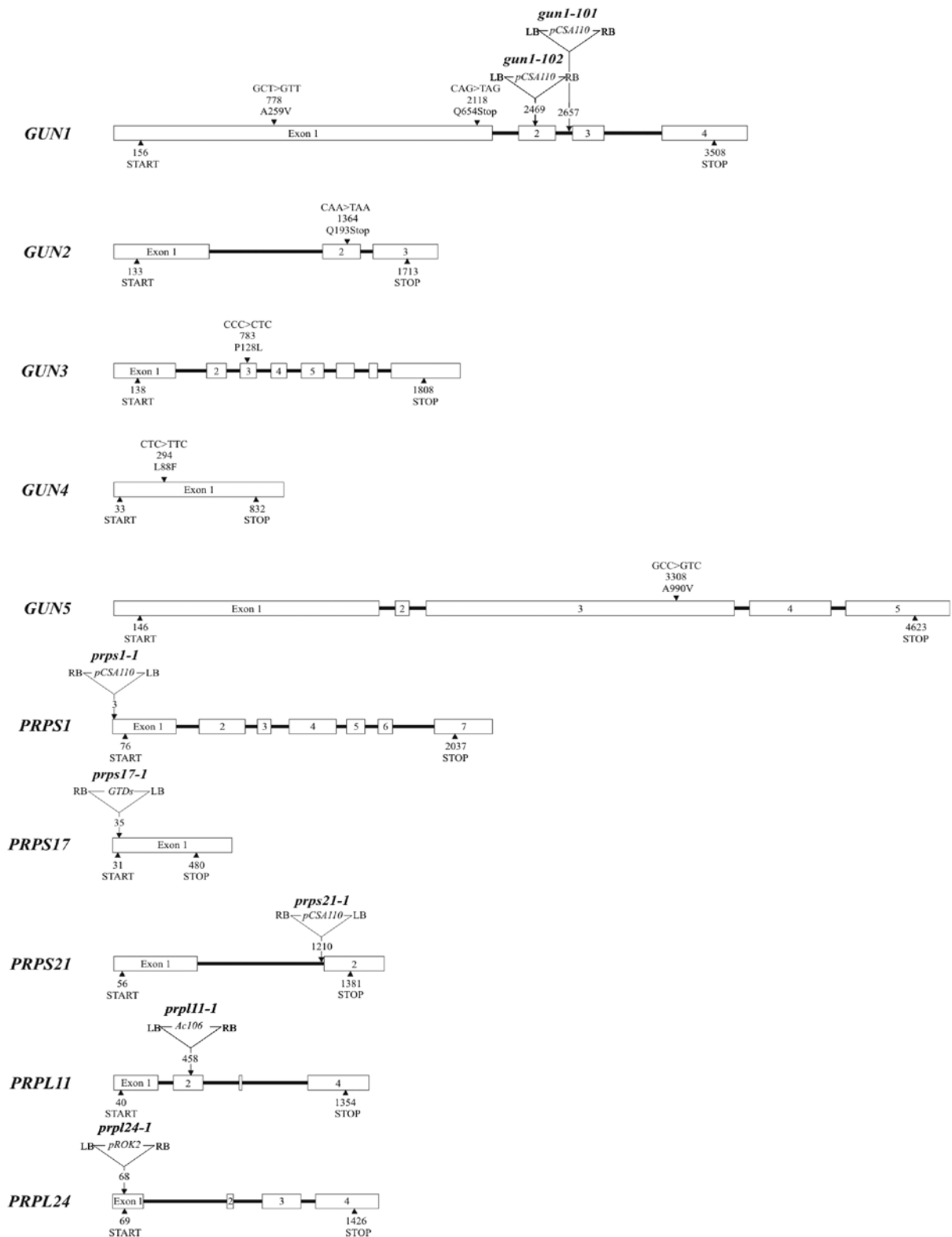


Figure 3.6 Schematic representation of the employed mutants alleles. Point mutations and T-DNA insertions are displayed within the genomic sequences. Introns are represented as black lines, exons as numbered boxes, LB and RB stand for left and right border of the T-DNA.

As described before, *gun1* mutant plants did not show any obvious phenotype at 28 d.a.p. and no difference in growth or leaf photosynthetic efficiency could be detected at this stage. However, when four independent *gun1* alleles (Figure 3.6), generated via either T-DNA insertions or point mutations, were introduced into the *prpl11* mutant background, mature-albinotic embryos and albino seedlings were observed in the progeny of the double heterozygous mutant plants (Figure 3.7).

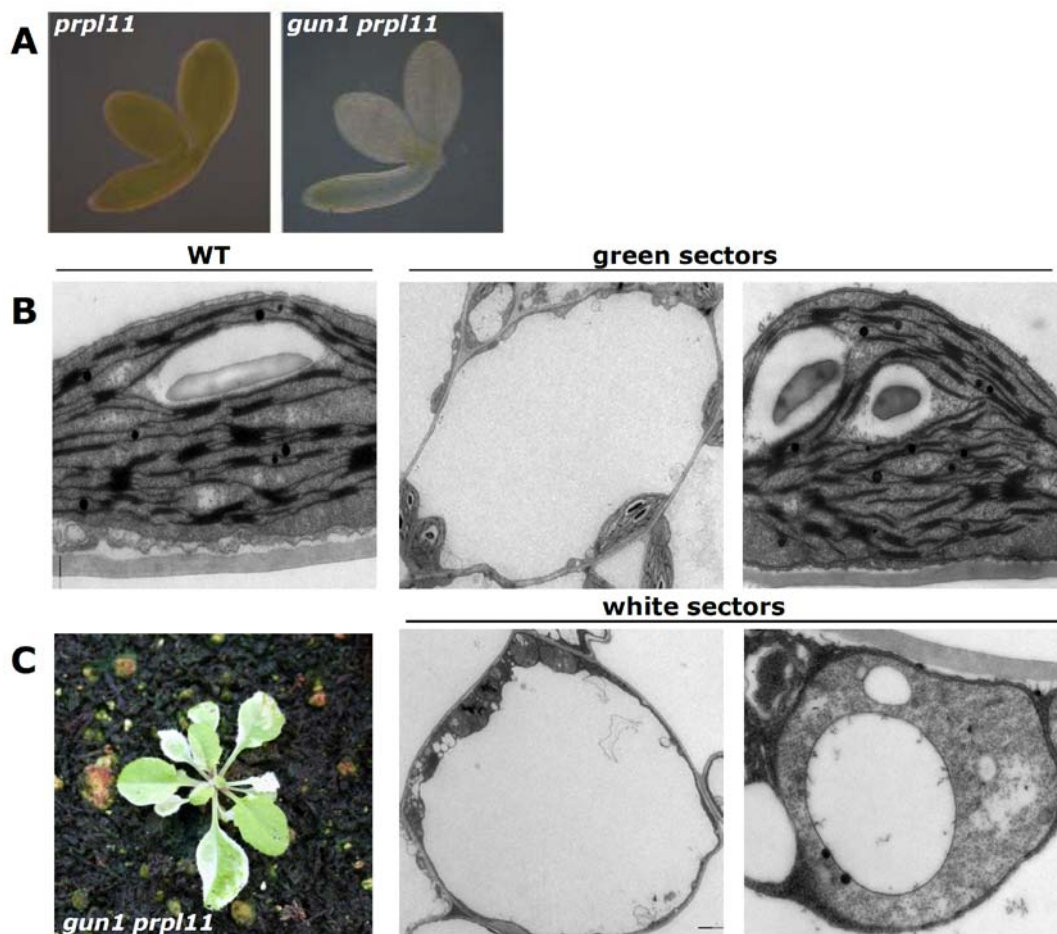


Figure 3.7 Phenotypic analysis of *gun1 prpl11* mutant. In most of the cases *gun1 prpl11* is an albinotic-seedling (A), rarely *gun1 prpl11* overcomes the seedling-stage and develops variegated leaves (C). TEM analyses revealed a pro-plastid-like structure which fails to develop a thylakoid membrane system (C) contrarily the green sectors contain WT-like fully developed chloroplasts (B).

PCR analysis identified the albinotic-seedlings as the *gun1 prpl11* double mutant. Segregation analyses on the *gun1/GUN1 prpl11/prpl11* F1 generation demonstrated that a part of the progeny fail to germinate. The four *gun1* alleles analyzed showed a different ratio between albinotic-seedlings and non-germinated seeds (Table 3.3).

Table 3.3 Segregation analyses on the progeny of four *gun1* alleles introduced into the *prpl11* mutant background. Plants were grown for 7 days on soil as described in Material and Methods.

Segregating mutant background	Albino	Not-germinated	Green	Total
WT	0	0	106	106
<i>prpl11/prpl11 GUN1/gun1-1</i>	11	4	91	106
<i>prpl11/prpl11 GUN1/gun1-9</i>	4	29	73	106
<i>prpl11/prpl11 GUN1/gun1-101</i>	11	10	85	106
<i>prpl11/prpl11 GUN1/gun1-102</i>	16	9	81	106

However, few viable *gun1 prpl11* double mutants were identified (Figure 3.7B). These plants appeared in rare numbers (~1:500), very variable in size and growth and show a variegated phenotype with alternating white and green leaf sectors. Transmittance electron microscopy (TEM) was used to compare the plastid morphology between the green and white sectors. Even though the green sectors contained fully developed WT like chloroplasts, the white sectors showed proplastid-like structures that fail to develop into thylakoid membrane containing chloroplast (Figure 3.7B).

To further investigate whether the variegated phenotype of viable *gun1 prpl11* double mutants is due to environmental stress conditions, as in the case of variegated plants lacking the plastid terminal oxidase (PTOX), *immutans* and *gun1 prpl11* plants were grown both under low- and growth-light conditions. As shown in Figure 3.8, *immutans* plants were characterized by white leaf sectors and a marked reduction in size under standard light conditions, in comparison to an almost WT like appearance

when grown under low light conditions. On the contrary, the variegated phenotype of *gun1 prpl11* leaves appeared similarly severe under both light conditions, indicating that the *gun1 prpl11* leaf phenotype is not influenced by light intensities and thus is rather due to a developmental defect (Figure 3.8).

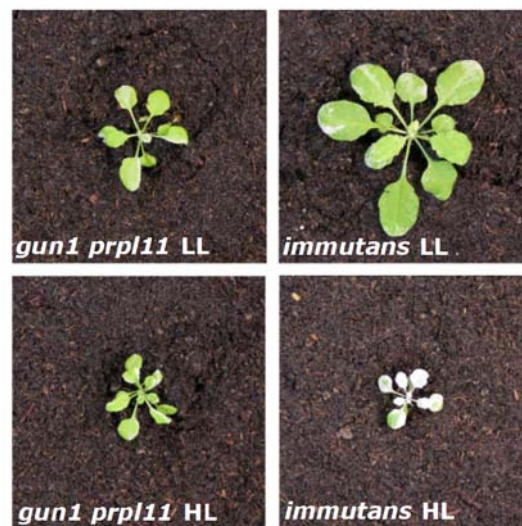


Figure 3.8 Phenotypic characterization of 26 days old *gun1 prpl11* and *immutans* plants. Plants were grown under low-light (LL, upper panel) and high-light (HL, bottom panel) conditions.

To investigate the involvement of the other GUN proteins in the plastid-to-nucleus communication, also the *gun2*, *gun3*, *gun4* and *gun5* mutations were introduced into the *prpl11* knock-out background. In these cases the double mutants were viable and behaved like the respective parental lines (Figure 3.9)

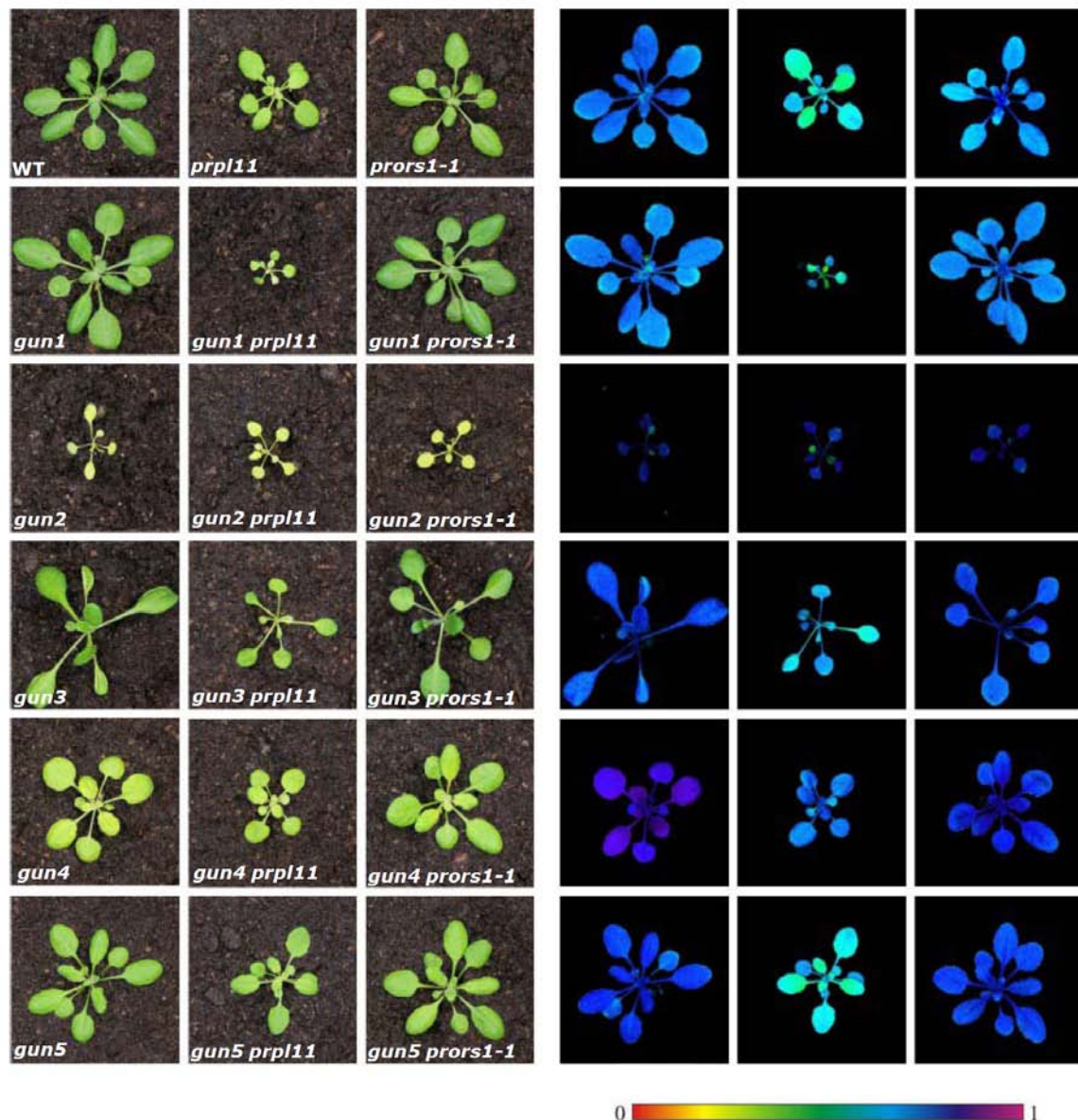


Figure 3.9 Phenotypes of the *gun1-gun5*, *prpl11* and *prors1-1* single and *gun prpl11* and *gun prors1-1* double mutants. Imaging-PAM pictures represent the PSII yield (Φ_{II}), values are visualized according to the color scale on the bottom, violet color for 1 and red color for 0.

As described above, mutants with a reduced PSII antenna size absorb less light and for this reason are less photo-sensitive. This appears also to be the case for *gun2*, *gun3*, *gun4* and *gun5* that show higher F_v/F_m and Φ_{II} values than the WT control. Similarly, the *gun2 prpl11*, *gun3 prpl11*, *gun4 prpl11* and *gun5 prpl11* double mutants showed a total or partial rescue of the decreased *prpl11* photosynthetic performance (Table 3.4).

Table 3.4 Photosynthetic performance analyses of *gun1-gun5*, *prpl11* and *prors1-1* single and double mutants. In the table are represented the PSII efficiency of dark-adapted plants (F_v/F_m) and light-adapted plants (Φ_{II}). The 1-qP value reflects the redox-state of the PQ pool.

	F_v/F_m	Φ_{II}	1-qP
WT	0,81±0,02	0,75±0,01	0,06±0,02
<i>gun1</i>	0,82±0,01	0,76±0,02	0,05±0,02
<i>gun2</i>	0,85±0,03	0,78±0,02	0,05±0,02
<i>gun3</i>	0,86±0,02	0,77±0,01	0,04±0,02
<i>gun4</i>	0,85±0,03	0,79±0,01	0,04±0,01
<i>gun5</i>	0,85±0,01	0,76±0,02	0,05±0,02
<i>prpl11</i>	0,71±0,03	0,64±0,02	0,07±0,02
<i>gun2 prpl11</i>	0,85±0,02	0,75±0,02	0,06±0,01
<i>gun3 prpl11</i>	0,79±0,01	0,67±0,02	0,05±0,01
<i>gun4 prpl11</i>	0,77±0,02	0,69±0,03	0,07±0,03
<i>gun5 prpl11</i>	0,73±0,02	0,66±0,03	0,07±0,02
<i>prors1-1</i>	0,78±0,02	0,68±0,02	0,06±0,02
<i>gun1 prors1-1</i>	0,81±0,01	0,73±0,02	0,05±0,01
<i>gun2 prors1-1</i>	0,86±0,03	0,78±0,03	0,06±0,02
<i>gun3 prors1-1</i>	0,84±0,01	0,76±0,02	0,06±0,01
<i>gun4 prors1-1</i>	0,84±0,03	0,76±0,02	0,05±0,02
<i>gun5 prors1-1</i>	0,83±0,01	0,76±0,03	0,06±0,02

Nevertheless, the improved photosynthetic efficiency observed in the double mutants did not correspond to a rescue of the plant's physiological performance, since no improvement in the growth rate of the different double mutants could be observed (Figures 3.9 and 3.10).

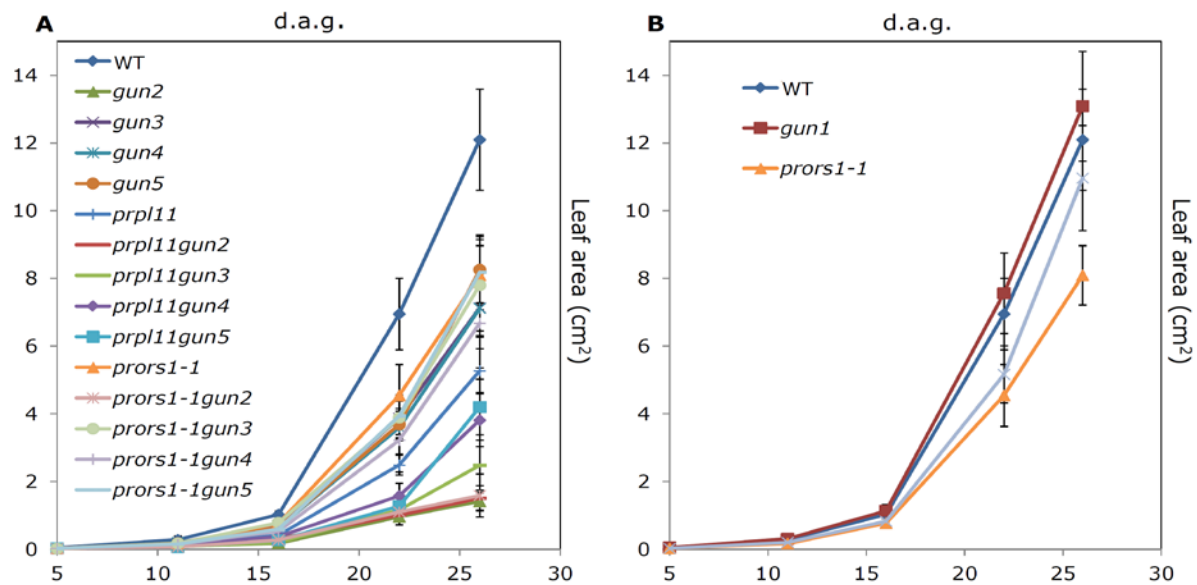


Figure 3.10 Growth ratio measurements of *gun* mutants in *prpl11* and *prors1-1* genetic background. The leaf area of at least 12 plants per genotype was measured from 5 to 26 d.a.g. Leaf areas are expressed cm².

To investigate further the role of GUN1 and to understand whether GUN1 is specifically and functionally interacting with the *prpl11* mutation, rather than with the translational machinery, the entire set of *gun* mutations was introduced into the *prors1-1* mutant background. Not surprisingly, *gun2-gun5 prors1-1* double mutants were slightly smaller than the parental lines with photosynthetic parameters being close to those of the *gun2-gun5* single mutants (Table 3.4). On the contrary, *gun1 prors1-1* showed a better photosynthetic performance in terms of maximum (F_v/F_m) and effective quantum yield of PSII (Φ_{II}) and an improved growth kinetics compared to *prors1-1* (Table 3.4, Figure 3.9 and 3.10). This implies that the lack of GUN1 partially restored the *prors1-1* phenotype in *gun1 prors1-1* plants. To summarize, *gun1* is genetically interacting with the *prpl11* mutation. This observation suggests a functional interaction of GUN1 with the plastid ribosome and a possible role in plastid gene expression. GUN1 is indeed essential in combination with *prpl11* for plastid development. On the other hand, GUN1 is not essential in the *prors1-1* mutant background, in fact *gun1 prors1-1* showed a partially restored phenotype. The other *gun2-gun5* mutants conversely did not show any

additive phenotype in combination with mutants impaired in plastid translation.

3.2.2 GUN1 functionally interacts with different subunits of the plastid ribosomes

To further analyze the functional interaction between GUN1 and plastid ribosomes, the *gun1-102*, *gun1-1*, and *gun1-9* alleles were crossed with *prps1*, *prps17*, *prps21* and *prpl24* mutants, each of them lacking a specific subunit of either the large or small subunit of the plastid ribosomes (Figure 3.6 and 3.11). Albino seedlings incapable of autotrophic growth have been found in the *gun1/GUN1 prps17/prps17* progeny (Figure 3.11A). Similarly, no viable double mutants could be identified in the *gun1/GUN1 prpl24/prpl24* progeny, and many seeds fail to germinate. Analyses on siliques revealed the presence of albino-seedlings which aborted before reaching the seed maturation state. On the other hand, *gun1 prps1* and *gun1 prps21* were viable, pale green double mutants (Figure 3.11).

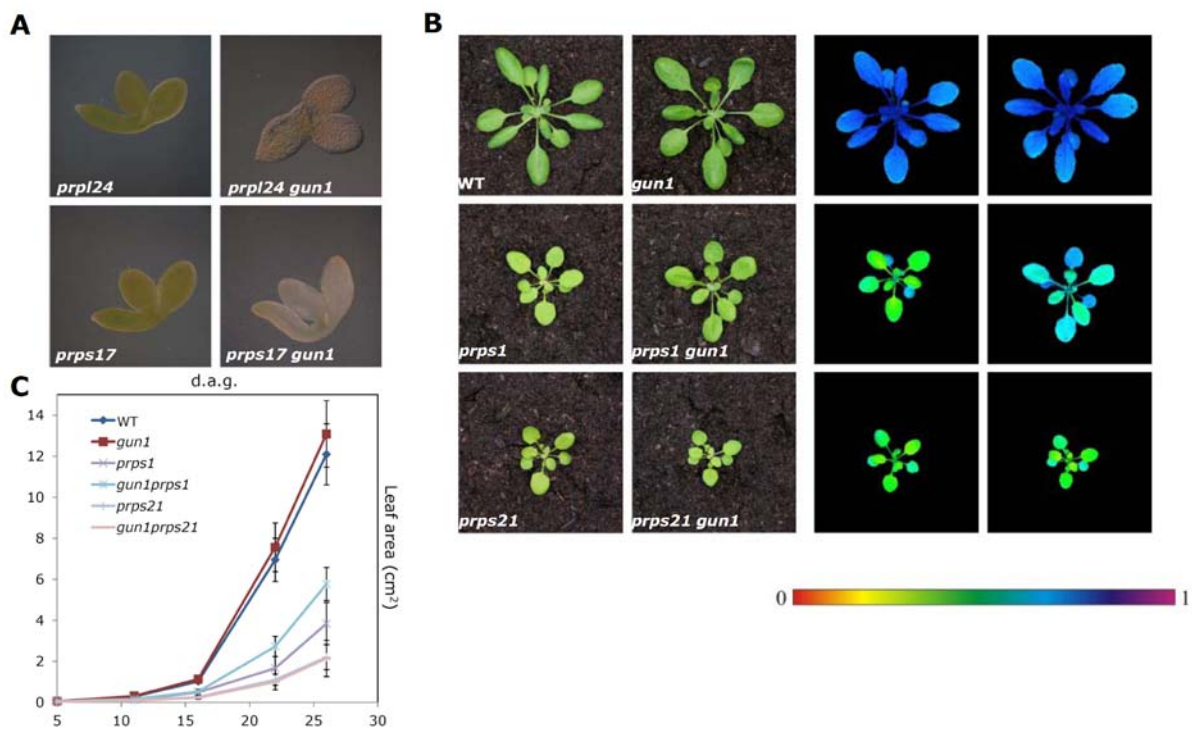


Figure 3.11 Phenotypic characterization of *gun1* and *prp* single and double mutants. Fully mature albinotic embryos isolated from *gun1/GUN1 prps17/prps17* and *gun1/GUN1 prpl24/prpl24* siliques (A). Bright field and imaging-PAM pictures of the effective quantum yield of PSII (Φ_{II}) of the *gun1 prp* viable mutants are represented on the right. Φ_{II} values are according to the color scale at the bottom, violet color for 1 and red color for 0 (B). Growth rate measurements for at least 12 plants are reported in the chart, the leaf area has been measured in different time points from 5 to d.a.p. (C).

In particular, *prps21* and *gun1 prps21* plants were phenotypically identical, whereas the *gun1 prps1* double mutant was slightly larger (150%) with respect to the *prps1* single mutant and showed a better photosynthetic performance in terms of F_v/F_m and Φ_{II} (Table 3.6).

Table 3.6 Photosynthetic efficiency measurements on *gun1 prps1* and *gun1 prps21* plants. The F_v/F_m is representative of the yield in the dark, Φ_{II} value indicates the PSII yield after light adaption and 1-qP depicts redox-state of the PQ pool.

	F_v/F_m	Φ_{II}	1-qP
WT	0,81±0,02	0,75±0,01	0,06±0,02
<i>gun1</i>	0,82±0,01	0,76±0,02	0,05±0,02
<i>prps1</i>	0,63±0,03	0,49±0,02	0,12±0,03
<i>prps1 gun1</i>	0,77±0,02	0,66±0,02	0,08±0,02
<i>prps21</i>	0,55±0,02	0,41±0,03	0,16±0,04
<i>prps21 gun1</i>	0,54±0,04	0,43±0,02	0,14±0,03

Taken together, these data clearly indicate that the lack of GUN1 is able to improve the plastid-related functional defects of the *prps1* mutant, similarly to the situation in *gun1 prors1-1*. Contrarily, it exacerbates the *prps17* and *prpl24* phenotypes leading to seedling- and embryo-lethality phenotypes of the corresponding double mutants. Interestingly, no additive phenotypic effects can be observed in *gun1 prps21* double mutant plants.

3.2.3 Discussion

It has been widely discussed that plastid-to-nucleus retrograde signaling involves GUN1-GUN6 proteins (Bienert et al., 2007; Mubarakshina et al.,

2010). In particular, GUN1 is proposed to be the major integrator of most of the plastid signals like the TRS, the OGE and the one derived from tetrapyrrole biosynthesis (Koussevitzky et al., 2007). A genetic approach was applied to investigate the functional interaction between *gun1-gun5* mutants and the OGE-defect mutants such as *prpl11* and *prors1-1*. Phenotypic analyses that focused on growth rate and photosynthetic efficiency showed no obvious functional interaction between *gun2-gun5* and the OGE mutations. The phenotypes of the double mutants only reflected the single mutant phenotypes without any significant over-additive effects. As described for *chaos*, *gun2-gun5* mutants had a diminished accumulation of chlorophyll and consequently a more oxidized TRS in comparison to WT. Therefore the TRS of *gun2-gun5 prpl11* and *gun2-gun5 prors1-1* mutants was restored to WT-levels. No particular signaling function could be deduced for *gun2-gun5* under altered OGE conditions, as already shown by Koussevitzky et al. (2007): *gun2-gun5* are indeed sensitive to lincomycin treatment like WT plants. On the other hand GUN1 is the only plastid-located protein of the pathway which shows a functional interaction with the OGE machinery and an involvement in OGE triggered signaling. The identification of lethal albinotic seedling mutants (*gun1 prpl11*, *gun1 prpl24* and *gun1 prprs17*) demonstrates that GUN1 is essential for plastid biogenesis when certain ribosomal subunits are absent even though embryogenesis is not affected in those double mutants. Indeed, TEM analyses and growth measurements of these double mutants under different light conditions demonstrated that the albinotic phenotype is rather due to the inability to perform the transition from pro-plastids to mature chloroplasts than a disruption of the chloroplasts. This kind of plastid phenotype resembles that of documented knock-out mutants of other pTAC components like pTAC3, pTAC6 and pTAC12 which are involved in plastid gene expression (Pfalz et al., 2006). However, only some of the *prp* mutants analyzed in combination with the *gun1* mutation resulted in embryo- seedling-lethality while *gun1* showed

no effect in the *prprs21* mutant background. It is therefore reasonable to assume that GUN1 function is related to only one or few specific ribosomal subunits/functions and not protein translation *per se*. Special cases of *gun1* OGE-mutant interactions are represented by *gun1 prors1-1* and *gun1 prps1*. Indeed, the lack of GUN1 was improving growth and photosynthetic performance of the *prors1-1* and *prps1* mutants, as indicated by the partially restored phenotypes observed in the double mutants. In both of the two double mutants the TRS was mitigated by introduction of the *gun1* mutation. Different from the situation of *chaos* and *gun2-gun5*, *gun1* neither showed an increased oxidization of TRS nor a reduced chlorophyll accumulation. The reason for the partial rescue of the *prors1-1* and *prps1* phenotype by a lack of GUN1 must therefore involve some different mechanisms. To summarize, we can conclude that GUN1 is the only GUN protein functionally interacting with the OGE machinery in the chloroplast, supporting the *gun1*-specificity regarding the lincomycin treatment observed by Koussevitzky et al. (2007).

3.3 GUN1 and the molecular mechanism behind

3.3.1 GUN1 is a component of the pTAC complex and interacts with the Mg-Chelatase

To further define the role of GUN1 at the molecular level and to explain the genetic interactions described so far, we tried to elucidate the functional mechanism of GUN1. Since we could raise no GUN1 antibody, a 35S:GUN1-GFP line was generated. The chimeric GUN1-GFP protein was able to complement the lethal *gun1 prp111* phenotype, thus showing its functionality. GUN1-GFP signals was observed inside the chloroplast, forming distinct spots as shown by Koussevitzky et al., (2007) (Figure 3.12).

In addition, western-blot analyses allowed to detect the GFP signal both, in thylakoids and even more abundant in the soluble stromal fraction. Moreover, immuno-decoration of GUN1-GFP resulted in two bands of approximately 90 and 95 kDa. Interestingly, the ratio of the two bands changed upon variations in light intensity, with high-light exposure favoring the accumulation of the higher molecular band. This observation suggests that GUN1 exists in two alternative forms (of possibly activity), most probably based on post-translation modifications (Figure 3.12).

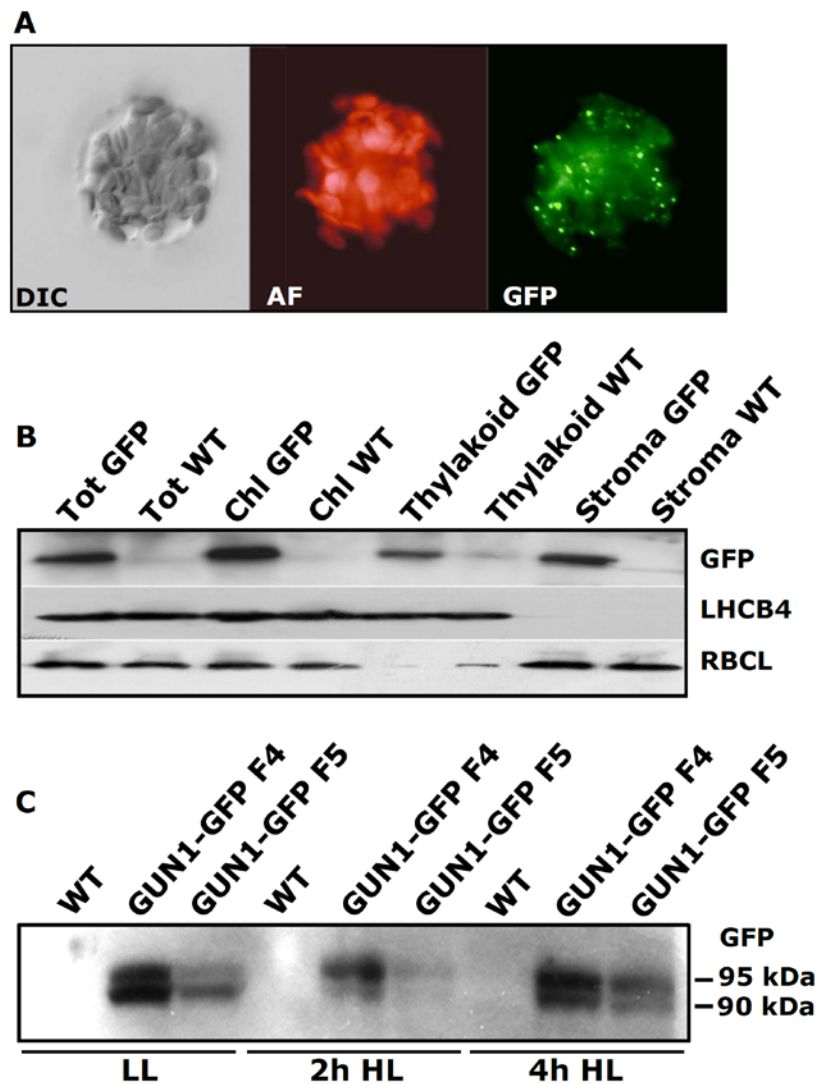


Figure 3.12 GUN1-GFP localization. Fluorescence microscopy of protoplasts revealed GUN1-GFP to form distinct spots in the chloroplasts (A). Immuno-blot analysis localized GUN1-GFP both, to thylakoids and the soluble stromal fraction of chloroplasts (B). GUN1-GFP immuno-decoration detected a double band, with the relative abundance of the higher molecular weight band increasing under high-light conditions (C).

To identify putative GUN1 interaction partners, a yeast-two-hybrid assay was carried out. First, GUN1 interaction with PRPL11 and PRPL24 was tested to see whether the functional interactions with the plastid ribosome subunits could be explained by their physical interaction. The yeast-based 2-hybrid assay indicated that no interaction occurs, although GUN1 showed the ability to form homo-dimers. Interestingly *GUN1* gene is co-regulated with pentatricopeptide and tricopeptide-repeat proteins, other

pTAC components like RH50 and the enzymes of the tetrapyrrole-biosynthesis pathway (Table 3.7).

Table 3.7 Co-regulation data of GUN1 with the entire *Arabidopsis thaliana* transcriptome. The co-regulation score is between 0 (no co-regulation) and 1 (identical regulation). Here a short list of genes most similarly co-regulated with *GUN1* is shown.

Genes	Score	Description
At2g31400	1,0000	GUN1
At4g01690	0,7901	protoporphyrinogen oxidase (PPOX)
At3g06980	0,7873	DEAD/DEAH box helicase (RH50)
At4g36390	0,7870	radical SAM domain-containing protein / TRAM domain-containing
At4g16390	0,7842	chloroplastic RNA-binding protein P67, putative
At5g46580	0,7835	pentatricopeptide (PPR) repeat-containing protein
At3g63190	0,7823	ribosome releasing factor, chloroplast, putative
At3g51140	0,7820	expressed protein
At3g02450	0,7809	cell division protein ftsH, putative
At1g70200	0,7807	RNA recognition motif (RRM)-containing protein
At5g08280	0,7687	hydroxymethylbilane synthase (HEMC)
At1g74850	0,7684	pentatricopeptide (PPR) repeat-containing protein
At1g01320	0,7655	tetratricopeptide repeat (TPR)-containing protein
At1g06190	0,7644	expressed protein
At4g29060	0,7610	elongation factor Ts family protein
At1g11750	0,7604	ATP-dependent Clp protease proteolytic subunit (ClpP)
At3g48730	0,7597	glutamate-1-semialdehyde 2,1-aminomutase 2 (GSA 2)
At4g38160	0,7594	mitochondrial transcription termination factor (mTERF)-related
At3g12930	0,7592	expressed protein
At3g19810	0,7590	expressed protein
At5g49030	0,7583	tRNA synthetase class I (I, L, M and V) family protein
At1g03475	0,7581	coproporphyrinogen III oxidase, putative
At1g02150	0,7577	pentatricopeptide (PPR) repeat-containing protein
At5g58250	0,7572	expressed protein
At5g45390	0,7566	ATP-dependent Clp protease proteolytic subunit (ClpP4)
At5g52520	0,7548	tRNA synthetase class II (G, H, P and S) family protein
At2g17033	0,7544	pentatricopeptide (PPR) repeat-containing protein
At3g63500	0,7532	expressed protein
At2g41950	0,7526	expressed protein

Based on gene expression co-regulation data, the potential interaction of GUN1 with these enzymes was tested. In particular, GUN1 interaction with

enzymes such as HEMA, GSA1, GSA2, HEMC, HEME1, HEME2, HEMF1, PPOX, CHLI1, CHLI2 and CHLD has been assayed (Figure 1.2). No interaction was detected between GUN1 and HEMA, GSA1, GSA2, HEME1, HEMF1, PPOX, CHLI1 and CHLI2. However, GUN1 was able to interact strongly with HEMC, HEME2, and CHLD (Table 3.8). The *gun1-1* allele, caused by a point mutation that induces the amino acid substitution A259V (Koussevitzky et al., 2007), was also tested in the yeast two-hybrid assay together with HEMC, HEME2 and CHLD, to see whether the mutated amino-acid residue is crucial for their interaction and therefore responsible for the *gun1-1* phenotype. GUN1-1 was shown to interact as strongly with HEMC, HEME2, and CHLD as the WT allele.

Table 3.8 Data of the yeast-two-hybrid assay using GUN1 as bait. Positive interactions are indicated by +, negative interactions are indicated by -. Note that similar data was obtained by using GUN1 as a prey.

	<i>GUN1</i>	<i>PRPL11</i>	<i>PRPL24</i>	<i>HEMA</i>	<i>GSA1</i>	<i>GSA2</i>	<i>HEMC</i>	prey
<i>GUN1</i> (bait)	+	-	-	-	-	-	+	

	<i>HEME1</i>	<i>HEME2</i>	<i>HEMF1</i>	<i>PPOX</i>	<i>CHLI1</i>	<i>CHLI2</i>	<i>CHLD</i>	prey
<i>GUN1</i> (bait)	-	+	-	-	-	-	+	

Further support of the above identified interactions was obtained by Bimolecular Fluorescence Complementation (BiFC) assays. Although no HEME2-GUN1 interaction could be detected, protoplasts co-transformed with nYFP-HEMC and cYFP-GUN1 showed a distinct spotted YFP fluorescence signal in the chloroplasts. This signal pattern resembling the fluorescence distribution observed in the GUN1-GFP line (Figure 3.12). However, an interaction could not be observed in the reciprocal combination, using the chimeric variants nYFP-GUN1 and cYFP-HEMC. On the contrary, the CHLD-GUN1 interaction was reproducible in both combinations again resembling the GUN1-GFP spotting pattern (Figure 3.13). GUN1-GUN4 interaction, which was also tested by BiFC, resulted as

negative (not shown). Taken together, these observations support the idea that GUN1 may be part of the Mg-chelatase complex similar to CHLD, CHLI, GUN4, and GUN5.

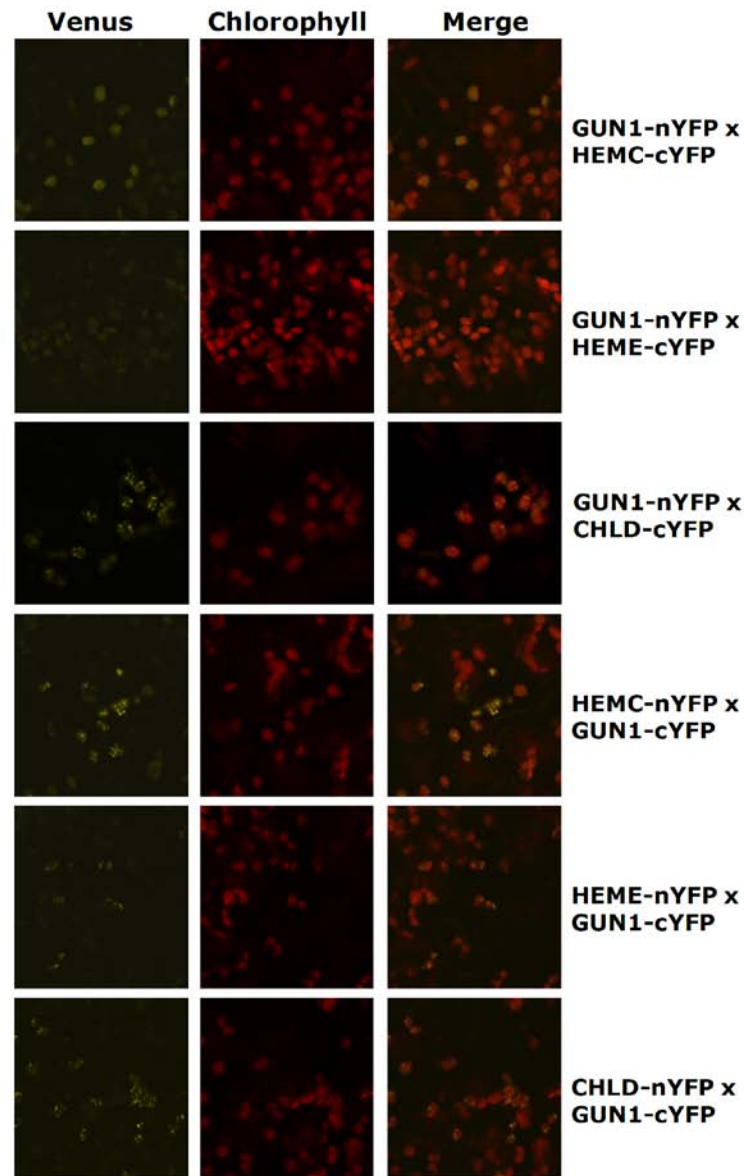


Figure 3.13 BiFC assays to test the interaction of GUN1 with each of the following tetrapyrrole enzymes: HEMC, HEME, and CHLD. Results of the interaction with both chimeric protein combinations are shown. The Venus channel in the first column represents the YFP fluorescence, in the second column is shown the chlorophyll fluorescence to highlight the chloroplasts.

Unfortunately immuno-precipitation on GUN1-GFP experiments never allowed for the detection of CHLD (not shown). However, supporting this

observation, preliminary immuno-blot analyses suggest that the presence of GUN1 influences the abundance of components of the Mg-chelatase enzymatic complex. The accumulation of CHLD was reduced in the *gun1* single mutant and enriched when the chimeric GUN1-GFP was highly abundant (35S:GUN1-GFP line). Also the GUN4 subunit accumulates to lower levels in the absence of GUN1, whereas CHLH appeared to accumulate to higher levels than in the WT both, in the presence (35S:GUN1-GFP line) and absence (*gun1*) of the GUN1 protein (Figure 3.14).

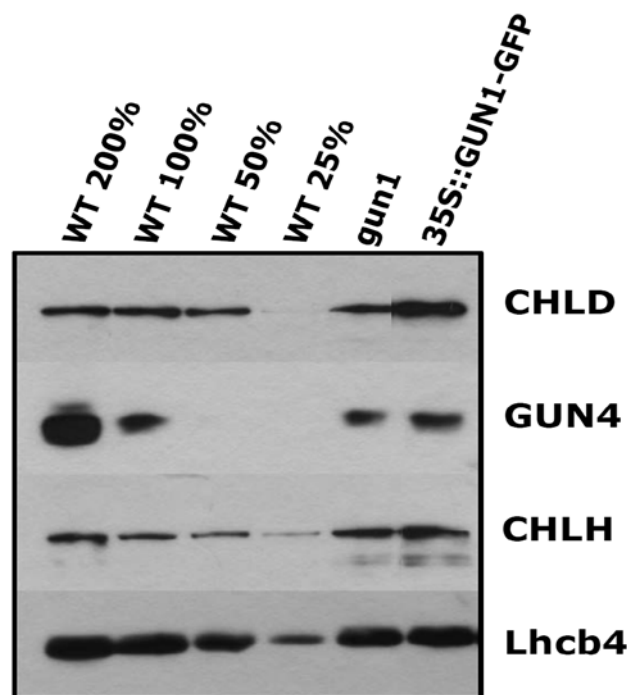


Figure 3.14 Immuno-blot analyses on the accumulation of Mg-chelatase subunits in leaves of WT, *gun1* and 35S:GUN1-GFP transgenic lines. Immuno-blotting on Lhcb4 was used as a loading control.

3.3.2 Discussion

The GUN1 protein was found to be associated with the pTAC complexes, immuno-localization experiments identify GUN1-GFP either in the insoluble fraction or in the stromal soluble matrix. Yeast two-hybrid experiments,

supported by BiFC assays and immuno-blot analyses suggested an interaction of GUN1 with the D subunit of the magnesium chelatase, possibly by stabilizing the CHLD subunit and modulating the activity of the Mg-chelatase. Nevertheless CHLD, as well as the other tetrapyrrole biosynthesis enzymes, have not been isolated with the pTACs yet. On the other hand no physical interaction between GUN1 and the PGE machinery (plastid ribosomal proteins) was identified. Moreover, *in-vivo* experiments such as co-immuno-precipitation did not allow for the detection of the CHLD subunit in the GUN1-GFP immuno-precipitated samples. One of the possible reasons could be that the CHLD-GUN1 interaction is only transient and the two proteins are too weakly associated with each other to be pulled down reciprocally. Another explanation might be that the CHLD-GUN1 complex needs activation to be assembled. As documented by immuno-blot analyses, GUN1-GFP appears in two forms probably due to post-translational modifications or degradation. The larger GUN1-GFP variant is induced under stress-conditions like highlight. Therefore, it might be possible that GUN1 interacts with CHLD to modulate enzyme activity in response to high-light stress. This scenario might explain why a lack of GUN1 leads to a *gun* phenotype on norflurazon (NF) similarly to the other Mg-chelatase subunit mutants (Davis et al., 1999; Mochizuki et al., 2001; Larkin et al., 2003). However, further immuno-precipitation experiments under stress conditions are needed to support this model. The recent discovery of the PhD transcription factor (PTM) being the physical link between the plastid and the nuclear part of the GUN1-mediated retrograde signaling pathway speaks in favor of this hypothesis. Indeed, PTM needs to be stress-activated in order to migrate into the nucleus (Sun et al., 2011). Our model proposes GUN1 to function as a key regulator which coordinates tetrapyrrole biosynthesis in the chloroplast with the plastid translational machinery and photosynthetic nuclear gene expression. Another role recently proposed for GUN1 is to act upstream of the heme-branch in the tetrapyrrole biosynthesis pathway and not

downstream as signal integrator (Koussevitzky et al., 2007; Terry and Smith, 2013). According to this hypothesis GUN1 controls either the synthesis or the availability of the tRNA^{GLU}, in this way modulating the positive signal transduced by the free heme (Terry and Smith, 2013). In this respect GUN1 might act as a negative regulator of NGE promoting chlorophyll biosynthesis and/or the opponent of FC1 which represents a positive NGE regulator by affecting heme synthesis. Therefore, the behavior of the double mutants described above could be explained by the sum of positive and negative signals being affected by their mutations. If the positive heme-related signal prevails the mutant phenotype is restored by the lack of GUN1, as described for *gun1 prps1* and *gun1 prors1-1*. Contrarily, when the negative signal dominates the result is an exacerbated phenotype, as observed in *gun1 prpl11*, *gun1 prpl24*, and *gun1 prps17*. Thus, the behavior *gun1 prps21*, which shows the same mutant phenotype as *prps21*, can be explained by equal signals cancelling each other out. To prove this signal-related theory it will be crucial to analyze the behavior of triple mutants like *gun1 prps1 fc1* and *gun1 prors1-1 fc1* or *gun1 prpl11 gun4* and *gun1 prpl24 gun4*. If the hypothesis is correct, the introduction of the *fc1* mutation might restore the *prps1* and *prors1-1* phenotype, whereas the introduction of *gun4* might complement the *gun1 prpl11* and *gun1 prpl24* phenotypes.

3.4 The RH50 component of the pTAC complex shows similar features of GUN1 with respect to retrograde signalling

3.4.1 RH50 and GUN1 are subunits of the pTAC complex

To further investigate the involvement of the pTAC complex in retrograde signaling, we selected two *rh50* mutant alleles, silenced by a T-DNA insertion in the gene encoding the RH50 DEAD-box helicase (Figure 3.15).

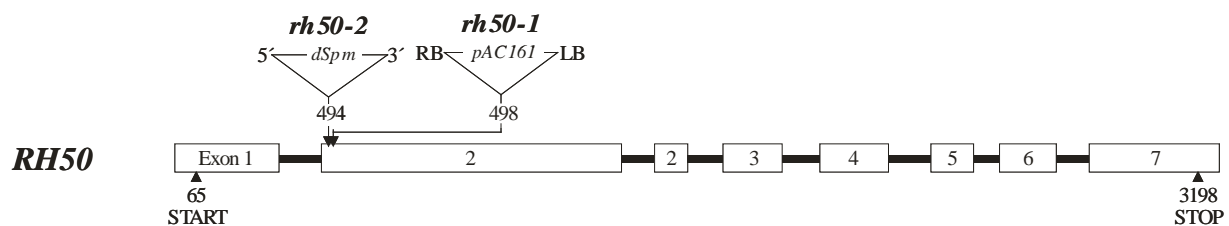


Figure 3.15 RH50 genomic locus and the employed T-DNA alleles. The two mutant alleles *rh50-1* and *rh50-2* including the T-DNA and transposon insertion sites are displayed within the genomic sequences, 5' and 3' indicate the orientation of the transposon, RB and LB the orientation of the T-DNA.

Besides the enzymes involved in tetrapyrrole biosynthesis also the *RH50* gene appears to be highly co-regulated with GUN1 (Table 3.7). Furthermore, mass spectrometry analyses identified RH50 to be a member of the pTAC complexes (Olinares et al., 2010). To confirm the localization of RH50, transgenic lines carrying the 35S:RH50-YFP construct were generated in the *rh50* genetic background. Subsequently, the 35S:RH50-YFP line was crossed with 35S:GUN1-GFP, a line carrying a fluorescence marker for pTACs, to clarify whether the two proteins co-localize with the pTAC complexes. Protoplasts were isolated from the F1 generation and analyzed with a fluorescence microscope employing YFP and GFP filters. Since the localization pattern of the two fluorescent proteins was widely overlapping, one can conclude that RH50 is a member of pTAC complexes similar GUN1 (Figure 3.16).

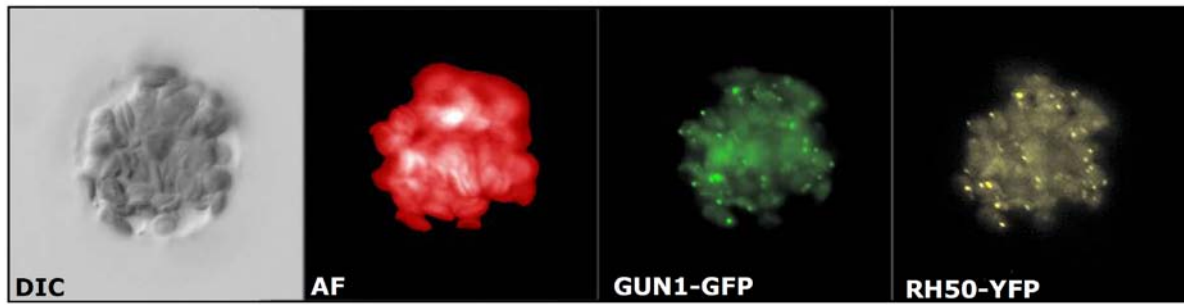


Figure 3.16 Co-localization of 35S:RH50-YFP and 35S:GUN1-GFP in *A. thaliana* protoplasts. DIC, differential interference contrast; AF, chlorophyll auto-fluorescence; GUN1-GFP, green fluorescence of the chimeric GUN1-GFP; RH50-YFP, yellow fluorescence emitted by the chimeric RH50-YFP.

To identify some putative components of RH50 protein complex, the same set of yeast-two-hybrid plasmids used for GUN1 was employed to identify RH50 interaction partners. However, with this approach no putative interacting-polypeptide was identified. RH50 did not show any interaction with GUN1, PRPL11, PRPL24, HEMA, GSA1, GSA2, HEMC, HEME1, HEMF1, PPOX, CHLI, CHLI2, or CHLD (not shown).

3.4.2 RH50 is involved in plastid transcript processing

Northern blot analyses was performed on 14 days old leaf material obtained from WT, *gun1*, *rh50*, and *gun1 rh50* double mutants to investigate putative roles of GUN1 and RH50 in plastid rRNA processing.

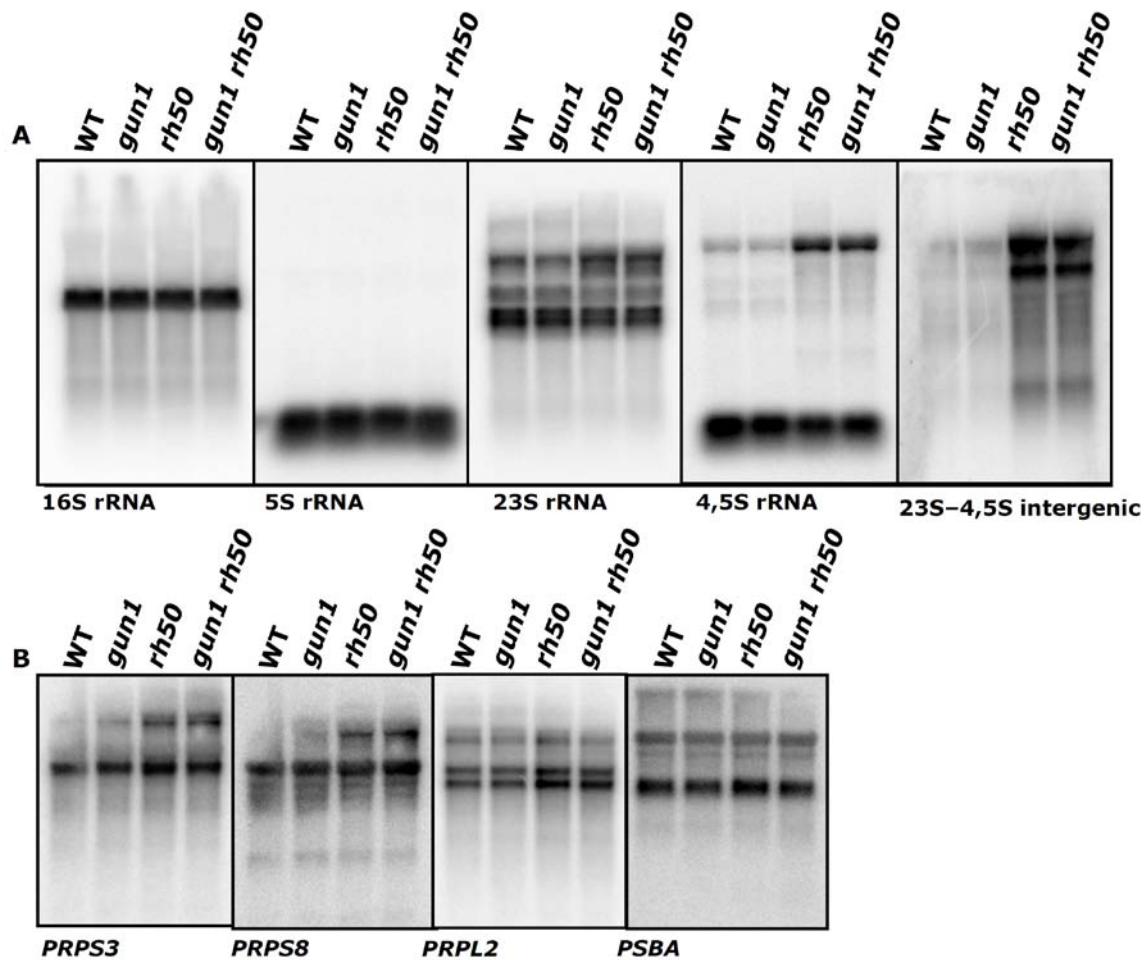


Figure 3.17 Northern blot analyses on leaves from 14 days old *gun1*, *rh50* and *gun1 rh50* plants. Analyses were performed to monitor plastid rRNA processing (A) and transcripts of other plastid-encoded genes (B).

The obtained data displayed no defects in 16S and 5S rRNA transcription and maturation in all the analyzed mutants. Nevertheless, the *rh50* and *gun1 rh50* mutants clearly showed a processing defect of the 23S and 4,5S rRNA transcripts. The mature transcript of these genes was slightly reduced and an unprocessed transcript was enriched when compared to Col-0 and *gun1*. The 23S-4,5S intergenic region was also analyzed by northern blot employing a complementary probe of 80 nucleotides in length to localize the region where alterations in splicing occur. This resulted in only faint signal being detectable in WT and *gun1* leaves. Contrarily, transcripts of this region strongly accumulated in *rh50* and *gun1 rh50* mutant plants (Figure 3.17). This observation indicates that RH50 is involved in the processing of the 23S-4,5S intergenic region and

as a consequence responsible for the efficient maturation of the 23S and 4,5S rRNAs. Further expression analyses showed additional processing defects in other plastid transcripts such as *PRPS3* and *PRPS8* in *rh50* and *gun1 rh50* leaves. As in the case of the rRNAs, the processing defects lead to the accumulation of the mRNA precursors. However, levels of the mature mRNAs were not affected. On the other hand, no splicing defects were detectable in *PRPL2* and *PSBA* transcripts from WT and mutant leaves (Figure 3.17).

3.4.3 RH50 and GUN1 show similar genetic interactions

Similarly to *gun1*, *rh50* shows a WT-like phenotype, as indicated by a WT growth rate and photosynthetic efficiency (Figures 3.18 and 3.19), whereas the *gun1 rh50* double mutant displayed a reduction in size (50% of the WT at 26 d.a.p.) although its photosynthetic efficiency was similar to WT (Figure 3.18, Figure 3.19 and Table 3.9). In the *prors1-1* mutant background the effect of the *rh50* mutation was comparable to the one of *gun1* with the *rh50 prors1-1* double mutant being slightly bigger than the *prors1-1* single mutant (130%), but still smaller than the WT control (85%). Also its photosynthetic performance was restored to WT levels.

Similarly, *rh50 prps1* plants were significantly larger than the *prps1* ones (160%) showing an improved photosynthetic performance as indicated by increased F_v/F_m and Φ_{II} parameters (Table 3.9). The *rh50 prps21* plants on the other hand showed a phenotype similar to the *prps21* single mutant.



Figure 3.18 Phenotypic analyses of the *rh50* mutation in *prp* and *prors1-1* mutant genetic backgrounds. Imaging-PAM representations of the yield of PSII (Φ_{II}) are reported on the right, violet color for 0, red color for 1 (A). Optical microscopy observations allowed for the identification of *rh50 prpl24* embryo-lethal mutant (B).

On the contrary, different effects could be observed for *rh50 prpl11* plants, as they were strongly reduced in size at 26 d.a.g. (30% of *prpl11* and 10% of Col-0) and exacerbated in their F_v/F_m and Φ_{II} values (Table 3.9).

In addition, the two *rh50* alleles (Figure 3.15) were also crossed with *prpl24*, but segregation analyses performed on the F2 generation did not allow for the identification of a *rh50 prpl24* double mutant.

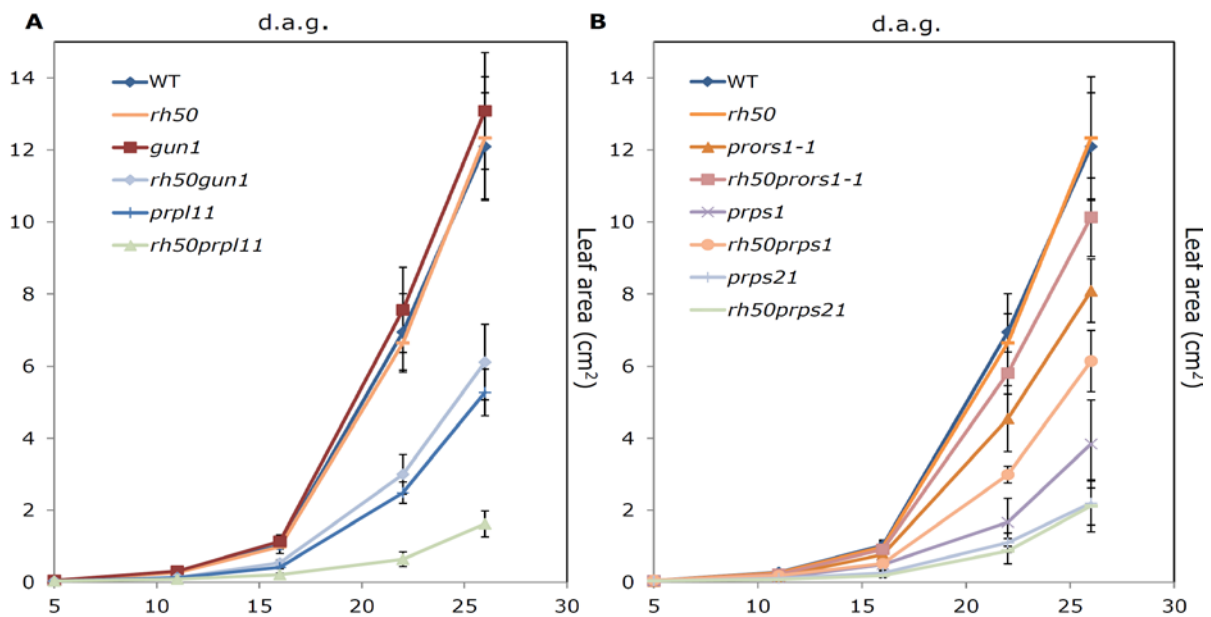


Figure 3.19 Growth rate analyses of *rh50* mutant in combination with *gun1* and the OGE mutants. The charts represent the leaf area (in cm²) measured during 26 days of observation.

Light microscopy of *rh50/RH50 prpl24/prpl24* siliques revealed that in one out of four ovules the embryo development was arrested at the globular stage, thus *RH50* and *PRPL24* seem to be essential for a proper embryo development (Figure 3.18). Similarly, analyses on *rh50-1/RH50 prps17/prps17* and *rh50-2/RH50 prps17/prps17* progeny did not allow for an identification of the corresponding double knock-out. Also in the case of a *prps17* genetic background *RH50* seems to be essential for embryo development.

Table 3.9 Photosynthetic parameters (F_v/F_m , Φ_{II} and 1-qP) of *rh50*, *gun1*, *prors1-1*, *prpl11*, *prps1* and *prps21* single and double mutants. F_v/F_m and Φ_{II} are representative of PSII efficiency, 1-qP is indicative for the redox-state of the PQ pool.

	F_v/F_m	Φ_{II}	1-qP
WT	0,81±0,02	0,75±0,01	0,06±0,02
<i>rh50</i>	0,82±0,01	0,75±0,01	0,05±0,01
<i>gun1</i>	0,82±0,01	0,76±0,02	0,05±0,02
<i>rh50 gun1</i>	0,82±0,01	0,75±0,02	0,06±0,02
<i>prors1-1</i>	0,78±0,02	0,68±0,02	0,06±0,02
<i>rh50 prors1-1</i>	0,82±0,02	0,73±0,02	0,07±0,02
<i>prpl11</i>	0,71±0,03	0,64±0,02	0,07±0,02
<i>rh50 prpl11</i>	0,49±0,04	0,39±0,03	0,12±0,03
<i>prps1</i>	0,63±0,03	0,49±0,02	0,12±0,03
<i>rh50 prps1</i>	0,67±0,02	0,54±0,02	0,08±0,03
<i>prps21</i>	0,55±0,02	0,41±0,03	0,16±0,04
<i>rh50 prps21</i>	0,53±0,02	0,40±0,03	0,14±0,03

Taken together the phenotypic observations on this set of double mutants, compared to the *gun1 prp* and *gun1 prors1-1* phenotypic data, strongly suggest a common function of RH50 and GUN1 possibly by acting within the same signaling pathway.

3.4.4 Discussion

As previously described by Olinares et al. (2010), the RH50 DEAD-box helicase protein is part of the pTACs and shows a co-localization with GUN1 in distinct spots within the plastid. Approaches like the Y2H assay that aimed at identifying direct interacting components of RH50 failed. On the other hand, expression analyses on 14 days old leaf material revealed the involvement of RH50 in plastid rRNA and mRNA processing with plastid encoded genes like 23S rRNA, 4,5S rRNA, *PRPS3* and *PRPS8* showing defects in RNA maturation in *rh50* and *rh50 gun1* mutant plants.

The incorrect processing of the 23S-4,5S intergenic region leads to the accumulation of 23S rRNA and 4,5S rRNA precursors and the reduction of both of the mature rRNAs. In contrast, GUN1 is not involved in these rRNA and mRNA processing steps since no additive effect can be observed in the *gun1 rh50* double mutant. The lethal phenotype of *rh50 prpl24* could therefore be explained by the adding up of two different defects in 23S rRNA accumulation since both, *rh50* and *prpl24* show a reduced abundance of the mature 23S rRNA. (this dissertation; Romani et al., 2012). The RH50 DEAD-box helicase represents a promising candidate for being involved in the GUN1-mediated retrograde signaling pathway. The *RH50* gene was considered because of its high co-regulation score with *GUN1* and mass-spectrometry data that have identified RH50 in pTAC complexes together with GUN1 (Olinares et al., 2010). Even though *gun1* and *rh50* show both a WT-like phenotype, the *gun1 rh50* double mutant displays an altered growth-rate phenotype suggesting a common molecular function in some chloroplast located process. The genetic interaction profile determines for the *rh50* mutant is widely congruent with the *gun1* mutant, both showing embryo-lethality in combination with *prpl24* and *prps17*. Interestingly, the *rh50 prpl24* double mutant is not able to complete its embryogenesis similar to the *gun1 prpl24* double mutant, which shows a less severe phenotype with an arrest only after reaching the torpedo stage. The *rh50 prpl24* double mutant shows an arrest already at the globular stage of seed development similar to many documented *prp* mutants like *prps20*, *prpl1*, *prpl4*, *prpl21*, *prpl27* or *prpl35* (Romani et al., 2012; Yin et al., 2012). The transition stage between the globular and the torpedo stage corresponds to the phase where pro-plastids develop to chloroplasts and fatty acid biosynthesis becomes essential for the embryo (Mansfield et al., 1991; Kobayashi et al., 2007). An opposite scenario must be noticed for the genetic interaction with *prpl11*. Here, *gun1* and *rh50* show a different effect even though both exacerbate the *prpl11* phenotype. Indeed *gun1 prpl11* is

albinotic and seedling-lethal whereas the *rh50 prpl11* double mutation produces small and pale plants that are still viable. If PRPL11 is lacking, GUN1 seems to be more crucial than RH50 for plastid functionality. Besides some minor differences, the *rh50* and *gun1* mutants behave similarly in combination with *prps1*, *prps21* and *prors1-1*. These mutations lead indeed to a partial rescue of the phenotype for *rh50 prps1*, *gun1 prps1* (if compared with *prps1*), *rh50 prors1-1* and *gun1 prors1-1* (in comparison to *prors1-1*) and a neutral effect in *prps21* mutant background. Similarly to *gun1*, *rh50* displays a partial restoration of *prps1* and *prors1-1* phenotypes concerning growth rate and photosynthetic performance (F_v/F_m and Φ_{II}). As described for *gun1*, even in this case the mitigation effect of the TRS is not due to the chlorophyll content of the mutant, but to a real improvement of the plastid functions. More experiments are needed to test the OGE in these genetic backgrounds to clarify whether transcription/translation is truly restored in these lines or rather more stress-adaption mechanisms are involved. Our observations strongly suggest an involvement of RH50 in the GUN1-mediated retrograde signaling pathway. However, NF sensitivity tests did not reveal a *gun* phenotype for the *rh50* mutant. Since GUN1 has been proposed to be the integrator of both, the tetrapyrrole biosynthesis and the plastid gene expression pathway and *rh50* shows a functional interaction only with the OGE pathway, we hypothesize that RH50 might function upstream of GUN1 in a plastid gene expression specific pathway. Therefore, OGE inhibitor studies are needed to check whether *rh50* shows a *gun* phenotype.

3.5 GUN1 and RH50 are involved in the regulation of NGE

3.5.1 GUN1 and RH50 act as repressors of NGE in the *prors1-1* genetic background

Organelles are known to be able to modulate NGE according to their physiological needs alterations, chloroplasts and mitochondria activities lead therefore to a reorganization of nuclear gene expression as observed in mutant backgrounds like *prors1-1* and *prors1-2* plants (Pesaresi et al., 2006; Woodson and Chory, 2008). As shown in this work, the *chaos* mutation is able to restore NGE in the *prors1-1* mutant background, indicating the importance of light absorption and the TRS in organelle-to-nucleus communication. To verify whether GUN1 and RH50 are part of the retrograde signaling pathway that is triggered by the effects of the *prors1-1* mutation, northern blot analyses were performed on the corresponding double mutants. In total 13 nuclear genes were analyzed and 10 of them were down-regulated in *prors1-1*, whereas *LHCA4*, *PSAO* and *PSBQ* were expressed at the same level or even higher than in the WT. As expected from growth-rate studies and photosynthetic efficiency analyses, the *gun1 prors1-1* double mutant shows higher expression levels of almost all the nuclear encoded genes except for *LHCB2* when compared to *prors1-1*. Several genes like *Lhca1*, *Lhcb1-2*, *Lhcb6*, *PsaE1*, *PsaK*, *PsaO* and *RbcS* were up-regulated even in the *gun1* single mutant in comparison to the WT. As a control for plastid encoded genes, *psaB* and *RbcL* radio-labeled probes were exploited and both genes resulted up-regulated in *prors1-1*. Surprisingly, *RbcL* and *psaB* were stronger up-regulated in *gun1 prors1-1* than in the *prors1-1* single mutant, indicating that the two mutations have a synergic effect on plastid transcription (Figure 3.20).

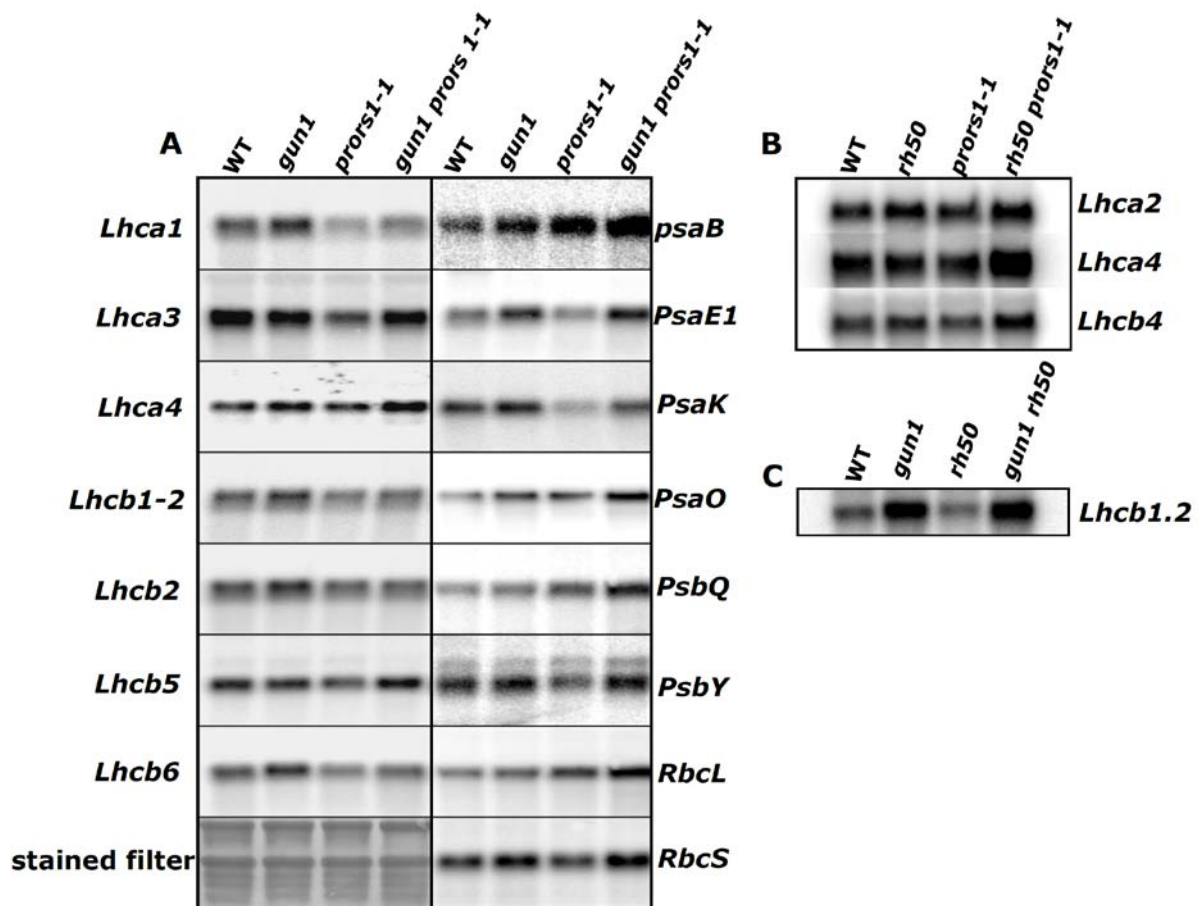


Figure 3.20 Northern blot analyses on NGE in *gun1*, *rh50* and *prors1-1* single and double mutant backgrounds. Expression analyses on nuclear- and plastid-encoded photosynthetic genes in the *gun1*, *prors1-1* and *gun1 prors1-1* genetic background. RNA stained filter shown as loading control (A). Expression of nuclear-encoded photosynthetic genes in *rh50*, *prors1-1* and *rh50 prors1-1* mutants (B). WT, *gun1*, *rh50*, and *gun1 rh50* mutants were grown on MS medium in the presence of 5 mM NF followed by the analysis of *Lhcb1.2* transcript accumulation via northern blot (C).

To check whether *rh50* has a similar effect on NGE as *gun1*, *Lhca2*, *Lhca4* and *Lhcb4* expression were assessed in the *prors1-1 rh50* double mutant by northern blot analysis. As expected, all analysed *Lhc* genes showed a reduced accumulation in *prors1-1* and an accumulation in *rh50 prors1-1* that is even higher than in the WT. These expression analyses strongly suggest that GUN1 and RH50 play a role in organelle-to-nuclear communication. Based on these data we propose that RH50 represents a new player of the GUN1-mediated retrograde signaling pathway, despite

the fact that the *rh50* mutant did not show a *gun*-like phenotype when grown on MS supplemented with 5 μ M NF (Figure 3.20).

3.5.2 Discussion

Expression analyses performed on *gun1 prors1-1* and *rh50 prors1-1* (compared to *prors1-1*) reveal that the restoration of the physiological functions of *prors1-1* implies changes in the NGE which, in fact, is restored to a WT-like level. In case of *gun1 prors1-1*, all the genes analyzed are higher expressed than in *prors1-1*, in particular *Lhca4*, *Lhcb5*, *PsaE1*, *PsaO*, *PsbQ* and *RbcS* are more abundant than in the WT control. *Lhca3*, *Lhcb1-2*, *PsaK* and *PsbY* are expressed at WT levels and *Lhca1*, *Lhcb2* and *Lhcb6* accumulated to levels between WT and *prors1-1*. As documented already for *gun1 sig2*, GUN1 seems to act as a repressor of NGE in the *prors1-1* genetic background (Woodson et al., 2013). The plastid-encoded genes *psaB* and *RbcL* used as controls, with both of them being up-regulated in *prors1-1* and even more so in *gun1 prors1-1* demonstrate the specificity of GUN1 for nuclear photosynthetic genes. Preliminary tests on *rh50 prors1-1* show the same NGE-rescue effect documented for *gun1 prors1-1*. *Lhca2*, *Lhca4* and *Lhcb4*, the nuclear genes tested so far, are indeed down-regulated in *prors1-1* and up-regulated in *rh50 prors1-1*, even more than the WT level. RH50 and GUN1 seem to act as repressors of NGE. However, further tests are needed to see whether RH50 and GUN1 have the same target gene specificity or whether they act in a common pathway in regulating NGE. The common role described for GUN1 and RH50 in regulating NGE strongly suggests the pTAC complexes as the main regulators in the OGE-mediated signaling to the nucleus. According to this hypothesis, different components of the complex, with different molecular functions, might interfere at various levels with the signaling pathway. The signals might then be integrated by GUN1 before being transduced from the chloroplast to the nucleus.

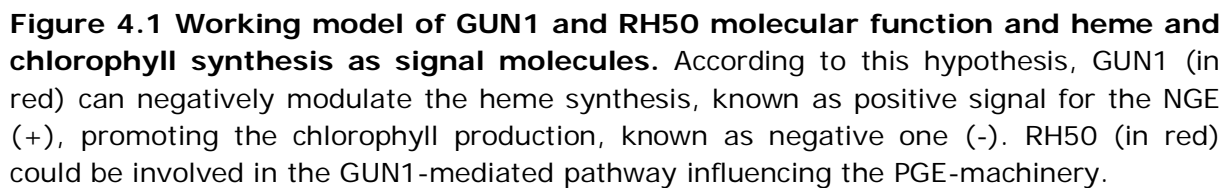
4. Conclusions

In this work we analyzed the role of several molecular players involved in the retrograde plastid-to-nucleus signaling pathway. The functional interaction between light absorption and plastid protein synthesis were studied by combining the *prors1-1* mutation, which is responsible for an altered protein synthesis in organelles, with the *chaos* mutation. This mutation leads to a hyper-oxidized TRS as a consequence of the reduced size of the PSII antenna (Klimyuk et al., 1999; Pesaresi et al., 2006). Perturbations in OGE lead to an imbalanced stoichiometry between nuclear- and plastid-encoded proteins of the photosystems which results in the reduction of the photosynthetic performance and imply changes in the TRS. As a consequence of an altered photosynthetic efficiency the nuclear-encoded photosynthetic genes are down-regulated, with the aim to adapt the chloroplast to the developmental and metabolic needs (Woodson and Chory, 2008). On the other hand the OGE machinery is under the control of the TRS, hence kinases and thioredoxins are indeed able to modify the activity and the stability of the OGE machinery (Balmer et al., 2003; Balmer et al., 2004; Stroher and Dietz, 2008; Tillich et al., 2009; Stern et al., 2010). The *prors1-1 chaos* double mutant analyses allowed us to understand how OGE and the TRS interact with the aim to adapt plastid and nuclear gene expression to the plant's physiological needs. A more oxidized TRS due to the *chaos* mutation is able to restore a WT-like TRS in the *prors1-1* genetic background, which shows as a highly-reduced TRS. The reduction of electron flow through the impaired photosystems can mitigate the stress produced across the electron transport chain itself. The restoration of a WT-like TRS does not imply any improvement on the translational level, since the OGE machinery in *prors1-1 chaos* is similarly reduced in its efficiency as in *prors1-1* mutant however the attenuation of the TRS is influencing NGE which is partially restored to WT-levels. We can therefore conclude that in the plastid-to-

nucleus retrograde signaling the TRS-dependent pathway acts downstream of the OGE-dependent signaling pathway in modulating NGE.

A similar rescue effect in NGE in the *prors1-1* genetic background can be observed for *gun1 prors1-1*. In this case, the TRS of *prors1-1* is restored to a WT-like level by the introduction of the *gun1* mutation. The GUN1 protein has been proposed to be the integrator of all the signaling pathways within the chloroplast as GUN1 is the only GUN protein able to respond to chemicals like NF and Lin which affect tetrapyrrole biosynthesis and OGE, instead, GUN2-to-GUN6 are involved solely in the tetrapyrrole biosynthesis pathway (Davis et al., 1999; Mochizuki et al., 2001; Larkin et al., 2003; Koussevitzky et al., 2007; Woodson et al., 2011). In contrast to the *chaos* mutation, *gun1* is able to restore the TRS of *prors1-1* mutant without changing the pigment composition of the thylakoids. Whether this rescue of NGE is due to an improvement of OGE efficiency or to more complex compensatory effects remains unclear, certainly the signaling cascade modulates the TRS which is perceived to a nuclear level. A genetics approach has allowed us to clarify that only GUN1 of the GUN proteins is functionally interacting with the plastid translation machinery. The *gun1* mutation in the background of different OGE mutants resulted in diverse phenotypic effects, ranging from embryo-, seedling-lethality in case of *gun1 prpl11*, *gun1 prpl24* and *gun1 prps17* to a partial rescue phenotype in *gun1 prps1* and *gun1 prors1-1*. As demonstrated by TEM analyses on variegated *gun1 prpl11* leaves, GUN1 is involved in chloroplast development which is unique in comparison to the other *gun* mutants. Furthermore, GUN1 is shown to physically interact with components of the tetrapyrrole biosynthesis pathway. By stabilizing the D-subunit of the Mg-chelatase under stress conditions GUN1 might be able to promote either heme or chlorophyll biosynthesis. Heme biosynthesis has been reported to act as a positive signal source for NGE (Woodson et al., 2011), whereas chlorophyll precursors have been shown to constitute a negative signal for NGE (Figure 4.1). These observations enable us to

define a molecular model for GUN1 acting as a superior integrator of stress signals within the chloroplast. According to this working model, GUN1 can integrate positive signals from heme and negative signals from chlorophyll biosynthesis to coordinate chloroplast development (Figure 4.1). Interestingly, the loss-of-function mutant of the RH50 DEAD-box helicase, another chloroplast-located protein associated with the pTACs (Olinares et al., 2010), shows a strong phenotypic overlap with the *gun1* mutation in its genetic profile of double mutants. The functional interaction of RH50 and OGE was further shown on the molecular level with *rh50* mutants showing processing defects in plastid transcripts of some rRNAs and ribosomal proteins. Even though the *rh50* mutant failed to show a *gun* phenotype on NF, RH50 shares a similar role with GUN1 in repressing NGE in the *prors1-1* genetic background. According to these observations, RH50 could represent a new player in the GUN1-mediated signaling pathway, which might constitute a regulatory domain within the pTAC protein complex (Figure 4.1).



References

- Adamska, I.** (1995). Regulation of early light-Inducible protein gene expression by blue and red light in etiolated seedlings involves nuclear and plastid factors. *Plant Physiol* **107**, 1167-1175.
- Allen, J.F., and Pfannschmidt, T.** (2000). Balancing the two photosystems: photosynthetic electron transfer governs transcription of reaction centre genes in chloroplasts. *Philos Trans R Soc Lond B Biol Sci* **355**, 1351-1359.
- Apel, K., and Hirt, H.** (2004). Reactive oxygen species: metabolism, oxidative stress, and signal transduction. *Ann Rev Plant Biol* **55**, 373-399.
- Aseeva, E., Ossenbuhl, F., Sippel, C., Cho, W.K., Stein, B., Eichacker, L.A., Meurer, J., Wanner, G., Westhoff, P., Soll, J., and Vothknecht, U.C.** (2007). Vipp1 is required for basic thylakoid membrane formation but not for the assembly of thylakoid protein complexes. *Plant Physiol Biochem* **45**, 119-128.
- Balmer, Y., Koller, A., del Val, G., Manieri, W., Schurmann, P., and Buchanan, B.B.** (2003). Proteomics gives insight into the regulatory function of chloroplast thioredoxins. *Proc Natl Acad Sci USA* **100**, 370-375.
- Balmer, Y., Vensel, W.H., Tanaka, C.K., Hurkman, W.J., Gelhaye, E., Rouhier, N., Jacquot, J.P., Manieri, W., Schuurmann, P., Droux, M., and Buchanan, B.B.** (2004). Thioredoxin links redox to the regulation of fundamental processes of plant mitochondria. *Proc Natl Acad Sci USA* **101**, 2642-2647.
- Banroques, J., Cordin, O., Doere, M., Linder, P., and Tanner, N.K.** (2011). Analyses of the functional regions of DEAD-Box RNA "Helicases" with deletion and chimera constructs cested *in vivo* and *in vitro*. *J Mol Biol* **413**, 451-472.
- Barajas-Lopez Jde, D., Blanco, N.E., and Strand, A.** (2013). Plastid-to-nucleus communication, signals controlling the running of the plant cell. *Biochim Biophys Acta* **1833**, 425-437.
- Barbrook, A.C., Santucci, N., Plenderleith, L.J., Hiller, R.G., and Howe, C.J.** (2006). Comparative analysis of dinoflagellate chloroplast genomes reveals rRNA and tRNA genes. *BMC Genomics* **7**, 297.
- Bienert, G.P., Moller, A.L.B., Kristiansen, K.A., Schulz, A., Moller, I.M., Schjoerring, J.K., and Jahn, T.P.** (2007). Specific aquaporins facilitate the diffusion of hydrogen peroxide across membranes. *J Biol Chem* **282**, 1183-1192.
- Bradbeer, J.W., Atkinson, Y.E., Borner, T., and Hagemann, R.** (1979). Cytoplasmic synthesis of plastid polypeptides may be controlled by plastid-synthesized RNA. *Nature* **279**, 816-817.
- Buchanan, B.B.** (1980). Role of light in the regulation of chloroplast enzymes. *Ann Rev Plant Physiol* **31**, 341-347.
- Chow, W.S., Hope, A.B., and Anderson, J.M.** (1989). Oxygen per flash from leaf-disks quantifies photosystem-II. *Biochim Biophys Acta* **973**, 105-108.

- Cordin, O., Banroques, J., Tanner, N.K., and Linder, P.** (2006). The DEAD-box protein family of RNA helicases. *Gene* **367**, 17-37.
- Davis, S.J., Kurepa, J., and Vierstra, R.D.** (1999). The *Arabidopsis thaliana* HY1 locus, required for phytochrome-chromophore biosynthesis, encodes a protein related to heme oxygenases. *Proc Natl Acad Sci USA* **96**, 6541-6546.
- Elstner, E.F.** (1991). Mechanisms of oxygen activation in different compartments of plant cells. *Curr Top Plant Phys* **6**, 13-25.
- Escoubas, J.M., Lomas, M., Laroche, J., and Falkowski, P.G.** (1995). Light-intensity regulation of cab gene-transcription is signaled by the redox state of the plastoquinone pool. *Proc Natl Acad Sci USA* **92**, 10237-10241.
- Estavillo, G.M., Crisp, P.A., Pornsiriwong, W., Wirtz, M., Collinge, D., Carrie, C., Giraud, E., Whelan, J., David, P., Javot, H., Brearley, C., Hell, R., Marin, E., and Pogson, B.J.** (2011). Evidence for a SAL1-PAP chloroplast retrograde pathway that functions in drought and high light signaling in *Arabidopsis*. *Plant Cell* **23**, 3992-4012.
- Farber, A., Young, A.J., Ruban, A.V., Horton, P., and Jahns, P.** (1997). Dynamics of xanthophyll-cycle activity in different antenna subcomplexes in the photosynthetic membranes of higher plants. The relationship between zeaxanthin conversion and nonphotochemical fluorescence quenching. *Plant Physiol* **115**, 1609-1618.
- Foyer, C.H., and Noctor, G.** (2005). Redox homeostasis and antioxidant signaling: A metabolic interface between stress perception and physiological responses. *Plant Cell* **17**, 1866-1875.
- Gehl, C., Waadt, R., Kudla, J., Mendel, R.R., and Hansch, R.** (2009). New GATEWAY vectors for high throughput analyses of protein-protein interactions by bimolecular fluorescence complementation. *Mol Plant* **2**, 1051-1058.
- Gray, J.C., Sornarajah, R., Zabron, A.A., Duckett, C.M., and Khan, M.S.** (1995). Chloroplast control of nuclear gene expression. *Photosynthesis: from light to biosphere Vol III*, 543-550.
- Gray, J.C., Sullivan, J.A., Wang, J.H., Jerome, C.A., and MacLean, D.** (2003). Coordination of plastid and nuclear gene expression. *Philos Trans R Soc Lond B Biol Sci* **358**, 135-144.
- Hess, W.R., and Borner, T.** (1999). Organellar RNA polymerases of higher plants. *Int Rev Cytol*, **190**, 1-59.
- Hess, W.R., Muller, A., Nagy, F., and Borner, T.** (1994). Ribosome-deficient plastids affect transcription of light-induced nuclear genes: genetic evidence for a plastid-derived signal. *Mol Gen Genet* **242**, 305-312.
- Hoefnagel, M.H.N., Atkin, O.K., and Wiskich, J.T.** (1998). Interdependence between chloroplasts and mitochondria in the light and the dark. *Biochim Biophys Acta* **1366**, 235-255.

Huang, Y.S., and Li, H.M. (2009). Arabidopsis CHL2 can substitute for CHL1. *Plant Physiol* **150**, 636-645.

Ignatowicz, A., Pesaresi, P., Varotto, C., Richly, E., Schneider, A., Jahns, P., Salamini, F., and Leister, D. (2004). Mutants for photosystem I subunit D of *Arabidopsis thaliana*: effects on photosynthesis, photosystem I stability and expression of nuclear genes for chloroplast functions. *Plant J* **37**, 839-852.

Kakizaki, T., Matsumura, H., Nakayama, K., Che, F.S., Terauchi, R., and Inaba, T. (2009). Coordination of Plastid Protein Import and Nuclear Gene Expression by Plastid-to-Nucleus Retrograde Signaling. *Plant Physiol* **151**, 1339-1353.

Klenell, M., Morita, S., Tiemblo-Olmo, M., Muhlenbock, P., Karpinski, S., and Karpinska, B. (2005). Involvement of the chloroplast signal recognition particle cpSRP43 in acclimation to conditions promoting photooxidative stress in *Arabidopsis*. *Plant Cell Physiol* **46**, 118-129.

Klimyuk, V.I., Persello-Cartieaux, F., Havaux, M., Contard-David, P., Schuenemann, D., Meierhoff, K., Gouet, P., Jones, J.D.G., Hoffman, N.E., and Nussaume, L. (1999). A chromodomain protein encoded by the *Arabidopsis* CAO gene is a plant-specific component of the chloroplast signal recognition particle pathway that is involved in LHCP targeting. *Plant Cell* **11**, 87-99.

Kobayashi, K., Kondo, M., Fukuda, H., Nishimura, M., and Ohta, H. (2007). Galactolipid synthesis in chloroplast inner envelope is essential for proper thylakoid biogenesis, photosynthesis, and embryogenesis. *Proc Natl Acad Sci USA* **104**, 17216-17221.

Koussevitzky, S., Nott, A., Mockler, T.C., Hong, F., Sachetto-Martins, G., Surpin, M., Lim, J., Mittler, R., and Chory, J. (2007). Signals from chloroplasts converge to regulate nuclear gene expression. *Science* **316**, 715-719.

Larkin, R.M., Alonso, J.M., Ecker, J.R., and Chory, J. (2003). GUN4, a regulator of chlorophyll synthesis and intracellular signaling. *Science* **299**, 902-906.

Leister, D. (2005). Genomics-based dissection of the cross-talk of chloroplasts with the nucleus and mitochondria in *Arabidopsis*. *Gene* **354**, 110-116.

Leister, D. (2012). Retrograde signaling in plants: from simple to complex scenarios. *Front Plant Sci* **3**, 135.

Linder, P., and Jankowsky, E. (2011). From unwinding to clamping - the DEAD box RNA helicase family. *Nat Rev Mol Cell Biol* **12**, 505-516.

Mansfield, S.G., Briarty, L.G., and Erni, S. (1991). Early embryogenesis in *Arabidopsis thaliana*. 1. The mature embryo sac. *Can J Bot* **69**, 447-460.

Martin, W., and Kowallik, K.V. (1999). Annotated english translation of Mereschkowsky's 1905 paper *Über Natur und Ursprung der Chromatophoren im Pflanzenreiche*. *Eur J Phycol* **34**, 287-295.

- Martin, W., Rujan, T., Richly, E., Hansen, A., Cornelsen, S., Lins, T., Leister, D., Stoebe, B., Hasegawa, M., and Penny, D.** (2002). Evolutionary analysis of *Arabidopsis*, cyanobacterial, and chloroplast genomes reveals plastid phylogeny and thousands of cyanobacterial genes in the nucleus. *Proc Natl Acad Sci USA* **99**, 12246-12251.
- Mochizuki, N., Brusslan, J.A., Larkin, R., Nagatani, A., and Chory, J.** (2001). *Arabidopsis* genomes uncoupled 5 (GUN5) mutant reveals the involvement of Mg-chelatase H subunit in plastid-to-nucleus signal transduction. *Proc Natl Acad Sci USA* **98**, 2053-2058.
- Mochizuki, N., Tanaka, R., Tanaka, A., Masuda, T., and Nagatani, A.** (2008). The steady-state level of Mg-protoporphyrin IX is not a determinant of plastid-to-nucleus signaling in *Arabidopsis*. *Proc Natl Acad Sci USA* **105**, 15184-15189.
- Moulin, M., McCormac, A.C., Terry, M.J., and Smith, A.G.** (2008). Tetrapyrrole profiling in *Arabidopsis* seedlings reveals that retrograde plastid nuclear signaling is not due to Mg-protoporphyrin IX accumulation. *Proc Natl Acad Sci USA* **105**, 15178-15183.
- Mubarakshina, M.M., Ivanov, B.N., Naydov, I.A., Hillier, W., Badger, M.R., and Krieger-Liszkay, A.** (2010). Production and diffusion of chloroplastic H₂O₂ and its implication to signalling. *J Exp Bot* **61**, 3577-3587.
- Mullineaux, P., and Karpinski, S.** (2002). Signal transduction in response to excess light: getting out of the chloroplast. *Curr Opin Plant Biol* **5**, 43-48.
- Oelmüller, R., Levitan, I., Bergfeld, R., Rajasekhar, V.K., and Mohr, H.** (1986). Expression of Nuclear Genes as Affected by Treatments Acting on the Plastids. *Planta* **168**, 482-492.
- Oelze, M.L., Kandlbinder, A., and Dietz, K.J.** (2008). Redox regulation and overreduction control in the photosynthesizing cell: complexity in redox regulatory networks. *Biochim Biophys Acta* **1780**, 1261-1272.
- Olinares, P.D., Ponnala, L., and van Wijk, K.J.** (2010). Megadalton complexes in the chloroplast stroma of *Arabidopsis thaliana* characterized by size exclusion chromatography, mass spectrometry, and hierarchical clustering. *Mol Cell Proteomics* **9**, 1594-1615.
- Pesaresi, P.** (2011). Studying translation in *Arabidopsis* chloroplasts. *Methods Mol Biol* **774**, 209-224.
- Pesaresi, P., Schneider, A., Kleine, T., and Leister, D.** (2007). Interorganellar communication. *Curr Opin Plant Biol* **10**, 600-606.
- Pesaresi, P., Varotto, C., Meurer, J., Jahns, P., Salamini, F., and Leister, D.** (2001). Knock-out of the plastid ribosomal protein L11 in *Arabidopsis*: effects on mRNA translation and photosynthesis. *Plant J* **27**, 179-189.
- Pesaresi, P., Masiero, S., Eubel, H., Braun, H.P., Bhushan, S., Glaser, E., Salamini, F., and Leister, D.** (2006). Nuclear photosynthetic gene expression is

synergistically modulated by rates of protein synthesis in chloroplasts and mitochondria. *Plant Cell* **18**, 970-991.

Pesaresi, P., Hertle, A., Pribil, M., Kleine, T., Wagner, R., Strissel, H., Ihnatowicz, A., Bonardi, V., Scharfenberg, M., Schneider, A., Pfannschmidt, T., and Leister, D. (2009). Arabidopsis STN7 kinase provides a link between short- and long-term photosynthetic acclimation. *Plant Cell* **21**, 2402-2423.

Pfalz, J., Liere, K., Kandlbinder, A., Dietz, K.J., and Oelmüller, R. (2006). pTAC2, -6, and -12 are components of the transcriptionally active plastid chromosome that are required for plastid gene expression. *Plant Cell* **18**, 176-197.

Pfannschmidt, T., and Yang, C. (2012). The hidden function of photosynthesis: a sensing system for environmental conditions that regulates plant acclimation responses. *Protoplasma* **249 Suppl 2**, S125-136.

Pfannschmidt, T., Nilsson, A., Tullberg, A., Link, G., and Allen, J.F. (1999). Direct transcriptional control of the chloroplast genes *psbA* and *psaAB* adjusts photosynthesis to light energy distribution in plants. *IUBMB Life* **48**, 271-276.

Pogson, B.J., Woo, N.S., Forster, B., and Small, I.D. (2008). Plastid signalling to the nucleus and beyond. *Trends Plant Sci* **13**, 602-609.

Pursiheimo, S., Mulo, P., Rintamäki, E., and Aro, E.M. (2001). Coregulation of light-harvesting complex II phosphorylation and *lhcb* mRNA accumulation in winter rye. *Plant J* **26**, 317-327.

Ramel, F., Birtic, S., Ginies, C., Soubigou-Taconnat, L., Triantaphylides, C., and Havaux, M. (2012). Carotenoid oxidation products are stress signals that mediate gene responses to singlet oxygen in plants. *Proc Natl Acad Sci USA* **109**, 5535-5540.

Romani, I., Tadini, L., Rossi, F., Masiero, S., Pribil, M., Jahns, P., Kater, M., Leister, D., and Pesaresi, P. (2012). Versatile roles of *Arabidopsis* plastid ribosomal proteins in plant growth and development. *Plant J.* **72**, 922-934

Ruckle, M.E., DeMarco, S.M., and Larkin, R.M. (2007). Plastid signals remodel light signaling networks and are essential for efficient chloroplast biogenesis in *Arabidopsis*. *Plant Cell* **19**, 3944-3960.

Schägger, H., and von Jagow, G. (1987). Tricine-sodium dodecyl sulfate-polyacrylamide gel electrophoresis for the separation of proteins in the range from 1 to 100 kDa. *Anal Biochem* **166**, 368-379.

Shiina, T., Tsunoyama, Y., Nakahira, Y., and Khan, M.S. (2005). Plastid RNA polymerases, promoters, and transcription regulators in higher plants. *Int Rev Cytol* **244**, 1-68.

Small, I.D., and Peeters, N. (2000). The PPR motif - a TPR-related motif prevalent in plant organellar proteins. *Trends Biochem Sci* **25**, 46-47.

Stern, D.B., Goldschmidt-Clermont, M., and Hanson, M.R. (2010). Chloroplast RNA Metabolism. *Annu Rev Plant Biol* **61**, 125-155.

- Strand, A., Asami, T., Alonso, J., Ecker, J.R., and Chory, J.** (2003). Chloroplast to nucleus communication triggered by accumulation of Mg-protoporphyrinIX. *Nature* **421**, 79-83.
- Stroher, E., and Dietz, K.J.** (2008). The dynamic thiol-disulphide redox proteome of the *Arabidopsis thaliana* chloroplast as revealed by differential electrophoretic mobility. *Physiol Plant* **133**, 566-583.
- Sullivan, J.A., and Gray, J.C.** (1999). Plastid translation is required for the expression of nuclear photosynthesis genes in the dark and in roots of the pea *lip1* mutant. *Plant Cell* **11**, 901-910.
- Sun, X.W., Feng, P.Q., Xu, X.M., Guo, H.L., Ma, J.F., Chi, W., Lin, R.C., Lu, C.M., and Zhang, L.X.** (2011). A chloroplast envelope-bound PHD transcription factor mediates chloroplast signals to the nucleus. *Nat Comm* **2**.
- Susek, R.E., Ausubel, F.M., and Chory, J.** (1993). Signal-transduction mutants of *Arabidopsis* uncouple nuclear *Cab* and *Rbcs* gene expression from chloroplast development. *Cell* **74**, 787-799.
- Tadini, L., Romani, I., Pribil, M., Jahns, P., Leister, D., and Pesaresi, P.** (2012). Thylakoid redox signals are integrated into organellar-gene-expression-dependent retrograde signaling in the *prors1-1* mutant. *Front Plant Sci* **3**, 282.
- Terry, M.J., and Smith, A.G.** (2013). A model for tetrapyrrole synthesis as the primary mechanism for plastid-to-nucleus signaling during chloroplast biogenesis. *Front Plant Sci* **4**, 14.
- Tillich, M., Le Sy, V., Schulerowitz, K., von Haeseler, A., Maier, U.G., and Schmitz-Linneweber, C.** (2009). Loss of *matK* RNA editing in seed plant chloroplasts. *Bmc Evol Biol* **9**.
- Timmis, J.N., Ayliffe, M.A., Huang, C.Y., and Martin, W.** (2004). Endosymbiotic gene transfer: organelle genomes forge eukaryotic chromosomes. *Nat Rev Genet* **5**, 123-135.
- Walter, M., Chaban, C., Schutze, K., Batistic, O., Weckermann, K., Nake, C., Blazevic, D., Grefen, C., Schumacher, K., Oecking, C., Harter, K., and Kudla, J.** (2004). Visualization of protein interactions in living plant cells using bimolecular fluorescence complementation. *Plant J* **40**, 428-438.
- Waters, M.T., Moylan, E.C., and Langdale, J.A.** (2008). GLK transcription factors regulate chloroplast development in a cell-autonomous manner. *Plant J* **56**, 432-444.
- Waters, M.T., Wang, P., Korkaric, M., Capper, R.G., Saunders, N.J., and Langdale, J.A.** (2009). GLK Transcription Factors Coordinate Expression of the Photosynthetic Apparatus in *Arabidopsis*. *Plant Cell* **21**, 1109-1128.
- Woodson, J.D., and Chory, J.** (2008). Coordination of gene expression between organellar and nuclear genomes. *Nat Rev Genet* **9**, 383-395.
- Woodson, J.D., Perez-Ruiz, J.M., and Chory, J.** (2011). Heme synthesis by plastid ferrochelatase I regulates nuclear gene expression in plants. *Curr Biol* **21**, 897-903.

- Woodson, J.D., Perez-Ruiz, J.M., Schmitz, R.J., Ecker, J.R., and Chory, J.** (2013). Sigma factor-mediated plastid retrograde signals control nuclear gene expression. *Plant J* **73**, 1-13.
- Xiao, Y., Savchenko, T., Baidoo, E.E., Chehab, W.E., Hayden, D.M., Tolstikov, V., Corwin, J.A., Kliebenstein, D.J., Keasling, J.D., and Dehesh, K.** (2012). Retrograde signaling by the plastidial metabolite MEcPP regulates expression of nuclear stress-response genes. *Cell* **149**, 1525-1535.
- Yadegari, R., Paiva, G., Laux, T., Koltunow, A.M., Apuya, N., Zimmerman, J.L., Fischer, R.L., Harada, J.J., and Goldberg, R.B.** (1994). Cell differentiation and morphogenesis are uncoupled in *Arabidopsis* raspberry embryos. *Plant Cell* **6**, 1713-1729.
- Yin, T., Pan, G., Liu, H., Wu, J., Li, Y., Zhao, Z., Fu, T., and Zhou, Y.** (2012). The chloroplast ribosomal protein L21 gene is essential for plastid development and embryogenesis in *Arabidopsis*. *Planta* **235**, 907-921.
- Yoshida, R., Sato, T., Kanno, A., and Kameya, T.** (1998). Streptomycin mimics the cool temperature response in rice plants. *J Exp Bot* **49**, 221-227.

Acknowledgements

I would like to thank Prof. Dr. Dario Leister for giving me the opportunity and the funding to accomplish my Ph.D. in his research group.

To Prof. Dr. Jörg Nickelsen for taking over the “Zweitgutachter”.

I would like to thank Dr. Paolo Pesaresi for all the good ideas, for the supervision and the motivation I got every single day.

Additionally, I would like to thank Dr. Mathias Pribil for the help and the support he gave me.

Thanks to Nico, for helping me a lot with doctors and broken bones while I was writing this thesis.

To Stefania, for offering me a shelter and care when I was not able to manage things by myself.

All the people in the lab for their help and for all the good and bad time we spent together.

My friends here and on the other side of the alps, for listening to my complaining and cheering me up in blue days.

Thanks to my family, for everything.

A Papá.

Curriculum vitae

Personal details

Name: Luca Tadini

Date of birth: 04/04/1984

Place of birth: Treviglio (BG), Italy

Citizenship: Italian

Education

October 2003 – December 2006

Bachelor degree in Biology. Final grade: 103/110

Università degli studi di Milano (Milan, Italy)

October 2006 – March 2009

Master degree in Molecular Cell Biology. Final grade: 110/110 with honor

Università degli studi di Milano (Milan, Italy)

Research experience

September 2006 – December 2006

Bachelor thesis in Prof. Anna Moroni´s group, Università degli studi di Milano (Milan, Italy)

Aim of the work: Extraction and purification of heterologous proteins in yeast

January 2008 –may 2009

Master thesis in Prof. Martin Kater´s group, Università degli studi di Milano (Milan, Italy)

Aim of the work: Study of imprinted polycomb genes involved in seed development in rice (ERA-PG Seeds for Growth Project)

June 2009 – October 2009

Six months fellowship in Prof. Martin Kater´s group, Università degli studi di Milano (Milan, Italy)

Aim of the work: Study of imprinted polycomb genes involved in seed development in rice (ERA-PG Seeds for Growth Project)

Publications

Romani I*, Tadini L*, Rossi F, Masiero S, Pribil M, Jahns P, Kater M, Leister D, Pesaresi P. (2012) Versatile roles of Arabidopsis plastid ribosomal proteins in plant growth and development. *Plant J.* 2012 Aug 18.

Tadini L, Romani I, Pribil M, Jahns P, Leister D, Pesaresi P. (2012) Thylakoid redox signals are integrated into organellar-gene-expression-dependent retrograde signaling in the *prors1-1* mutant. *Front Plant Sci* 3, 282.

Allahverdiyeva Y*, Suorsa M*, Rossi F, Pavesi A, Kater MM, Antonacci A, Tadini L, Pribil M, Schneider A, Wanner G, Leister D, Aro EM, Barbato R, Pesaresi P. (2013) Arabidopsis plants lacking PsbQ

and PsbR subunits of the oxygen-evolving complex show altered PSII super-complex organization and short-term adaptive mechanisms. *Plant J* 2013 May 7.

Armbruster U*, Ruehle T*, Kreller R, Strotbek C, Zuehlke J, Tadini L, Blunder T, Hertle A, Qi Y, Rengstl B, Nickelsen J, Frank W, Leister D. (2013) The PAM68LIKE protein evolved from a PSII assembly factor to mediate assembly of the chloroplast NDH complex in flowering plants. *Plant Cell*, submitted.

* authors contributed equally

publications related to this dissertation

Declaration / Eidesstattliche Erklärung

Ich versichere hiermit an Eides statt, dass die vorgelegte Dissertation von mir selbständig und ohne unerlaubte Hilfe angefertigt ist.

München, den

Luca Tadini